Institute of Thermoelectricity, Academy of Sciences and Ministry of Education and Science of Ukraine

# Journal of THERMOELECTRICITY

International Research

Founded in December, 1993

published 4 times a year

*No. 2* *2022*

## Editorial Board



## International Editorial Board

Founders – National Academy of Sciences, Ukraine
Institute of Thermoelectricity of National Academy of Sciences and Ministry of Education and Science of Ukraine

Certificate of state registration № КВ 15496-4068 ПР



Address of editorial office:
Ukraine, 58002, Chernivtsi, General Post Office, P.O. Box 86.
Phone: +(380-372) 90 31 65.
Fax: +(380-3722) 4 19 17.
E-mail: jt@inst.cv.ua
http://www.jt.inst.cv.ua

Signed for publication 24.03.2022. Format 70×108/16. Offset paper №1. Offset printing.
Printer's sheet 11.5. Publisher's signature 9.2. Circulation 400 copies. Order 5.

Printed from the layout original made by "Journal of Thermoelectricity" editorial board
in the printing house of "Bukrek" publishers,
10, Radischev Str., Chernivtsi, 58000, Ukraine

## CONTENTS

**L.M. Vykhor,** *DSc (Phys-Math)* [1]
**P.V. Gorskyi,** *DSc (Phys-Math)* [1,2]
**V.V. Lysko,** *Cand.Sc (Phys-Math)* [1,2]

[1]Institute of Thermoelectricity of the NAS and MES of Ukraine,
1, Nauky str., Chernivtsi, 58029, Ukraine;
[2]Yuriy Fedkovych Chernivtsi National University,
2, Kotsiubynsky str., Chernivtsi, 58012, Ukraine
*e-mail: anatych@gmail.com*

# METHODS FOR MEASURING CONTACT RESISTANCES OF "METAL – THERMOELECTRIC MATERIAL" STRUCTURES (PART 1)

*An overview of existing methods for measuring electrical contact resistance is presented. An analysis of their accuracy, advantages and disadvantages, as well as the possibilities of using them in thermoelectricity for the study and optimization of "metal – thermoelectric material" structures is conducted. Bibl. 11, Figs 14.*

**Key words:** electrical contact resistance, measurement, accuracy, thermoelectric power converters.

## Introduction

Reducing the cost of manufacturing thermoelectric power converters is a pressing issue in thermoelectricity. Solving this issue will significantly increase the competitiveness of both cooling and generating thermoelectric modules and expand the areas of their practical use.

In particular, the use of thermoelectricity for waste heat recovery is important. Almost all technological processes in industry, as well as the production of electrical energy, are associated with the use of fuels, including nuclear, to produce thermal energy. Most of this energy in industry, after the implementation of technological processes, is dissipated into the environment by gaseous or liquid heat carriers.

In heat engines, only 25 – 40 % of thermal energy is converted into mechanical energy. The remaining more than 50 % is given to the environment, which leads to its thermal pollution and disruption of the Earth's heat balance. This thermal power can be converted into electrical energy. The use of thermoelectric recuperators allows to extract from this heat as much electrical energy as all nuclear power plants generate. Thus, thermoelectric recuperators can become an important factor in the overall environmental improvement, and therefore are important for the interests of the human community.

At the same time, the main obstacle to the widespread practical use of thermoelectricity for the recovery of waste heat is the high cost of thermoelectric energy converters, the largest share of which is the cost of thermoelectric material. The cost of thermoelectric energy converters can be reduced by tens of times and approach the required for wide practical applications due to their miniaturization.

However, attempts to create miniature modules encounter the growing influence of contact resistances, which cause a catastrophic decrease in the quality of the modules.

The development and optimization of technologies for creating contact resistances necessary to

meet practical needs is carried out experimentally by studying the influence of various technological factors on the value of contact resistance. The latter is possible only if reliable methods and equipment for measuring contact resistances are available.

The purpose of this work is to analyze existing methods and equipment for determining the values of contact resistances and the possibilities of their use for the study and optimization of "metal – thermoelectric material" structures.

## 1. Methods for measuring electrical contact resistance

### 1.1 Methods used in microelectronics

The most modern methods for measuring electrical contact resistance include the Cox-Streck method, the transmission line method, the Kelvin method, and the boundary probing method. These methods are successfully used in microelectronics [1 – 10].

The authors of [1] proposed contacts made of silver alloy with indium and germanium for *n*-type gallium arsenide and contacts made of silver alloy with indium and zinc for *p*-type gallium arsenide. Depending on the specific resistance of gallium arsenide, the resistance of such contacts is from $10^{-4}$ to $10^{-3}$ Ohm·cm$^2$.

In [2], it is shown that the contact resistance is significantly affected by the technology of cleaning the semiconductor surface. In particular, sputtering cleaning instead of chemical etching significantly reduces the contact resistance.

In [3], various methods for measuring contact resistance and common sources of error are discussed. A number of methods are described, in particular the transmission line method. The results of measuring contact resistances for aluminum-silicon contacts over a wide range of doping levels of the silicon surface layer are presented and discussed.

In [4], a method for separating the contact resistance from the resistance of a bulk sample was proposed. This method is based on measuring the angular dependence of the geometric magnetoresistance. Its efficiency was tested on the Gunn diodes. The error is less than 0.5 % of the total resistance of the device.

In [5], a setup for simultaneous measurement of electrical and thermal contact resistances between metals is described. It allows measuring electrical contact resistance with an error of 0.003 % and thermal contact resistance with an error of 4.4 %. The measurement results for real contacts are in good agreement with theoretical calculations available in the literature.

In [6], a device for measuring electrical contact resistance is described. It can be used to measure contact resistances of the order of 10 μΩ. It uses a current through the contact of about 1 mA, which prevents the formation of an electric arc.

In [7], it is indicated that the measurement of the contact resistance of a "metal-high-resistance semiconductor" is associated with significant difficulties, so that the error can reach five orders of magnitude. It is shown that the transmission line method is inapplicable if the contact resistance is less than $10^{-3}$Ω·cm$^2$.

In [8], a device was developed for measuring the contact resistance between metal wafers as a function of pressure and the corresponding dependence for a pair of copper wafers was investigated.

In [9], the electrical contact resistance between contacts made of *Fe-Cr* alloy and thermoelectric material $Ca_3Co_4O_9$ was measured. The maximum contact resistance obtained was $1.2\cdot10^{-7}$Ohm·cm$^2$.

The essence of the main methods for measuring contact resistance in microelectronics is presented in [10]. Methods for measuring contact resistance are divided into four categories:

1) two-contact two-terminal;
2) multi-contact two-terminal,
3) four-terminal,
4) six-terminal.

None of these methods are applicable to the measurement of surface resistivity $\rho_i$. Instead, the specific contact resistance $\rho_c$ is determined, which is not the actual surface resistance of the metal-semiconductor interface, but it is a practically applicable numerical characteristic that describes the real contact. From this point of view, comparing theory and experiment is quite difficult, since theory cannot accurately predict $\rho_c$, and experimentally it is difficult to accurately measure $\rho_i$. It is often difficult even to unambiguously measure $\rho_c$. We will limit ourselves to discussing experimental techniques.

### 1.1.1 Two-contact two-terminal method

This method is the earliest. Its accuracy is rather questionable and it is rarely used. Its simplest schematic implementation is shown in Fig. 1.

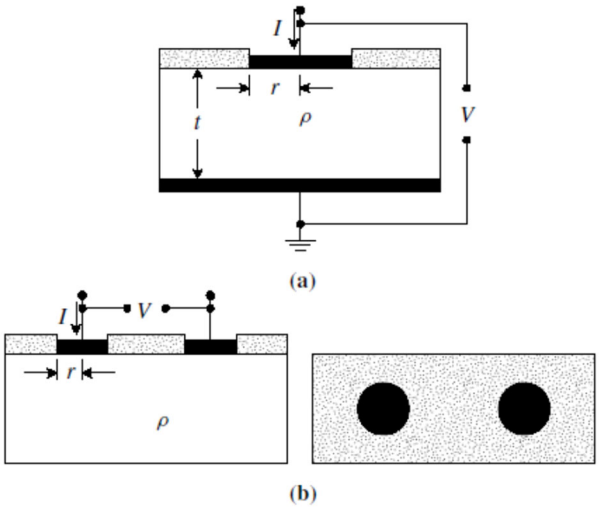


*Fig. 1. Vertical two-terminal structure (a) and surface two-terminal structure (b) for measuring contact resistance [10].*

For a homogeneous semiconductor with resistivity $\rho$ and thickness $t$, the total resistance $R_t = V/I$ measured according to diagram (a) by passing current $I$ through the sample with determination of the voltage $V$ between the contacts is equal to:

$$R_T = R_c + R_{sb} + R_{cb} + R_p . \quad (1)$$

When measuring according to diagram (b), instead of (1), the following relation is used:

$$R_T = 2R_c + 2R_{sb} + 2R_p . \quad (2)$$

In these formulae, $R_c$ – the contact resistance of the upper contact, $R_{sb}$ – the spreading resistance directly under the contact, $R_{cb}$ – the contact resistance of the lower contact, $R_p$ – the resistance of the probe or wire. Typically, the lower contact has a large area, and, therefore, a relatively low associated contact resistance. Therefore, the contact resistance of the lower contact is often neglected. Similarly,

the probe resistance is also assumed to be low.

The spreading resistance of a flat non-penetrating contact of circular shape with radius $r$ on the surface of a semiconductor with resistivity $\rho$ and thickness $t$ is equal to:

$$R_{sp} = \frac{\rho}{2\pi r}\operatorname{arctg}\left(2t/r\right) \tag{3}$$

In the case $2t >> r$ the following relation is valid:

$$R_{sp} = \frac{C\rho}{4r}. \tag{4}$$

In this formula, $C$ is the correction factor, which depends on $\rho, r$ and current distribution. For widely spaced contacts, as in diagram (b), located on a homogeneously doped semi-confined substrate, $C = 1$. If the current flows vertically into the upper contact, as in diagram (a), then the contact resistance is:

$$R_c = \rho_c / A_c = \rho_c / \pi r^2 \tag{5}$$

Relation (1) shows that with low $R_{cb}$ and $R_p$ the contact resistance will be the difference between the total resistance and spreading resistance. But the spreading resistance cannot be measured independently. Therefore, even small errors in the spreading resistance will lead to significant errors in the value of contact resistance. Hence, the two-terminal method works best when $R_{sp} << R_c$, that is, in the case of contacts of small radius.

A modification of the two-terminal method is the use of upper contacts of different diameters. Therefore, from the known values of $R_T$ it is possible to determine and plot the dependence of $R_c$ on $1/A_c$ and to determine $\rho_c$ by the slope of the corresponding plot. Alternatively, it is possible to plot the total resistance as a function of $1/r$. Using contacts of different diameters, from the shape of the curve it is possible to determine whether the data are anomalous.

The two-terminal method is most often implemented using the horizontal (surface) structure shown in Fig. 2.

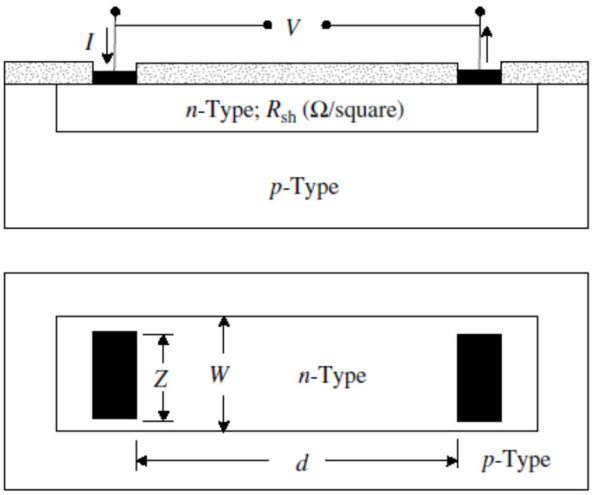


*Fig. 2. Surface (horizontal) structure for implementing the two-terminal method of measuring contact resistance in section and plan view [10].*

It differs from the structure shown in Fig. 1*b* in that the current is limited by an n-type island. The test structure consists of two contacts separated by a distance. In order to limit the current, the area in which the contacts are located must be isolated from the rest of the substrate by doping or diffusion so that, for example, an n-type region is formed in the p-substrate by planar technology or by chemical etching of the region surrounding the island, leaving a "mesa". The island in this example has a width $W$ and ideally the contacts should have the same width. However, this is difficult to do, so the width of the contacts $Z$ usually differs from $W$ . In this case, the analysis is complicated by the horizontal flow of current, the increase in its density near the contacts and the geometry of the sample. For the geometry shown in Fig. 2, the total resistance is:

$$R_T = R_{sh} d / W + R_d + R_w + 2R_c \,. \tag{6}$$

In this formula, $R_{sh}$ – the surface resistance of the n-layer, $R_d$ – the correction for the current change near the contact, $R_w$ – the correction for the contact width, if $Z < W$ . The expressions for the resistances appearing in formula (6), are given in [10].

For the case of many contacts, the so-called "*contact chain method*" is used, the diagram of which is shown in Fig. 3.

In this diagram, the total resistance between each pair of contacts is defined as the sum of the semiconductor resistance, the contact resistance, and the metal resistance. The semiconductor resistance is calculated from the known surface resistance and the geometry of the circuit. Subtracting the semiconductor resistance from the total resistance gives the total contact resistance. The contact resistance of each contact is obtained by dividing the result by twice the number of contacts.

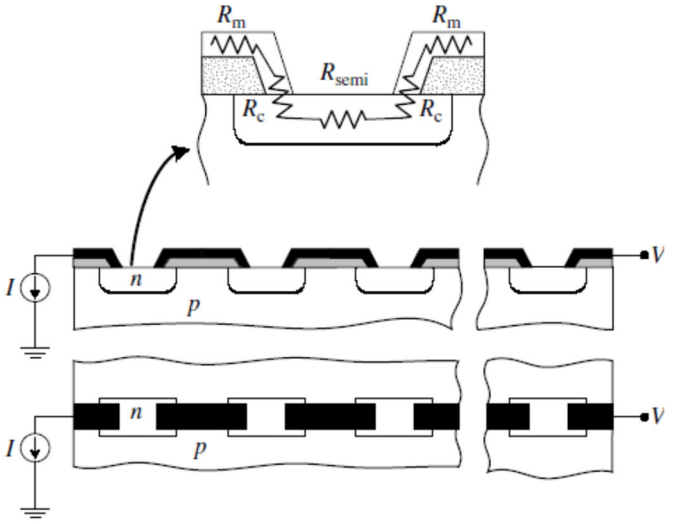


*Fig. 3. Diagram of the "contact chain" method and images of the test structure in plan and section [10].*

In this diagram, the total resistance between each pair of contacts is defined as the sum of the semiconductor resistance, the contact resistance, and the metal resistance. The semiconductor resistance is calculated from the known surface resistance and the geometry of the circuit. Subtracting the semiconductor resistance from the total resistance gives the total contact resistance. The contact resistance of each contact is obtained by dividing the result by twice the number of contacts. For a contact chain consisting of *N* islands and *2N* contacts of width *W*, separated by a distance, and neglecting the metal resistance, the following relation is valid:

$$R_T = \frac{NR_{sh}d}{W} + 2NR_c . \quad (7)$$

This method is too rough for accurate assessment of contact resistance. However, it is often used for process control.

### 1.1.2 Multi-contact two-terminal method

The diagram of the method is shown in Fig. 4, the test structure for its implementation is shown in Fig. 5.

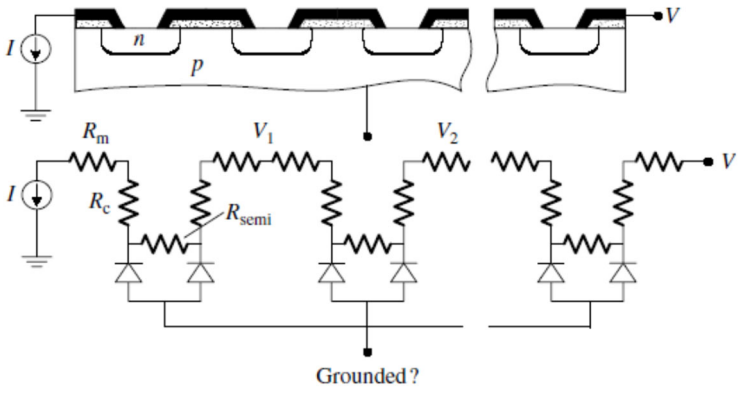


*Fig. 4. Diagram of multi-contact-two-terminal method [10].*

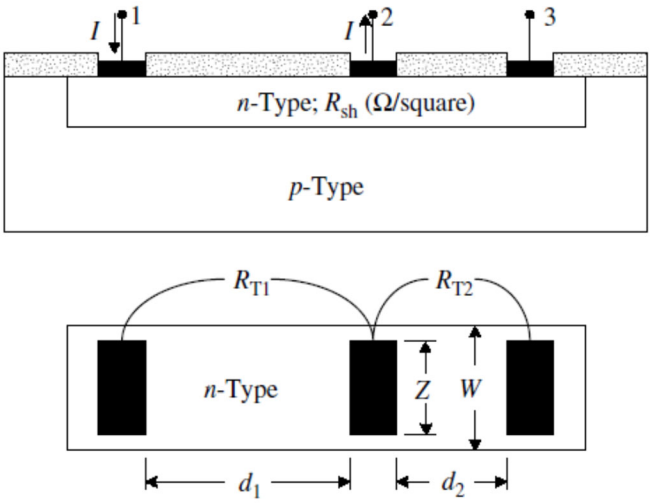


*Fig. 5. Test structure for the implementation of multi-contact two-terminal method [10].*

This method was developed to overcome the shortcomings of the two-contact two-terminal method. It creates three identical contacts to the semiconductor, separated by distances $d_1$ and $d_2$. Assuming that the contact resistances of all three contacts are the same, the total resistance can be determined as follows:

$$R_{Ti} = \frac{R_{sh}d_i}{W} + 2R_c . \quad (8)$$

Therefore, substituting $i = 1,2$ and solving the corresponding system of equations for $R_c$, we obtain:

$$R_c = \frac{R_{T_2} d_1 - R_{T_1} d_2}{2(d_1 - d_2)}. \quad (9)$$

This test structure does not have the uncertainties of a simple two-terminal structure, since it is not necessary to know the volume and surface resistance of the semiconductor. The assumption that the contact resistances of all three contacts are the same is somewhat questionable, but it is justified if the sample is not very large. The contact resistance is determined by the difference of two large values. This can be difficult, especially for contacts with low resistance. The determination of distances $d_1$ and $d_2$ is an additional source of inaccuracies. Incidentally, this method can also give a negative value for the contact resistance.

The structure in Fig. 5 allows only the contact resistance to be determined. The specific contact resistance cannot be directly determined from two resistance measurements. The determination requires a more detailed assessment of the current distribution in and outside the horizontal contact region. Early studies of the two-dimensional current distribution in diffusion resistors by Kennedy and Marley showed that there is current concentration at the contacts. Analysis under the assumption of zero contact resistance showed that only a portion of the contact length is active in the transfer of current from the semiconductor to the metal and vice versa. This portion was found to be approximately equal to the thickness of the diffusion semiconductor layer.

Let us now consider some test structures for measuring contact resistance, which are shown in Fig. 6.

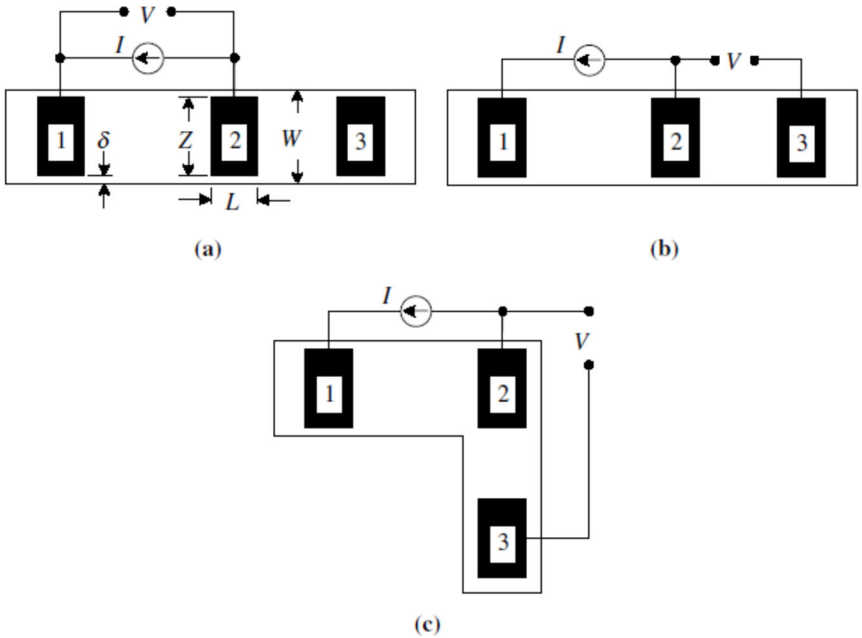


*Fig. 6. Test structures for measuring contact resistance: a) conventional; b) for measuring contact resistance of the end contact; c) Kelvin test structure of the "cross bridge" type [10].*

In all of these structures, the current flows from contact 1 to contact 2. In the test structure for implementing the line transmission method shown in Fig. 6a, which is also called the *structure for measuring the front contact resistance*, the voltage is measured between the same contacts as the current. In the test structure shown in Fig. 6b, the voltage is measured between contacts 2 and 3. In the test structure for measuring contact resistance by the Kelvin method (Fig. 6c), which is considered to be one

of the most accurate, the voltage is measured at right angles to the current.

Let us now consider the expressions for the resistances in these circuits. In diagram 6a, the resistance of the front contact is:

$$R_{cf} = V/I = \frac{\sqrt{R_{sh}\rho_c}}{Z}\operatorname{cth}\left(L/L_T\right) = \frac{\rho_c}{L_T Z}\operatorname{cth}\left(L/L_T\right), \tag{10}$$

if $Z = W$ . If the sample is wider than the contact, then formula (10) is only approximate.

It is usually considered that $R_{cf} = R_c$. The general formula (10) allows for a number of simplifications.

For instance, if $L < 0.5L_T$ ,then $\operatorname{cth}\left(L/L_T\right) \approx L_T/L$ , hence,

$$R_c = \frac{\rho_c}{LZ}. \tag{11}$$

If $L > 1.5L_T$ , then $\operatorname{cth}\left(L/L_T\right) \approx 1$ , hence

$$R_c = \frac{\rho_c}{L_T Z}. \tag{12}$$

In the first case, the true contact area coincides with its effective area. However, in the second case, the effective contact area is smaller than the true one. This leads to a number of important consequences. For example, consider a structure with a surface resistance of 20 Ohm/sq and a contact resistance of $10^{-7}$ Ohm·cm$^2$. In this case, the "characteristic transmission length" is 0.7 μm. For a contact 10 μm long and 50 μm wide, the true contact area is $5\cdot10^{-6}$ cm$^2$. However, the effective contact area is only $3.5\cdot10^{-7}$ cm$^2$.

Thus, the current density in the contact becomes 14 times higher than in the case when the entire contact is active. This increase in the current density in the contact causes problems associated with contact degradation. The reduced contact area burns out in extreme cases and the active area of the contact gradually shifts until it is completely destroyed.

The contact model shown in Fig. 6 may be oversimplified in the case of a series of contacts. For example, in the case of alloy contacts, the contact region consists of the metal, the alloy region, and an adjacent semiconductor layer. Contacts obtained by sputtering a metal onto a thin layer of a narrow-gap or wide-gap semiconductor also fall into this category. This requires a more complex transmission line model, and a symmetrical layer model. Then the corresponding equations become significantly more complicated.

When voltage is measured between contacts 2 and 3, while current flows between contacts 1 and 2 (Fig. 6b), the corresponding contact resistance is:

$$R_{ce} = V/I = \frac{\sqrt{R_{sh}\rho_c}}{Z\operatorname{sh}\left(L/L_T\right)} = \frac{\rho_c}{L_T Z\operatorname{sh}\left(L/L_T\right)}. \tag{13}$$

The measurement of contact end resistance can be used to determine the specific contact resistance by measuring $R_{ce}$ and iterating the relation (13). In the case of short contacts, $R_{ce}$ is sensitive to changes in the contact length, so the error in the determination of $L$ limits the accuracy of the method. For long contacts $R_{ce}$ becomes small and the accuracy of its determination is limited by the error of the

instruments. This can be seen by constructing the relation

$$\frac{R_{ce}}{R_{cf}} = \frac{1}{\mathrm{ch}\left(L/L_T\right)}, \tag{14}$$

which becomes very small for $L >> L_T$.

For the case of the Kelvin test structure (Fig. 6c), contact 3 is located away from contact line 1-2. Therefore, the measured voltage is the average value of the potential along the length of the contact, i.e.:

$$V = L^{-1}\int_0^L V\left(x\right)dx, \tag{15}$$

Integrating, we get:

$$R_c = V\Big/ I = \frac{\rho_c}{LZ}, \tag{16}$$

Equation (13) assumes that the width of contact Z is equal to the width of the semiconductor layer. This is rarely realized in practice. Usually $Z < W$. Experiments at Z=5 μm and W in the range from 10 to 60 μm show that the method of measuring the resistance of the end of the contact gives a falsely large contact resistance. The error increases if $\rho_c$ decreases. Or if $R_{sh}$ increases.

The source of error is the potential difference between the front and rear edges of the contact, as a result of which the current can flow around the edges of the contacts. The measured resistance is proportional to the surface resistance and is insensitive to the contact resistance for large $\delta$. For the validity of a simple one-dimensional theory, the test structure must satisfy the conditions $L \le L_T, Z >> L$ and $\delta << Z$. The "one-dimensional" analysis is not suitable if the specified conditions are not satisfied. However, an accurate determination of $\rho_c$ is possible if the numerical calculations (simulation) are properly adjusted to the measurement data.

The problem associated with $W \neq Z$ can be prevented by using a circular (annular) test structure consisting of a leading inner region of radius $L$, a gap of width *d*, and an inner contact region. The leading regions are usually metallic, and the gap width varies from a few microns to tens of microns. The structure is shown in Fig. 7.

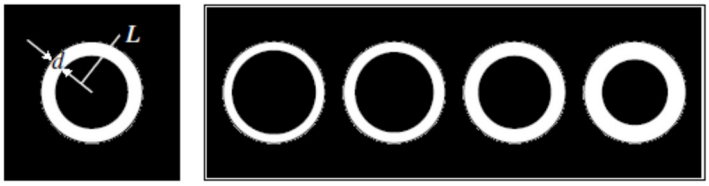


*Fig. 7. A separate element of the circular structure (a) and the structure as a whole (b). Black areas – metal [10].*

If the surface resistances of the semiconductor layer under the metal and in the gap are the same, then the following expression is valid for the total resistance between the external and internal contacts:

$$R_T = \frac{R_{sh}}{2\pi}\left[\frac{L_T}{L}\frac{I_0\left(L/L_T\right)}{I_1\left(L/L_T\right)} + \frac{L_T}{L+d}\frac{K_0\left(L/L_T\right)}{K_1\left(L/L_T\right)} + \ln\left(1+\frac{d}{L}\right)\right] \tag{17}$$

In these formulae, $I_m(z)$ and $K_m(z)-$ Bessel functions of imaginary argument and modified Bessel functions of corresponding indices.

For the circular transmission line test structure shown in Fig. 7, under the condition $L >> 4L_T$ the ratios $I_0/I_1$ and $K_0/K_1$ tend to unity, and, hence, expression (17) is simplified:

$$R_T = \frac{R_{sh}}{2\pi}\left[\frac{L_T}{L} + \frac{L_T}{L+d} + \ln\left(1+\frac{d}{L}\right)\right] \tag{18}$$

If, in addition, $L >> d$ , the expression (25) takes on the form:

$$R_T = \frac{R_{sh}C}{2\pi L}\left(d + 2L_T\right), \tag{19}$$

where

$$C = \frac{L}{d}\ln\left(1+\frac{d}{L}\right) \tag{20}$$

For practical radii of about 200 μm and gap widths in the range of 5 – 50 μm, a correction factor $d/L$ is needed to compensate for the difference between the results of the linear transmission line method and the consideration according to the circular diagram in order to obtain a linear smoothing of the experimental data. Without the correction factor, the specific contact resistance is underestimated. Similar to the case of the linear structure, the corrected data allow the characteristic transmission length and hence the specific contact resistance to be estimated.

The circular test structure has one significant advantage. It is that there is no need to isolate the semiconductor layer during measurements, since current can only flow from the centre contact to the surrounding contact. In a linear test structure, for the transmission line method, current can flow from contact to contact through the area outside the test structure, if it is not isolated. The circular test structure with four metal contacts is very similar to the Kelvin cross-bridge resistor discussed earlier (see Fig. 6 *c*).

Equations (10) and (13) were obtained on the assumption that $\rho_c > 0.2R_{sh}t^2$ , where $t$ – layer thickness. For $R_{sh} = 20\,\text{Ohm/sq}$ and $t = 1\,\mu\text{m}$ this condition leads to inequality $\rho_c > 4\times10^{-8}\,\text{Ohm·cm}^2$. The transmission line method must be modified if this condition is not satisfied, which is verified by experiments and simulations. However, most contact resistances are much larger, so the transmission line method is suitable.

The difficulty in deciding where to measure the voltage in the diagrams in Fig. 6 led to the emergence of the test structure shown in Fig. 8 and the corresponding "transmission length method" proposed by Shockley.

The structure for implementing this method is very similar to the structure shown in Fig. 2, but contains more than 3 contacts. The two contacts at the ends of the test structure serve to allow current to enter and exit the original "ladder" structure, and the voltage is measured between one of the large contacts and each of the successive narrow contacts as in Fig. 8a. Later, the structure shown in Fig. 8b was proposed, in which the voltage is measured between adjacent contacts.

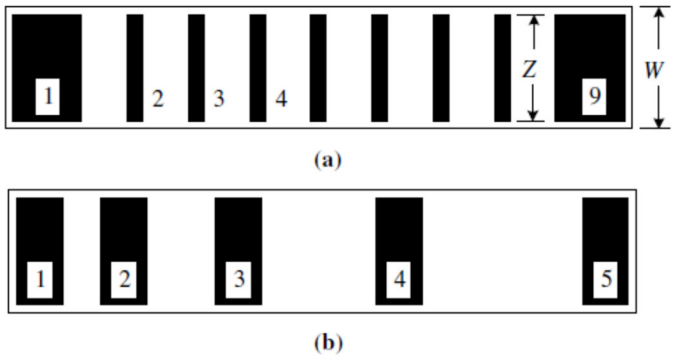


*Fig. 8. Test structures for implementing the "transmission length method" [10].*

The structure in Fig. 8b has certain advantages over the structure shown in Fig. 8a. If the voltage in the "ladder" structure is measured, for example, between contacts 1 and 4, then there is a current disturbance due to the presence of contacts 2 and 3. The influence of contacts 2 and 3 depends on the "characteristic transmission length $L_T$ and contact length $L$. If $L << L_T$, the current does not penetrate noticeably into contact 2 and, therefore, contacts 2 and 3 do not affect the measurement results. If, however, $L >> L_T$ , current flows in the metal and the contact can be imagined as two contacts of length $L_T$, which are located in a metal conductor Shunting the current by metal strips obviously affects the measured voltage value, and therefore the resistance. From this point of view, the structure in Fig. 8b is better, since it has a "pure" semiconductor between every two contacts (in the sense that the corresponding gap is sufficient for the current not to penetrate into the adjacent contact).

For contacts that satisfy the condition $L \geq 1.5L_T$, the following expression is valid for the measured resistance of the front contact:

$$R_T = R_{sh} d \Big/ Z + 2R_c \approx \frac{R_{sh}}{Z}\left(d + 2L_T\right), \tag{21}$$

where we used the same approximation that leads from formula (10) to formula (12).

The dependence of the measured contact resistance on $d$ is shown in Fig. 9.

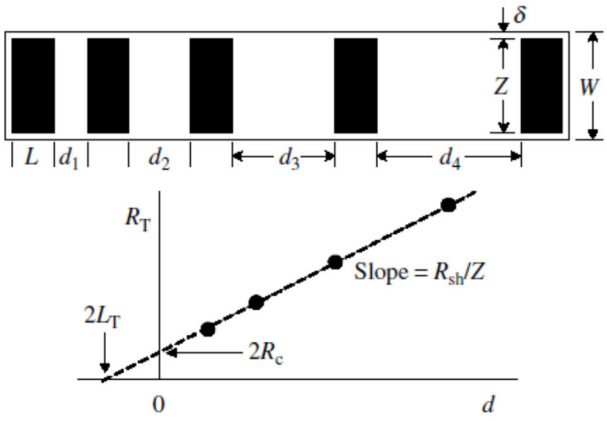


*Fig. 9. Test structure for implementing the "characteristic transmission length" method and the dependence of the measured total resistance on d [10].*

The slope of the line $\Delta d/d = R_{sh}/Z$ allows one to determine the surface resistance $R_{sh}$, if the contact width $Z$ is known from independent measurements. The intersection of the plot with the vertical axis, given $d = 0$ allows one to determine the total contact resistance. The intersection of the plot with the horizontal axis, given $R_T = 0$ allows one to determine the "characteristic transmission length", and, hence, the specific contact resistance, since the surface resistance $R_{sh}$ is known from the slope of the line. Thus, this method gives a complete characterization of the contact, including the surface resistance of the semiconductor layer, the total contact resistance and the specific contact resistance.

This method is usually used to measure contact resistance, but it has its own problems. For example, the point of intersection of the plot with the horizontal axis is not always clearly defined, which leads to an incorrect value of $L_T$, and, hence, of $\rho_c$. However, a more serious problem is the uncertainty of the surface resistance of the semiconductor layer under the contacts. Eq. (21) is valid assuming the same surface resistance of the semiconductor layer under the contacts and between them. However, these resistances can differ from each other due to effects associated with the formation of the contact. This is true for alloy and "silicide" contacts, when the semiconductor region under the contact is modified in the process of obtaining the contact. In this case, the following expressions are valid for the resistance of the front edge of the contact and the total resistance:

$$R_{cf} = \frac{\rho_c}{L_{Tk} Z} \operatorname{cth}\left(L/L_{Tk}\right). \tag{22}$$

$$R_T = \frac{R_{sh} d}{Z} + 2R_k \approx \frac{R_{sh} d}{Z} + \frac{2R_{sk} L_{Tk}}{Z} = \frac{R_{sh}}{Z}\left[d + 2\left(R_{sk}/R_{sh}\right)L_{Tk}\right]. \tag{23}$$

In formula (23), $R_{sk}$ – the modified surface resistance of semiconductor layer under the contact, $L_{Tk} = \sqrt{\rho_c / R_{sk}}$. The slope of the dependence of $R_T$ on $d$, as before, is determined by $R_{sh}/Z$ and the point of intersection with the vertical axis gives $2R_c$. However, the point of intersection with the horizontal axis gives $2\left(R_{sk}/R_{sh}\right)L_{Tk}$, therefore, the specific contact resistance is now impossible to determine, since $R_{sk}$ is unknown. Nevertheless, determining $R_{cf}$ by the method of "characteristic transmission length" and $R_{ce}$ by "contact end resistance" method, where:

$$R_{ce} = \frac{\sqrt{R_{sk}\rho_c}}{Z \operatorname{sh}\left(L/L_{Tk}\right)} = \frac{\rho_c}{Z L_{Tk} \operatorname{sh}\left(L/L_{Tk}\right)}; \frac{R_{ce}}{R_{cf}} = \frac{1}{\operatorname{ch}\left(L/L_{Tk}\right)}. \tag{24}$$

one can determine $L_{Tk}$ and $\rho_c$. Thus, it becomes possible to determine the contact resistance and specific contact resistance in addition to the resistance of the surface layer of the semiconductor between and under the contacts. It is also possible to separate $R_{sh}$ from $R_{sk}$ by etching the semiconductor between the contacts.

The determination of electrical parameters of contacts by the transmission line method is based on the assumption that the electrical and geometric parameters of the contacts are uniform across the sample cross-section. However, these parameters are usually scattered across the chip (wafer). Statistical simulation shows that the usual data acquisition procedure can lead to errors even if there are no errors in the measurement of electrical and geometric parameters. For the case of short contacts ($L < L_T$) $\rho_c$ can be determined, despite the scattering of other parameters, whereas the error in the determination of

$R_{sk}$ and $R_{sh}$ occurs only when $\rho_c$ is scattered across the wafer. In the case of long contacts, the found values of $\rho_c$ and $R_{sk}$ have an error when there is a measurement error. The best results are obtained when $L \geq 2L_T$. If a wafer has a non-uniform distribution of electrical parameters with fluctuations of 10-30%, then the error in the determination of $\rho_c$ and $R_{sk}$ can reach 100-1000%. The use of more than one test structure makes it possible to reduce the errors.

### 1.1.3 Four-terminal method for measuring contact resistance

The methods of measuring contact resistance considered earlier require knowledge of the value of the specific or surface resistance of the semiconductor layer. However, such methods of measuring $R_c$ and $\rho_c$ that would minimize the contribution of the resistance of the semiconductor layer or eliminate it altogether are preferable. The measurement method that is most suitable for this purpose is the Kelvin method, which is based on the Kelvin structure with "crossing bridges". This test structure was first used in 1972, but it was not until the early 1980s that it was seriously evaluated. In principle, this method allows the actual contact resistance to be measured, uncorrupted by the resistances of the semiconductor and metal. The measurement principle is illustrated in Fig. 10.

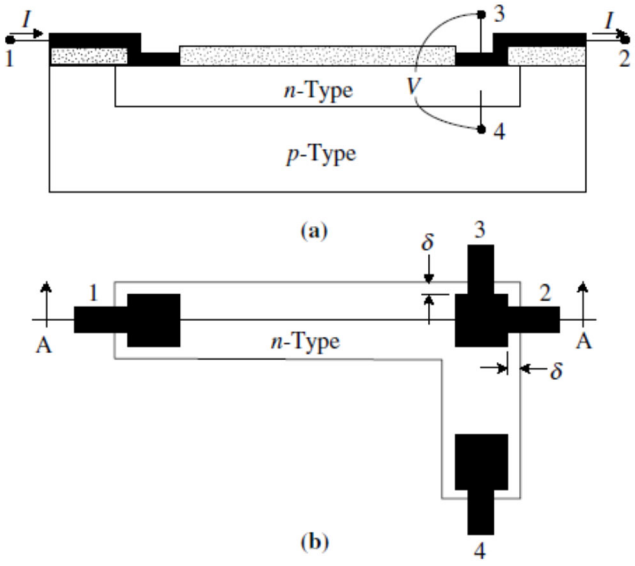


*Fig. 10. Kelvin test structure in section A-A and in plan [10].*

Current is passed between contacts 1 and 2, and voltage is measured between contacts 3 and 4. There are three voltage jumps between contacts 1 and 2. The first is between wafer 1 and the semiconductor layer, the second is along the surface of the semiconductor layer, and the third is between the n-layer and wafer 2/3. The high input impedance of the voltmeter causes very little current between contacts 3 and 4. Therefore, the potential at contact 4 is the same as the potential of the n-region directly below wafer 2/3, as illustrated in Fig. 10a by placing point 4 directly below contact 3. Thus, the measured voltage $V_{34}$ is entirely due to the jump at the metal-semiconductor contact. The contact resistance is then:

$$R_c = V_{34}/I\,, \tag{25}$$

therefore, the specific contact resistance is equal to

$$\rho_c = R_c A_c , \tag{26}$$

where $A_c$ – contact area.

This method is considered to be the most accurate, but the relation (26) does not always agree with the experimental data. The specific contact resistance calculated in accordance with (26) is an imaginary contact resistance distorted by the surface current concentration in the case when the contact windows are smaller than the diffusion gap, denoted as $\delta$ in Fig. 10. The curvature of the contact window to the diffusion layer and the horizontal diffusion of the dopant are taken into account under the condition $\delta > 0$. The ideal case $\delta = 0$ is illustrated in Fig. 11a. In a real contact, part of the current, shown by the arrows in Fig. 11b, flows around the metal contact. In the ideal case, when $\delta = 0$, the potential jump $V_{34} = IR_c$.

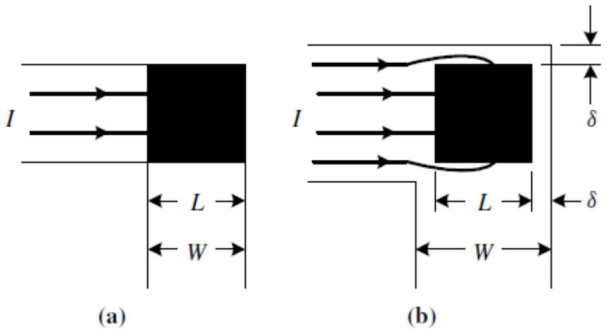


*Fig. 11. Kelvin test structures: a) ideal; b) taking into account horizontal current flow around and under the contact [10].*

In the case of $\delta \neq 0$ the horizontal current creates an additional voltage jump, which is included in $V_{34}$ and leads to a higher value of the measured voltage. According to relation (26) $\rho_c$ increases if the true contact area is used. The thus obtained value of $\rho_c$ is known as the imaginary specific contact resistance. The error introduced by the above geometric factor is greater for lower values of $\rho_c$, and (or) higher $R_{sh}$ and less for higher values of $\rho_c$, and (or) lower values of $R_{sh}$. The vertical voltage jump in the semiconductor, normal to the contact plane, is usually not taken into account, although it also introduces a correction.

### 1.1.4 Six-terminal method for measuring contact resistance

The diagram of the six-terminal method for measuring contact resistance is shown in Fig. 12.

The appropriate test structure is a four-terminal Kelvin test structure with two additional contacts to provide additional capabilities not available in the conventional Kelvin structure. This structure allows the determination of contact resistance, contact resistivity, contact start resistance, contact end resistance and semiconductor surface resistance. In the case of a conventional Kelvin structure, current is pumped between contacts 1 and 3 and voltage is measured between contacts 2 and 4. Then $R_c = V_{24}/I$, and, hence, $\rho_c = R_c/A_c$. The problems arising from consideration within the framework of a two-dimensional model remain for the six-terminal structure.

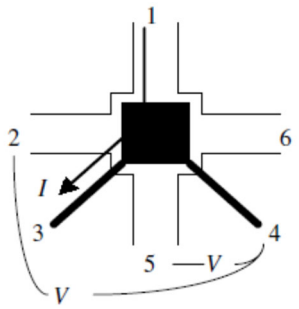


*Fig. 12. The diagram of the six-terminal method for measuring contact resistance, allowing simultaneous determination of* $R_c, R_{ce}, R_{cf}, R_{sk}$ *[10].*

To measure the resistance of the contact end in conformity with relation $R_{ce} = V_{54}/I$ current is passed between contacts 1 and 3, and voltage is measured between contacts 5 and 4. Given the contact resistance and the specific contact resistance known earlier, the surface resistance of the semiconductor under the contact can be determined through the resistances $R_{ce}$ and $R_{cf}$ from relations (10) and (24).

## 2. Measurement of electrical contact resistance in thermoelectricity

It is known that the influence of contact resistance on the efficiency of a thermoelectric device increases as it is miniaturized. Popular methods for measuring contact resistance in microelectronics are suitable for thin films, but cannot be directly transferred to the case of bulk TE materials. The authors of [11] propose a method for measuring contact resistance for the case of bulk TE materials by manufacturing and testing stacks of TE material wafers covered with metal using a traditional technological process for manufacturing thermoelectric devices. The thermoelectric figure of merit *Z* of the stack is used to isolate the contact resistance and reduce the sensitivity of the results to the resistance of the TE material. The advantage of this technique is that it reflects the real technological process of manufacturing TE devices and copies structures similar to real TE devices with maximum accuracy. The smallest values of the electrical contact resistance that were measured by this method at 300K were $1.1 \cdot 10^{-6}$ and $1.3 \cdot 10^{-6}$ Ω·cm$^2$ for n- and p-type materials, respectively. The measurement error for each sample is from 10 to 20%, which is acceptable when measuring contact resistances of the order of $10^{-6}$ Ω·cm$^2$.

The improved method for measuring contact resistance by thermoelectric figure of merit in cooling mode, described in [11], is as follows. It is known that the maximum cooling capacity of a thermocouple is defined as:

$$Q_{\max} = \frac{1}{2L}\left[\frac{\alpha^2 T_c^2}{(2\rho + 4\rho_c/L)} - k\Delta T\right]. \qquad (27)$$

In this formula, $L$ – the length of the thermoelectric leg, $\alpha$ – the Seebeck coefficient, $T_c$ – the cold junction temperature, $\rho$ – the resistivity of the semiconductor, $\rho_c$ – the contact resistance, $k$ – the thermal conductivity, $\Delta T$ – the temperature difference. The influence of contact resistance on the performance of the refrigerator is considered to be significant when the leg lengths are 200 μm or less. Specific contact resistance is difficult to measure when it is less than $10^{-6}$ Ohm·cm$^2$. In order to

quantitatively evaluate the contact resistance on $Bi_2Te_3$, a stack structure simulating a real device was developed and applied. The technological process of manufacturing a stack-like structure was similar to that of a real thermoelectric cooler, so that the contact resistance was well reproduced. The stack-like structure was made of several wafers of thermoelectric material. The wafers were soldered together in a single process and cut into "cubes", as shown in Fig. 13.

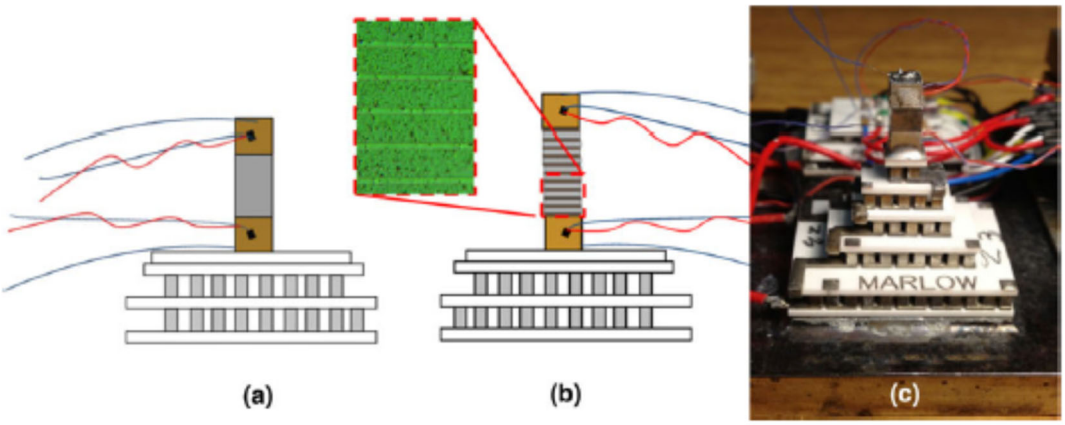


*Fig. 13. Method of measuring contact resistance by the figure of merit [11]: a) – control sample; b) – stack-shaped structure; c) – general view of the measuring setup.*

The process of sample manufacturing is shown in Fig. 14.

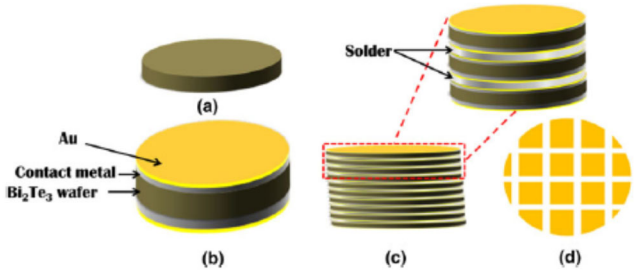


*Fig. 14. Sequential stages of sample manufacturing process [11]: a) – single wafer after lapping; b) – wafer after etching and deposition of contact layer; c) – finished stack of 10 wafers after soldering; d) – stack of wafers cut into cubes.*

The samples were manufactured as follows. First, the wafers were ground to a thickness of 250 µm. The composition of the TE materials was approximately as follows: *n*-type – $(Bi_2Te_3)_{0.9}(Bi_2Se_3)_{0.1}$, *p*-type – $(Sb_2Te_3)_{0.75\text{-}0.80}(Bi_2Te_3)_{0.2\text{-}0.25}$. After lapping, the wafers were subjected to surface treatment and metal deposition. Gold was deposited on the surface of the metal contacts to prevent surface oxidation and to ensure wetting with solder. After metal deposition, the wafers were placed in a special clamping device. Solder was applied manually using ceramic strips to ensure a flat and smooth surface. Then one wafer was placed on top of the other and carefully pressed. Excess solder was removed. The process continued until a stack of 10 plates was formed. Tin-antimony solder was used to form the stacks. After that, the finished stacks were inserted into the furnace. The uniformity of the solder and the reproducibility of the technological process of forming the stacks were checked by numerous tests. After that, the finished stacks were cut into squares with a side of 3.8 mm. Copper pads with conductive wires were soldered to the end of each stack. In order to produce control samples with the same thermoelectric properties, solid wafers 2.5 mm high were made from an adjacent piece of each

corresponding ingot. The control samples and stacks were placed in a figure of merit measurement setup and the thermoelectric properties were measured in the temperature range from 260 to 340 K.

The thermoelectric figure of merit was measured by the modified Harman method. The Seebeck coefficient $\alpha$ and the resistivity $\rho$ were also measured. The measuring setup was calibrated to ensure a measurement error of no more than 2 %.

The essence of the measurement method is as follows. The figure of merit of the control sample is:

$$Z_{\text{control}} = \frac{\alpha^2 L}{k\left(\rho L + 2\rho_c\right)}. \tag{28}$$

At the same time, the figure of merit of the device in the form of a stack is equal to:

$$Z_{\text{stack}} = \frac{\alpha^2}{k\left(\rho + 2\rho_c / t\right)}. \tag{29}$$

It is clear that due to the small average distance $t$ between the wafers in the stack the difference between $Z_{\text{control}}$ and $Z_{\text{stack}}$ can be made quite noticeable and, therefore, the accuracy of determining the specific contact resistance $\rho_c$ is significantly increased. Dividing (28) by (29) and solving the resulting equation for $\rho_c$, we obtain:

$$\rho_c = \frac{\rho L}{2}\left(\frac{Z_{\text{ratio}} - 1}{Lt^{-1} - Z_{\text{ratio}}}\right). \tag{30}$$

In this formula,

$$Z_{\text{ratio}} = Z_{\text{control}} / Z_{\text{stack}}. \tag{31}$$

To improve accuracy, it is necessary to make several control samples and stacks and take the average values of the corresponding figures of merit measured by the modified Harman method.

The authors of [11] used averaging over 5 stacks and 3 control samples. Thus, in each experiment, averaging was performed over more than 100 interfaces. Due to the main contribution of contact resistance to the change in the figure of merit of the stack, the temperature effect of the solder layers was not taken into account in the calculations. The results of the contact resistance calculations show that when using the standard process 1, the contact resistance is on average $3.6 \cdot 10^{-6}$ Ω·cm$^2$ and $2.7 \cdot 10^{-6}$ Ω·cm$^2$ for *p*- and *n*-type materials, respectively. For process 1, the accuracy of the contact resistance determination is consistent with the models and the results of measuring the cooling capacity of real coolers with leg lengths of 0.45 mm. Initial results for process 2 showed a significant decrease in the contact resistance. Namely, the contact resistances for *p*- and *n*-type materials were $1.1 \cdot 10^{-6}$ Ω·cm$^2$ and $1.3 \cdot 10^{-6}$ Ω·cm$^2$.

The maximum uncertainty in the contact resistance values does not exceed 20 %, which is good enough for determining contact resistances of the order of $10^{-6}$ Ω·cm$^2$. As the contact resistance decreases, the calculated value of $\rho_c$ becomes more sensitive to variations in the figure of merit of the samples. Therefore, to measure contact resistances within $5 \cdot 10^{-7}$ Ω·cm$^2$, the samples should be pre-tested for a decrease in the standard deviation of the measured figure of merit values. One of the many advantages of this method is the ability to determine contact resistance over a wide temperature range, and Table 1 shows the decrease in contact resistance with decreasing temperature, which clearly reflects the temperature dependence of volume resistances in accordance with "narrowing effects".

## Conclusions

1. The most accurate method for measuring electrical contact resistance is the Kelvin method in its six-terminal modification. This method is successfully used in microelectronics. There is no information in the literature about its application in thermoelectricity.
2. The only known method for measuring the contact resistance of soldered metal contacts to a thermoelectric material is a modified method based on measuring the figure of merit of a stack of TEM wafers with many contacts. This method needs improvement to reduce the error in measuring the contact resistance, which is 20%.

## References

1. Cox R.H., Strack H. (1969). *Sol. St. Electron*., 12, 89.
2. Heime K., Konig U., Kohn E., Wortmann A. (1974). *Sol. St. Electron*., 17, 835.
3. Berger H.H. J. (1972). Electrochem. Soc., 119, 507.
4. Gutai L., Mojres T. Appl.Phys. Lett. (1975). 26, 325.
5. Misra P., Nagaraju J. (2004). Test facility for simultaneous measurement of electrical and thermal contact resistance. *Rev. Sci. Instr*., Aug.2004, doi 10.1063/1.1775316
6. Maheshappa N.D., Nagaraju J., Krishna Murthy N.V. (1998). A facility for electrical resistance contact measurement. *Rev. Sci. Instr*., Mar.1998, doi 10.1063/1.1148810
7. Deepak, Krishna H. (2007). Measurement of small specific contact resistance of metals with resistive semiconductors. *J. El. Mat*., 36(5), 598-605, doi 10.1007/s11664-007-0091-y
8. Maheshappa H.D., Nagaraju J., Krishna Murthy M.V. (1998). A facility for electrical resistance contact measurement. *Rev. Sci. Instr*., Mar. doi 10.1063/1.1148810
9. Holgate T.C., Han L., Wu NY, Bojesen E.D., Cristensen M., Iversen Bo.B., Nong N.V., Pryds N. *Characterization of the interface between Fe-Cr alloy and the p-type thermoelectric oxide* $Ca_3Co_4O_9$.
10. Schroder D.K. (2006). *Semiconductor material and device characterization.* IEEE press. A John Wiley & Sons, Inc. Publication.
11. Gupta R.P., McCarty R., Sharp J. (2013). Practical contact resistance measurement method for bulk $Bi_2Te_3$ based thermoelectric devices. *J. El. Mat*.

Submitted 12.01.2022.

**Вихор Л.М.,** *доктор фіз.-мат. наук* [1]
**Горський П.В.,** *доктор фіз.-мат. наук* [1,2]
**Лисько В.В.,** *канд. фіз.-мат. наук* [1,2]

[1] Інститут термоелектрики НАН та МОН України,
вул. Науки, 1, Чернівці, 58029, Україна;
[2] Чернівецький національний університет імені Юрія Федьковича,
вул. Коцюбинського 2, Чернівці, 58012, Україна
*e-mail: anatych@gmail.com*

## МЕТОДИ ВИМІРЮВАННЯ КОНТАКТНИХ ОПОРІВ СТРУКТУР «МЕТАЛ – ТЕРМОЕЛЕКТРИЧНИЙ МАТЕРІАЛ» (ЧАСТИНА 1)

*Наведено огляд існуючих методів вимірювання електричного контактного опору. Проведено аналіз їх точності, переваг та недоліків, а також можливостей використання у термоелектриці для дослідження та оптимізації структур «метал – термоелектричний матеріал». Бібл. 11, рис. 14.*

**Ключові слова:** електричний контактний опір, вимірювання, точність, термоелектричні перетворювачі енергії.

## Література

1. Cox R.H., Strack H. (1969). *Sol. St. Electron*., 12, 89.
2. Heime K., Konig U., Kohn E., Wortmann A. (1974). *Sol. St. Electron*., 17, 835.
3. Berger H.H. J. (1972). Electrochem. Soc., 119, 507.
4. Gutai L., Mojres T. Appl.Phys. Lett. (1975). 26, 325.
5. Misra P., Nagaraju J. (2004). Test facility for simultaneous measurement of electrical and thermal contact resistance. *Rev. Sci. Instr*., Aug.2004, doi 10.1063/1.1775316
6. Maheshappa N.D., Nagaraju J., Krishna Murthy N.V. (1998). A facility for electrical resistance contact measurement. *Rev. Sci. Instr*., Mar.1998, doi 10.1063/1.1148810
7. Deepak, Krishna H. (2007). Measurement of small specific contact resistance of metals with resistive semiconductors. *J. El. Mat*., 36 (5), 598 – 605, doi 10.1007/s11664-007-0091-y
8. Maheshappa H.D., Nagaraju J., Krishna Murthy M.V. (1998). A facility for electrical resistance contact measurement. *Rev. Sci. Instr*., Mar. doi 10.1063/1.1148810
9. Holgate T.C., Han L., Wu NY, Bojesen E.D., Cristensen M., Iversen Bo.B., Nong N.V., Pryds N. *Characterization of the interface between Fe-Cr alloy and the p-type thermoelectric oxide* $Ca_3Co_4O_9$.
10. Schroder D.K. (2006). *Semiconductor material and device characterization.* IEEE press. A John Wiley & Sons, Inc. Publication.
11. Gupta R.P., McCarty R., Sharp J. (2013). Practical contact resistance measurement method for bulk $Bi_2Te_3$ based thermoelectric devices. *J. El. Mat*.

Надійшла до редакції: 12.01.2022.

**M.V. Havryliuk,** [1]
**V.V. Lysko,** *Cand.Sc (Phys-Math)* [1,2]
**O.S. Rusnak** [1]

[1]Institute of Thermoelectricity of the NAS and MES of Ukraine,
1, Nauky str., Chernivtsi, 58029, Ukraine;
[2]Yuriy Fedkovych Chernivtsi National University,
2, Kotsiubynsky str., Chernivtsi, 58012, Ukraine
*e-mail: anatych@gmail.com*

# EXPERIMENTAL STUDIES OF THERMOELECTRIC PARAMETERS OF MATERIALS FORMING PART OF THERMOELECTRIC MODULES

*The design of equipment for measuring the parameters of thermoelectric generator and cooling modules is presented, as well as a description of the method for determining the thermoelectric properties of materials used in these modules. The equipment was created on the basis of the absolute method, which makes it possible to determine the parameters of modules in real conditions of their operation and allows instrumental minimization of the main sources of measurement errors. The results of experimental studies of the parameters of thermoelectric modules carried out using the developed equipment are presented.*
**Key words:** thermoelectric module, electrical conductivity, thermoEMF, thermal conductivity, thermoelectric material, measurement.

## Introduction

*General characterization of the problem*

Quality control of thermoelectric converters of modules plays an important role in their development, as well as in the creation on the basis of these modules of thermoelectric devices for cooling and generation of electricity. Such control is carried out by measuring the parameters of thermoelectric modules - cooling capacity, coefficient of performance and temperature difference on the module for thermoelectric coolers; efficiency, electric power – for thermoelectric generators. One of the best measurement methods in this case is the absolute method [1, 2], which allows one to determine the parameters of modules in real conditions of their operation, makes it possible to instrumentally minimize the main sources of measurement errors, and also obtain information about the properties of the material forming part of the module, namely thermoEMF, electrical conductivity and thermal conductivity of a pair of thermoelectric legs [3 – 5].

The Institute of Thermoelectricity of the National Academy of Sciences and the Ministry of Education and Science of Ukraine has developed a universal electronic control system and automated measuring equipment based on it, which makes it possible to measure the parameters of thermoelectric modules and the thermoelectric properties of materials forming part of them for a wide range of operating temperatures: from – 50 to 100 °C for cooling modules and from 30 to 600 °C for generator modules [6 – 8].

*The purpose of this work* is to conduct experimental studies of the developed equipment and confirm its expected capabilities.

## 1. Description of method and equipment for determining the properties of thermoelectric materials forming part of thermoelectric power converters

The appearance of the developed equipment for measuring the parameters of thermoelectric modules and determining the thermoelectric properties of materials forming part of them is shown in Fig. 1.

*Fig. 1. Appearance of equipment for measuring parameters of thermoelectric modules.*

Diagrams of the absolute method, taken as a basis for creating equipment for determining the parameters of generator and cooling thermoelectric modules, are shown in Fig. 2 and Fig. 3, respectively.

To determine the parameters of the generator thermoelectric module, the latter is placed between two heat-equalizing plates, which in turn are located between the electric heater and the heat meter (Fig. 2). The other side of the heat meter is in contact with the thermostat. With the help of an electric heater, a given temperature difference is created on the module and the EMF $E_{TEM}$ which occurs at the module wires, is measured. Following that, a matched electrical load is connected to the module wires, whereby the voltage on the module wires will become equal to half the EMF. The values of the electric current $I_{TEM}$ passing through the module, the voltage on its wires $U_{TEM}$ are measured, and with the help of a heat meter, the value of the heat flux $Q_1$, removed from the cold side of the module to the thermostat, is determined. The electrical power of module $P$ and its efficiency η are determined by the formulae

$$P = I_{TEM} \cdot U_{TEM}, \tag{1}$$

$$\eta = \frac{P}{Q_1 + P_{TEM}} \tag{2}$$

where $I_{TEM}$ and $U_{TEM}$ is current and voltage of module, $Q_1$ is heat flux which is removed from the cold side of module and determined by means of a heat meter.

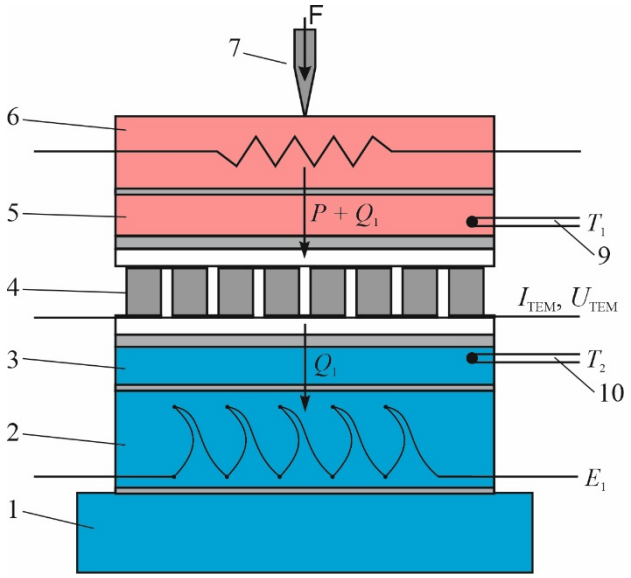


*Fig. 2. Absolute method of measuring parameters of thermoelectric generator modules: 1 – thermostat; 2 – heat meter; 3, 5 – heat-equalizing plates; 4 – module under study; 6 – heater; 8 – clamp; 10, 11 – thermocouples.*

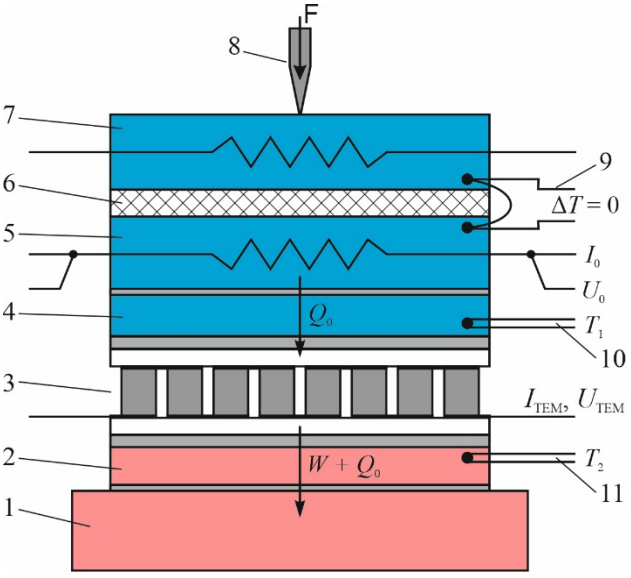


*Fig. 3. Absolute method of measuring parameters of thermoelectric cooling modules: 1 – thermostat; 2, 4 – heat-equalizing plates; 3 – module under study; 5 – reference heater; 6 – thermal insulation; 7 – protective heater; 8 – clamp; 9 – zero thermocouple; 10, 11 – thermolcouples.*

When determining the parameters of the cooling modules, a protective heater is additionally used, which prevents heat loss from the heater through the clamping mechanism (Fig. 3). The values of cooling capacity $Q_0$, temperature difference $\Delta T$ and coefficient of performance ε are determined by the formulae

$$Q_0 = I_0 \cdot U_0 , \tag{3}$$

$$\Delta T = T_1 - T_2 , \tag{4}$$

$$\varepsilon = \frac{Q_0}{W} , \tag{5}$$

where $I_0$ and $U_0$ is current through the heater and voltage drop thereupon, $T_1$ is the cold side temperature of module, $T_2$ is the hot side temperature of module, $W$ is electrical power consumption of the module.

To find the properties of the thermoelectric material forming part of the modules, the technique described in detail in [3, 5] was used.

The average values of electrical conductivity, thermoEMF, thermal conductivity and figure of merit of the material of thermoelectric module legs are determined by the formulae

$$\sigma = \frac{1}{R_M / 2N} \frac{h_1}{a_1 \cdot b_1} \cdot K_1, \tag{6}$$

$$\alpha = \frac{E / 2N}{\Delta T} \cdot K_2, \tag{7}$$

$$\kappa = \frac{Q / 2N}{\Delta T} \frac{h_1}{a_1 \cdot b_1} \cdot K_3, \tag{8}$$

$$Z = \frac{\alpha^2 \sigma}{\kappa}, \tag{9}$$

where $R_M$ is module resistance measured on the alternating current; $a_1$ x $b_1$ is cross-section of legs; $h_1$ is the height of legs; $N$ is the number of pairs; $E$ is module EMF; $\Delta T$ is temperature difference between thermocouples placed on heat-equalizing plates with a module under study arranged between them; $Q$ is heat flux through the module; $K_1 - K_3$ are correction factors to reduce the magnitude of measurement errors, calculated for a given design of the module and measuring equipment or determined experimentally.

## 2. Results of experimental studies

Figs. 4 and 5 show an example of the results of measuring the parameters of an Altec-22 type thermoelectric module on the developed equipment, namely, the dependence of the cooling capacity (Fig. 4) and the coefficient of performance (Fig. 5) on the power supply and temperature difference at $T_h$ = 20 °C.

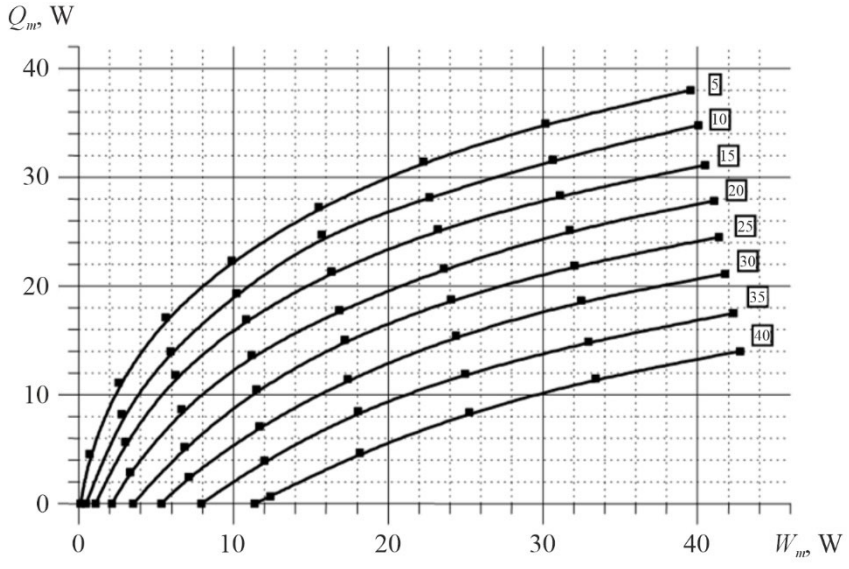


*Fig. 4. Dependence of cooling capacity $Q_m$ of thermoelectric module of the type Altec-22 on the power supply of module $W_m$ and temperature difference thereupon at $T_h$ = 20 °C.*

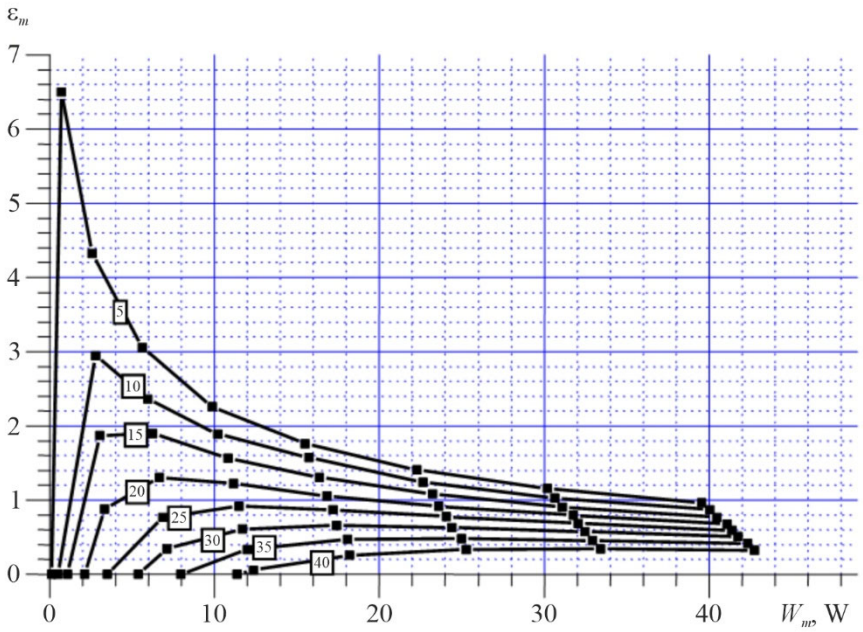


*Fig. 5. Dependence of coefficient of performance $\varepsilon_m$ of thermoelectric module of the type Altec-22 on the power supply of module $W_m$ and temperature difference thereupon at $T_h$ = 20 °C.*

Figs. 6, 7 show an example of the results of measuring the parameters of an Altec-1061 type thermoelectric module on the developed equipment, namely, the dependence of the efficiency and maximum useful electrical power of module on the hot side $T_h$ and cold side $T_c$ temperatures of module.

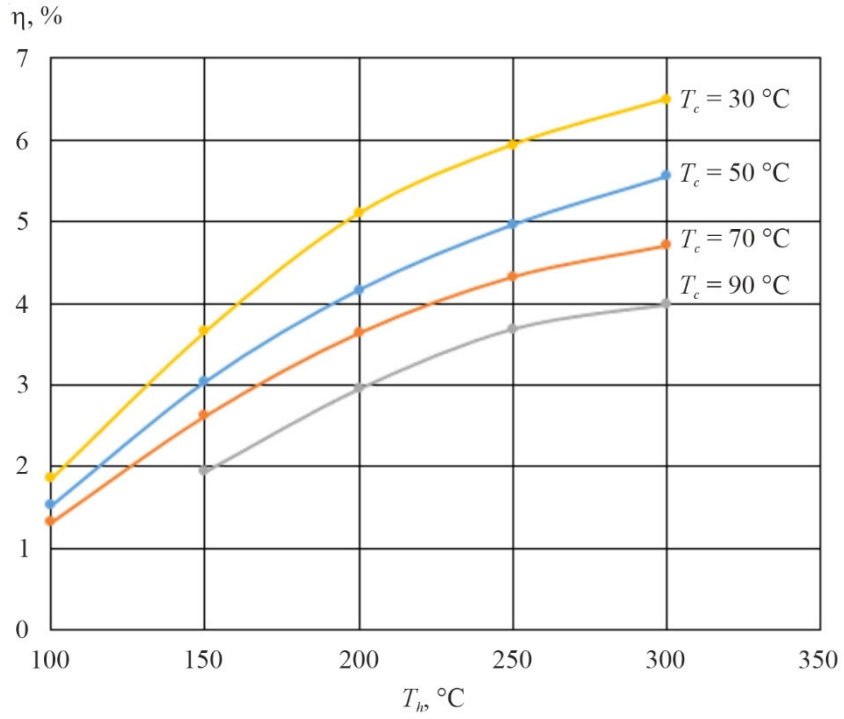


*Fig. 6. Dependence of the efficiency η of thermoelectric module of the type Altec-1061 on the hot side $T_h$ and cold side $T_c$ temperatures of module.*

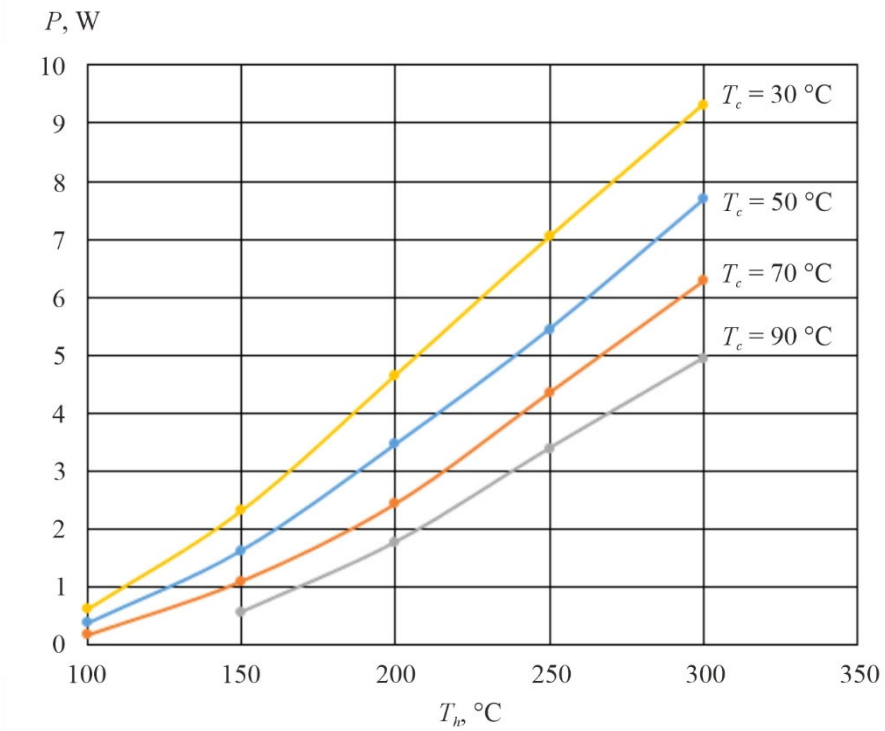


*Fig. 7. Dependence of maximum useful electrical power P of thermoelectric module of the type Altec-1061 on the hot side $T_h$ and cold side $T_c$ temperatures of module.*

According to the method detailed in paragraph 1, the thermoelectric properties of materials forming part of the cooling module of Altec-22 type and the generator module of Altec-1061 type were determined. The research results are presented in Table 1 and Table 2, respectively.

*Table 1*

*Results of determining the properties of thermoelectric materials used in cooling module of the type Altec-22*

| $T_1$, °C | $T_2$, °C | $T_{ave}$, °C | σ, $Ohm^{-1}\cdot cm^{-1}$ | α, μ/°C | κ, W/(m·°C) | $Z\cdot10^3$, 1/°C |
|---|---|---|---|---|---|---|
| 100 | 90 | 95 | 661 | 222.0 | 1.62 | 2.02 |
| 80 | 70 | 75 | 687 | 222.5 | 1.59 | 2.14 |
| 60 | 50 | 55 | 780 | 220.4 | 1.54 | 2.45 |
| 40 | 30 | 35 | 854 | 216.0 | 1.55 | 2.57 |
| 20 | 10 | 15 | 937 | 209.3 | 1.58 | 2.60 |
| 0 | – 10 | – 5 | 1028 | 200.3 | 1.64 | 2.52 |
| – 20 | – 30 | – 25 | 1078 | 194.9 | 1.68 | 2.44 |

*Table 2*

*Results of determining the properties of thermoelectric materials used in generator module of the type Altec-1061*

| $T_1$, °C | $T_2$, °C | $T_{ave}$, °C | σ, $Ohm^{-1}\cdot cm^{-1}$ | α, μ/°C | κ, W/(m·°C) | $Z\cdot10^3$, 1/°C |
|---|---|---|---|---|---|---|
| 40 | 30 | 35 | 1674 | 141.0 | 1.99 | 1.67 |
| 80 | 30 | 55 | 1550 | 147.3 | 1.92 | 1.75 |
| 120 | 30 | 75 | 1435 | 152.7 | 1.89 | 177 |
| 160 | 30 | 95 | 1328 | 157.2 | 1.89 | 1.74 |
| 200 | 30 | 115 | 1231 | 160.7 | 1.93 | 1.64 |
| 240 | 30 | 135 | 1142 | 163.3 | 2.01 | 151 |
| 280 | 30 | 155 | 1062 | 165.0 | 2.13 | 1.36 |
| 320 | 30 | 175 | 991 | 165.8 | 2.28 | 1.19 |

The errors of the method used (with regard to corrections) are: when determining electrical conductivity – 2 – 3 %, thermoEMF – 3 – 5 %, thermal conductivity – 5 – 7 %.

Comparison of the obtained results with the properties of the initial materials used to manufacture these modules, determined on the high-precision equipment "ALTEC-10001", allows obtaining information about such important module parameters as the effect of contact and interconnect resistance on its efficiency. This information is extremely important for improving modules design.

## Conclusions

1. The design of automated equipment for measuring the parameters of thermoelectric generator and cooling modules is described, as well as a method for determining the thermoelectric properties of materials in these modules. The equipment was created on the basis of the absolute method, which makes it possible to measure the parameters of thermoelectric modules and the thermoelectric properties of materials in them for a wide range of operating temperatures: from – 50 to 100 °C for cooling modules and from 30 to 600 °C for generator modules.
2. The developed equipment was used to study the parameters of serial thermoelectric cooling modules of Altec-22 type and generator modules of Altec-1061 type. The possibility of determining the properties of thermoelectric materials forming part of these modules has been experimentally confirmed.

## References

1. Kolodner P. (2014). High-precision thermal and electrical characterization of thermoelectric modules. *Review of Scientific Instruments*, 85(5), 054901/1-054901/11.

2. Anatychuk L.I., Havrylyuk M.V. (2011). Procedure and equipment for measuring parameters of thermoelectric generator modules. *J. Electronic Materials*, 40 (5), 1292 – 1297.
3. Anatychuk L.I., Lysko V.V. (2021). Method for determination of thermoelectric parameters of materials forming part of thermoelectric cooling modules. *J. Thermoelectricity*, 1, 49 – 54.
4. Anatychuk L.I., Lysko V.V. (2020). Determination of thermoelectric parameters of materials forming part of thermoelectric generator modules. *J. Thermoelectricity*, 3, 70 – 80.
5. Anatychuk L.I., Lysko V.V. (2021). Determination of the temperature dependences of thermoelectric parameters of materials used in generator thermoelectric modules with a rise in temperature difference. *J. Thermoelectricity*, 2, 53 – 57.
6. Anatychuk L.I., Havryliuk M.V., Lysko V.V. (2021). Computerization of processes of measuring thermoelectric parameters of materials forming part of generator and cooling thermoelectric modules. *J. Thermoelectricity*, 2, 62 – 66.
7. Anatychuk L.I., Havryliuk M.V., Lysko V.V. (2021). Automation and computerization of processes of measuring thermoelectric parameters of materials forming part of generator and cooling thermoelectric modules. *J. Thermoelectricity*, 3, 60 – 70.
8. Anatychuk L.I., Lysko V.V. (2021). Method for determining the thermoelectric parameters of materials forming part of thermoelectric cooling modules. *J. Thermoelectricity*, 3, 71 – 82.

Submitted 26.01.2022.

**Гаврилюк М.В.** [1],
**Лисько В.В.,** *канд. фіз.-мат. наук* [1,2],
**Руснак О.С.** [1]

[1] Інститут термоелектрики НАН та МОН України,
вул. Науки, 1, Чернівці, 58029, Україна;
[2] Чернівецький національний університет імені Юрія Федьковича,
вул. Коцюбинського 2, Чернівці, 58012, Україна
*e-mail: anatych@gmail.com*

# ЕКСПЕРИМЕНТАЛЬНІ ДОСЛІДЖЕННЯ ТЕРМОЕЛЕКТРИЧНИХ ПАРАМЕТРІВ МАТЕРІАЛІВ У СКЛАДІ ТЕРМОЕЛЕКТРИЧНИХ МОДУЛІВ

*Наведено конструкцію обладнання для вимірювання параметрів термоелектричних генераторних та холодильних модулів, а також опис методики визначення термоелектричних властивостей матеріалів у складі цих модулів. Обладнання створено на основі абсолютного методу, що дозволяє визначати параметри модулів у реальних умовах їх експлуатації та дає можливість інструментально мінімізувати основні джерел похибок вимірювань. Представлено результати експериментальних досліджень параметрів термоелектричних модулів, проведених за допомогою розробленого обладнання.*

**Ключові слова:** термоелектричний модуль, електропровідність, термоЕРС, теплопровідність, термоелектричний матеріал, вимірювання.

## Література

1. Kolodner P. (2014). High-precision thermal and electrical characterization of thermoelectric modules. *Review of Scientific Instruments*, 85 (5), 054901/1-054901/11.
2. Anatychuk L.I., Havrylyuk M.V. (2011). Procedure and equipment for measuring parameters of thermoelectric generator modules. *J. Electronic Materials*, 40 (5), 1292 – 1297.
3. Анатичук Л.І., Лисько В.В. Методика визначення термоелектричних параметрів матеріалів у складі термоелектричних модулів охолодження // Термоелектрика. – 2021, №1. – С. 49 – 54.
4. Анатичук Л.І., Лисько В.В. Визначення термоелектричних параметрів матеріалів у складі генераторних термоелектричних модулів // Термоелектрика. – 2020, №3. – С. 70 – 80.
5. Анатичук Л.І., Лисько В.В. Визначення температурних залежностей термоелектричних параметрів матеріалів у складі генераторних термоелектричних модулів при зростаючому перепаді температур // Термоелектрика. – 2021, №2. – С. 53 – 57.
6. Анатичук Л.І., Гаврилюк М.В., Лисько В.В. Комп'ютеризація процесів вимірювань термоелектричних параметрів матеріалів у складі генераторних та холодильних термоелектричних модулів // Термоелектрика. – 2021, №2. – С. 62 – 66.
7. Анатичук Л.І., Гаврилюк М.В., Лисько В.В. Автоматизація та комп'ютеризація процесів вимірювань термоелектричних параметрів матеріалів у складі генераторних та холодильних термоелектричних модулів // Термоелектрика. – 2021, №3. – С. 63 – 72.
8. Анатичук Л.І., Лисько В.В. Методика визначення термоелектричних параметрів матеріалів у складі термоелектричних модулів охолодження // Термоелектрика. – 2021, №3. – С. 73 – 85.

Надійшла до редакції: 26.01.2022.

**L.I. Anatychuk,** *Acad. NAS Ukraine* [1,2]
**R.R. Kobylianskyi,** *Cand. Sc (Phys &Math)* [1,2]
**R.V. Fedoriv** [1,2]

[1]Institute of Thermoelectricity of the NAS and MES of Ukraine,
1, Nauky str., Chernivtsi, 58029, Ukraine;
[2]Yuriy Fedkovych Chernivtsi National University,
2, Kotsiubynsky str., Chernivtsi, 58012, Ukraine
*e-mail: anatych@gmail.com*

# COMPUTER SIMULATION OF THE WORKING TOOL OF THERMOELECTRIC DEVICE FOR CRYODESTRUCTION WITHOUT TAKING INTO ACCOUNT PHASE TRANSITION

*The paper presents the results of computer simulation of the working tool of thermoelectric device for cryodestruction without taking into account phase transition, as well as cyclic temperature effect on the human skin in dynamic mode. A physical model of the working tool, a three-dimensional computer model of biological tissue taking into account thermophysical processes, blood circulation, heat exchange, metabolic processes and phase transitions, is constructed. As an example, a case is considered when the working tool is on the skin surface, the temperature of which changes cyclically according to a given law in the temperature range [– 50 ÷ + 50] °C. Temperature distributions in different layers of the human skin in cooling and heating modes were determined. The obtained results make it possible to predict the depth of freezing and warming of biological tissue at a given temperature effect.*

**Key words:** cryodestruction, working tool, temperature effect, human skin, dynamic mode, computer simulation.

## Introduction

Temperature effect is an important factor in the treatment of many diseases of the human body [1 – 12]. However, the devices used for this purpose are in most cases bulky, without adequate temperature regulation and thermal regime reproduction capabilities. To obtain lower temperatures, liquid nitrogen systems are used [13 – 17], which significantly limits the possibilities of their use in medical institutions where the supply of liquid nitrogen is problematic. In addition, the use of liquid nitrogen or the Joule-Thomson effect during gas expansion does not allow for the implementation of precisely required temperature regimes, which reduces the overall efficiency of using cold in treatment.

The use of thermoelectric cooling (heating) can solve this problem [12, 18 – 21]. The studies of thermal effects on biological tissue conducted over many years, the creation of thermoelectric devices based on them and their use in medical practice confirm their efficiency. Thermoelectric devices are promising in such areas of medicine as cryotherapy, cryosurgery, ophthalmology, traumatology, neurosurgery, plastic surgery, urology, dermatology [10 – 12].

However, the experience of using thermoelectric medical devices revealed a number of their shortcomings. Among them, the most important is the lack of ability to manage cooling and heating processes in time. The latter significantly narrows the possibilities of heat and cold treatment.

Studies show that cooling rates (their dynamics) play a decisive role in treatment [16, 22 – 34]. Thus, very fast cooling does not lead to the destruction of biological tissues at all. On the contrary, moderate but cyclical cooling promotes energetic destruction of tumors. The time functions of cooling and heating are also important in the treatment of other diseases.

Therefore, the general problem is to develop a thermoelectric device for the destruction of biological tissue or oncological neoplasms, which will provide the possibility of cyclic temperature effects on the tumor. This determines the relevance of the problem posed in the present work.

The importance of solving this problem is obvious, otherwise thermoelectric devices for medicine of a new generation with the possibility of cyclic temperature effects on the human skin cannot be developed.

Therefore, the purpose of this work is computer simulation of the working tool of thermoelectric device for cryodestruction without taking into account the phase transition.

## 1. Physical model of the working tool of thermoelectric device for destruction the walls of which are made of steel

Fig.1 shows a physical model consisting of housing 1, inside which substance 2 (25 % alcohol solution) with a phase transition temperature $T_1$ is placed. Housing 1 with a hemispherical end 3 touches the skin 4 with a plane 5 with a diameter d. Housing 1 is made of medical grade stainless steel. Skin model 4 takes into account its complex structure.

The model takes into account heat inleak $Q_1$ at the ambient air temperature $T_2$ = 25 °C, as well as heat inleak $Q_2$ from the ambient air. The upper part of housing 1 is adiabatically insulated ($q$ = 0). The diameter of the thermal contact 5 is 5 mm.

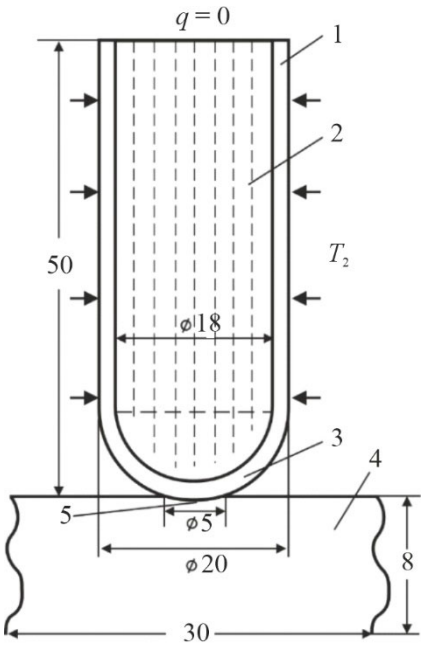


*Fig. 1. Physical model of the working tool of thermoelectric device for cryodestruction, the walls of which are made of steel.*

## 2. Computer model

A three-dimensional computer model of biological tissue was created in a cylindrical coordinate system, on the surface of which there is a thermoelectric medical device for local cooling. The Comsol

Multiphysics package of application programs [45] was used to build computer models, which makes it possible to simulate thermophysical processes in biological tissue, taking into account blood circulation, heat exchange, metabolic processes, and phase transition.

The calculation of temperature distributions and the density of heat flows in biological tissue and cold accumulator was carried out by the finite element method, the essence of which is that the object under study is divided into a large number of finite elements and in each of them the value of the function is sought, which satisfies the given second order differential equation with the corresponding boundary conditions. The accuracy of solving the given problem depends on the level of division and is ensured by the use of a large number of finite elements [45].

Thermophysical properties of the skin and the biological tissue of human body [35 – 38] in normal and frozen states are shown in Tables 1, 2.

*Table 1*

*Thermophysical properties of the biological tissue of human body [35 – 38]*

| Biological tissue layers | Epidermis | Dermis | Subcutaneous layer | Internal tissue |
|---|---|---|---|---|
| Thickness, $l$ (mm) | 0.08 | 2 | 10 | 30 |
| Specific heat, $C$ ($J \cdot kg^{-1} \cdot K^{-1}$) | 3590 | 3300 | 2500 | 4000 |
| Thermal conductivity, $\kappa$ ($W \cdot m^{-1} \cdot K^{-1}$) | 0.24 | 0.45 | 0.19 | 0.5 |
| Density, $\rho$ ($kg \cdot m^{-3}$) | 1200 | 1200 | 1000 | 1000 |
| Metabolism, $Q_{met}$ ($W/m^3$) | 368 | 368 | 368 | 368 |
| Blood perfusion rate, $\omega_b$ (ml/s·ml) | 0 | 0.0005 | 0.0005 | 0.0005 |
| Blood density, $\rho_b$ ($kg \cdot m^{-3}$) | 1060 | 1060 | 1060 | 1060 |
| Heat capacity of blood, $C_b$ ($J \cdot kg^{-1} \cdot K^{-1}$) | 3770 | 3770 | 3770 | 3770 |

*Table 2*

*Thermophysical properties of the biological tissue of human body in normal and frozen states [35 – 38]*

| Thermophysical properties of biological tissue | Value | Units of measurement |
|---|---|---|
| Heat capacity of normal biological tissue ($C_1$) | 3600 | $J/m^3$ °C |
| Heat capacity of frozen biological tissue ($C_2$) | 1800 | $J/m^3$ °C |
| Thermal conductivity of normal biological tissue ($\kappa_1$) | 0.5 | W/m °C |
| Thermal conductivity of frozen biological tissue ($\kappa_2$) | 2 | W/m °C |
| Latent heat of phase transition ($L$) | $250 \cdot 10^3$ | $J/m^3$ |
| Upper temperature of phase transition ($T_1$) | -1 | °C |
| Lower temperature of phase transition ($T_2$) | -8 | °C |

## 3. Computer simulation results

Fig. 2 shows temperature distributions in human skin, directly under the center of action of the working tool

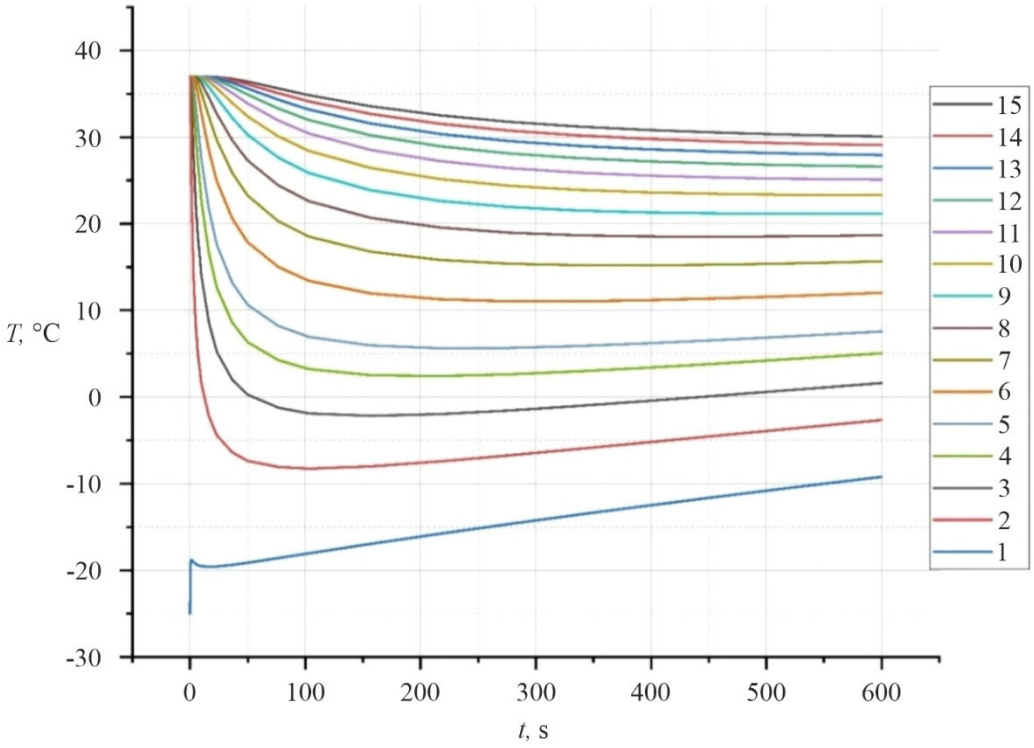


*Fig. 2. Dependences of temperature on time in the human skin at different depths: 1 – point of contact between working tool and skin; 2 – 0.5 mm; 3 – 1 mm; 4 – 1.5 mm; 5 – 2 mm; 6 – 2.5 mm; 7 – 3 mm; 8 – 3.5 mm; 9 – 4 mm; 10 – 4.5 mm; 11 – 5 mm; 12 – 5.5 mm; 13 – 6 mm; 14 – 6.5 mm; 15 – 7 mm.*

Fig. 3 shows temperature distributions in the skin directly under the centre of action of the working tool at time moments: 10 s, 60 s, 140 s, 200 s, 600 s.

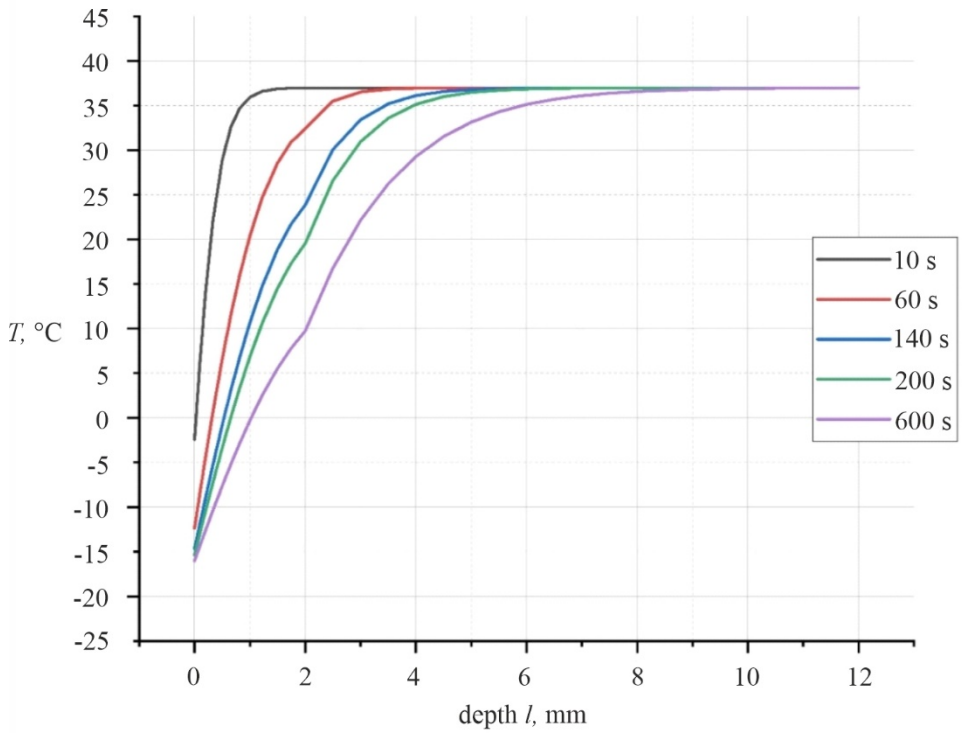


*Fig. 3. Dependences of temperature on skin depth at time moments: 10 s, 60 s, 140 s, 200 s, 600 s.*

Fig. 4 represents temperature distributions in the cold accumulator at different depths.

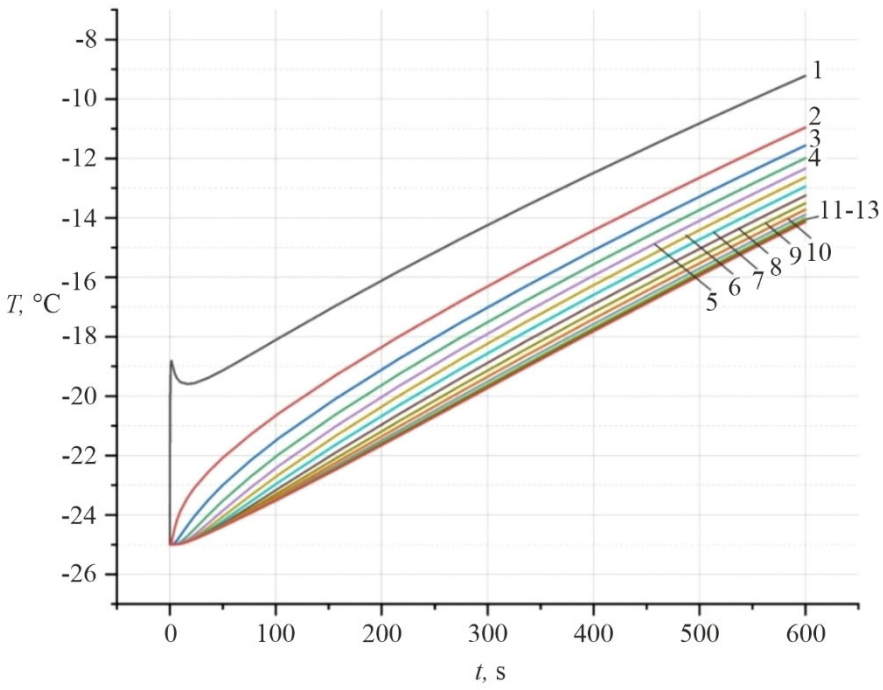


*Fig. 4. Dependences of temperature on time in the cold accumulator at different depths: 1 – point of contact between working tool and skin: 2 – 4 mm; 3 – 8 mm; 4 – 12 mm; 5 – 16 mm; 6 – 20 mm; 7 – 24 mm; 8 – 28 mm; 9 – 32 mm; 10 – 36 mm; 11 – 40 mm; 12 – 44 mm; 13 – 48 mm.*

Fig. 5 shows the distribution of temperatures in the cold accumulator at the following moments: 10 s, 60 s, 140 s, 200 s, 600 s.

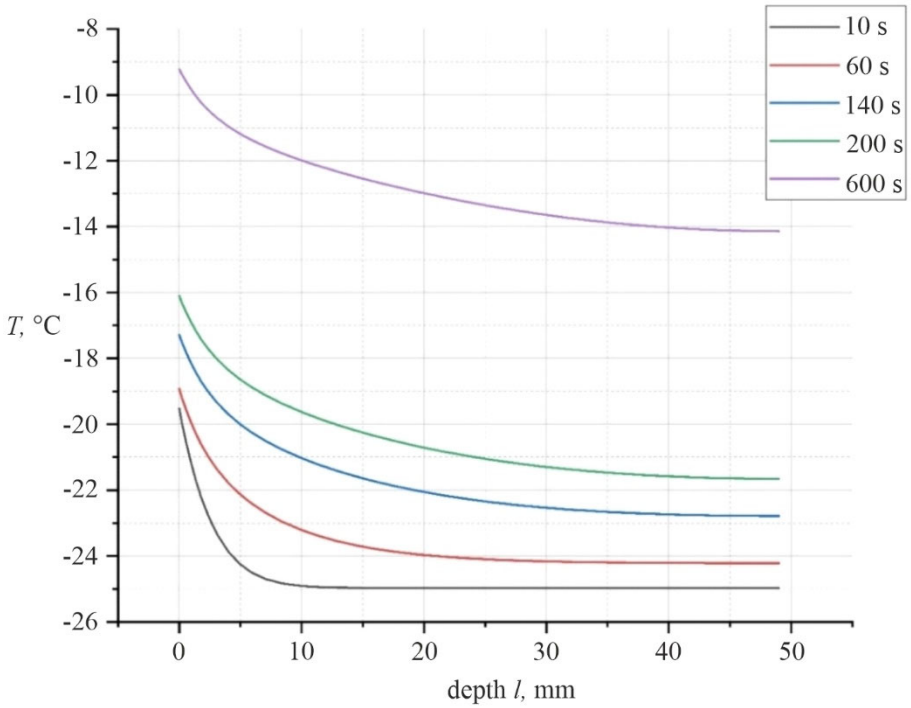


*Fig. 5. Dependences of temperature on time in the cold accumulator at time moments:10 s, 60 s, 140 s, 200 s, 600 s.*

## 4. Physical model of the working tool of thermoelectric device for destruction the walls of which are made of copper

Fig. 6 shows a physical model consisting of a housing 1, inside which a substance 2 (25 % alcohol solution) with a phase transition temperature T1 is placed. Housing 1 with its hemispherical end 3 touches skin 4 with a plane 5 of diameter d. Housing 1 is made of copper. The complex structure of skin 4 is taken into account in the model.

The model takes into account the heat inleak $Q_1$ at the ambient air temperature $T_2 = 25$ °C, as well as the heat inleak $Q_2$ from the ambient air. The upper part of the housing 1 is adiabatically insulated ($q = 0$). The diameter of the thermal contact is 5 mm.

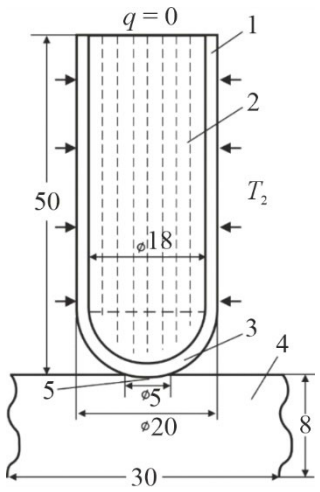


*Fig. 6. Physical model of the working tool of thermoelectric device for cryodestruction the walls of which are made of copper.*

## 5. Results of computer simulation

Fig. 7 shows temperature distributions in the human skin, directly under the center of action of the working tool.

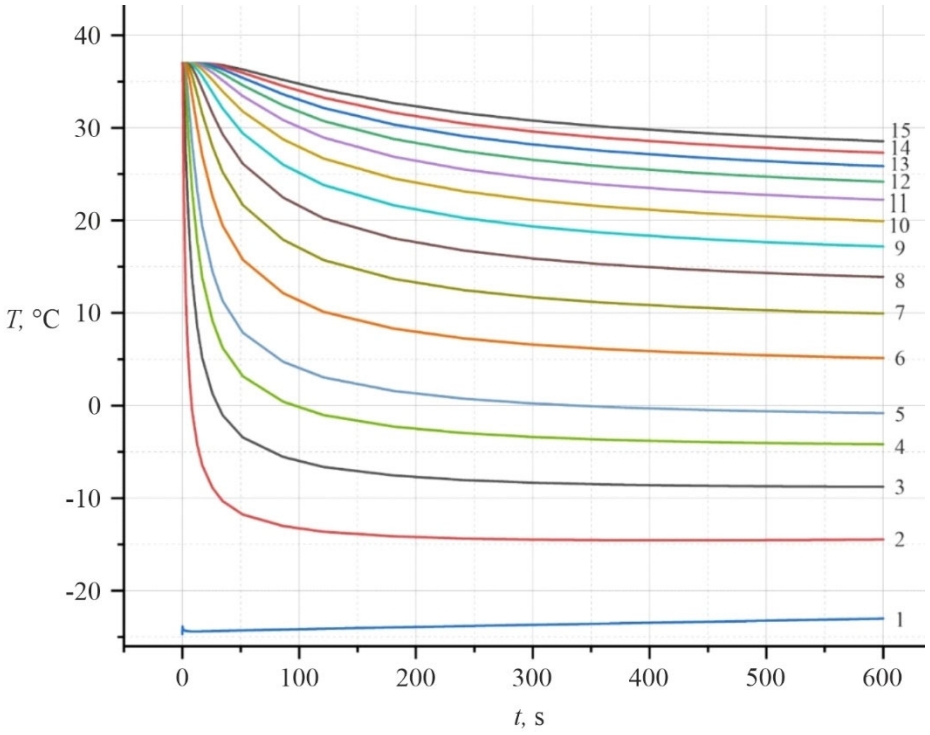


*Fig. 7. Dependences of temperature on time in the human skin at different depths: 1 – point of contact between the working tool and skin; 2 – 0.5 mm; 3 – 1 mm; 4 – 1.5 mm; 5 – 2 mm; 6 – 2.5 mm; 7 – 3 mm; 8 – 3.5 mm; 9 – 4 mm; 10 – 4.5 mm; 11 – 5 mm; 12 – 5.5 mm; 13 – 6 mm; 14 – 6.5 mm; 15 – 7 mm.*

Fig. 8 shows temperature distributions in the cold accumulator at different depths.

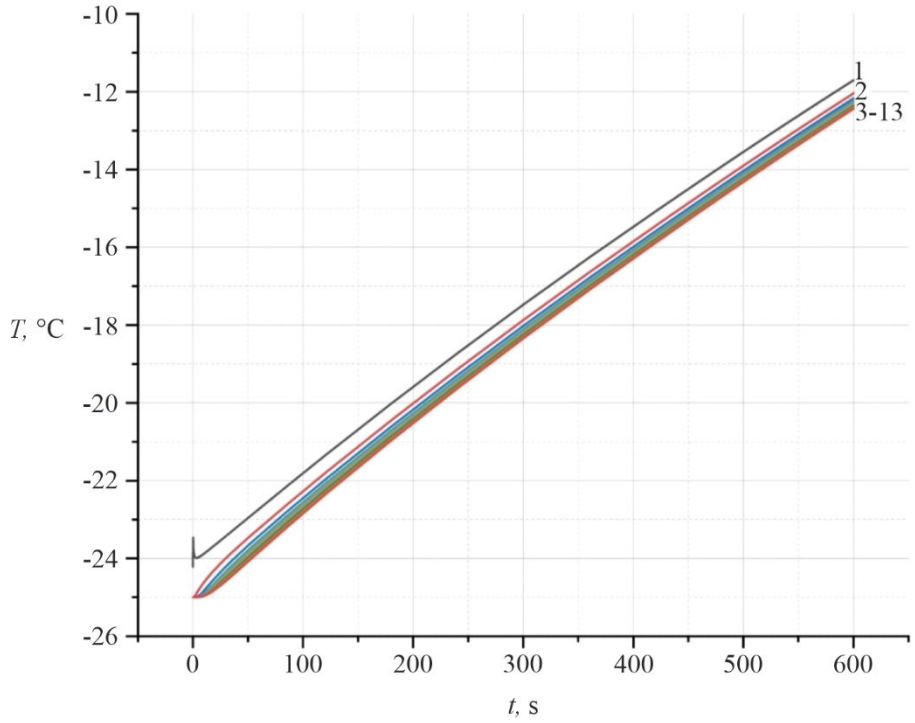


*Fig. 8. Dependences of temperature on time in the cold accumulator at different depths: 1 – point of contact between the working tool and skin; 2 – 4 mm; 3 – 8 mm; 4 – 12 mm; 5 – 16 mm; 6 – 20 mm; 7 – 24 mm; 8 – 28 mm; 9 – 32 mm; 10 – 36 mm; 11 – 40 mm; 12 – 44 mm; 13 – 48 mm.*

Fig. 9 shows the dependence of temperature on depth at time moments 60, 120, 240, 600 s and depending on the location under the working tool.

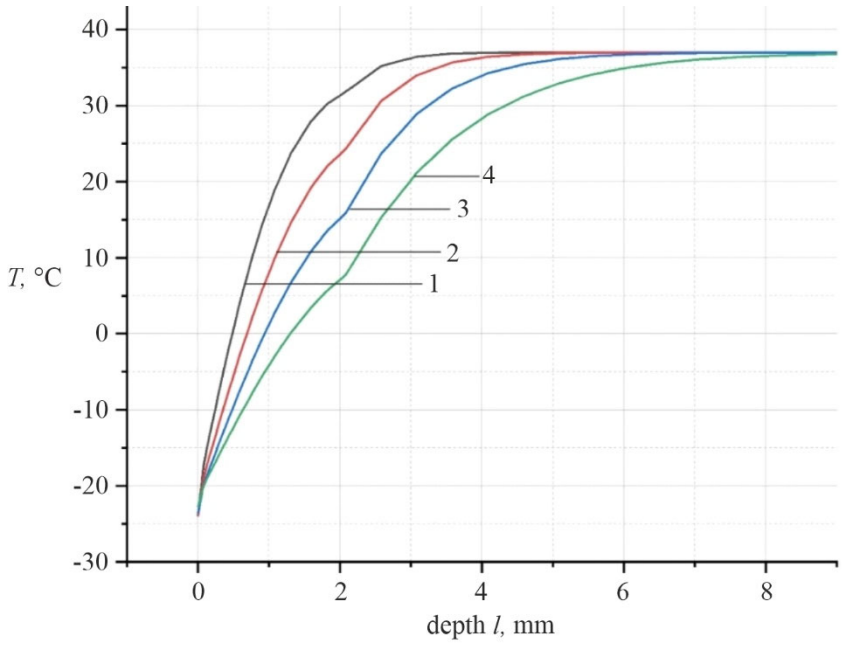


*Fig. 9. Dependence of the temperature on the depth directly under the center of the working tool at time moments: 1 – 60 s, 2 – 120 s, 3 – 240 s, 4 – 600 s.*

## Conclusions

1. The mechanism of cryodestruction was determined from the analysis of the literature and data was obtained that the use of excessive cooling is not necessary. It has been established that for cryodestruction it is sufficient to cool biological tissue to a temperature of – 20 ÷ – 50 °C, and the optimal cooling rate should be 40 – 50 °C/min. To increase the efficiency of cryodestruction, it is reasonable to use cyclic cooling and heating up to (+ 39 ÷ + 45) ºC, which indicates good prospects for using thermoelectric cooling in medical practice, since such conditions can be achieved by using the thermoelectric method of cooling and heating.
2. A method for computer simulation of temperature distribution in the human skin in dynamic mode has been developed, which makes it possible to predict the results of local temperature effects on the skin and determine at any moment in time the temperature distribution in different layers of the skin for a given arbitrary time function of change in the temperature of the working tool $T_f(t)$.
3. A computer model was developed and a computer simulation of the working tool of the thermoelectric device for destruction was performed for two design options in order to determine the temperature in the skin and the cold accumulator without taking into consideration the phase transition:
    a) the working tool made of medical steel without an internal cylinder;
    b) the working tool made of copper without an internal cylinder.
4. With the help of computer simulation, the temperature distributions in different layers of the skin and in the cold accumulator of the working tool of thermoelectric device for destruction at the initial temperature of – 25 ºC were determined. The obtained results make it possible to predict the depth of freezing of biological tissue.

## References

1. Anatychuk L.I. (2003). *Termoelektrichestvo. T. 2. Termoelektricheskiie preobrazovatelu energii [Thermoelectricity. Vol. 2. Thermoelectric energy converters]*. Kyiv, Chernivtsi: Naukova Dumka.
2. Moskalyk I.A., Manyk O.M. (2013). On the use of thermoelectric cooling in the practice of cryodestruction. *J. Thermoelectricity*, 6, 84 – 92.
3. Moskalyk I.A. (2015). On the use of thermoelectric devices in cryosurgery. *Physics and Chemistry of the Solid State*, 4, 742 – 746.
4. Anatychuk L.I., Denisenko O.I., Kobylianskyi R.R., Kadeniuk T.Ya. (2015). On the use of thermoelectric cooling in detrmatology and cosmetology. *J. Thermoelectricity*, 3, 57 – 71.
5. Kobylianskyi R.R., Moskalyk I.A. (2015) Computer simulation of local thermal effect on biological tissue. *J. Thermoelectricity*, 6, 57 – 65.
6. Kobylianskyi R.R., Kadeniuk T.Ya. (2016). On the prospects of using thermoelectriicty for the treatment of skin diseases with cold. *Scientific bulletin of Chernivtsi University: collected papers. Physics. Electronics*, 5 (1). Chernivtsi: Chernivtsi National University, 67 – 72.
7. Anatychuk L.I., Denisenko O.I., Kobylianskyi R.R., Kadeniuk T Ya., Perepichka M.P. (2017). Modern methods of cryotherapy in dermatological practice. *Clinical and Experimental Pathology*, XVI, (59), 150 – 156.
8. Anatychuk L.I., Kobylianskyi R.R., Denisenko O.I., Shulenina O.V., Mykytiuk O.P. (2018). Results of clinical application of thermoelectric device for the treatment of skin diseases. *J. Thermoelectricity*, 3, 51 – 64.

9. Kobylianskyi R.R., Manyk O.M., Vyhonnyi V.Yu. (2018). On the use of thermoelectric cooling for cryodestruction in dermatology. *J. Thermoelectricity*, 6, 35 – 44.
10. Anatychuk L.I., Denysenko O.I., Kobylianskyi R.R., Stepanenko V.I., Svyryd S.G., Stepanenko R.L., Perepichka M.P. (2019). Thermoelectric device for treatment of skin diseases. *J. Thermoelectricity*, 4, 63 – 73.
11. Anatychuk L.I., Todurov B.M., Kobylianskyi R.R., Dzhal S.A. (2019). On the use of thermoelectric microgenerators for powering cardiac pacemakers. *J. Thermoelectricity*, 5, 63 – 88.
12. Anatychuk L.I., Vikhor L.M., Kotsur M.P., Kobylianskyi R.R., Kadenyuk T.Ya. (2016). Optimal control of time dependence of cooling temperature in thermoelectric devices. *J. Thermoelectricity*, 5, 5 – 11.
13. Anatychuk L.I., Kobylianskyi R.R., Kadenyuk T.Ya. (2017). Computer simulation of local thermal effect on human skin. *J. Thermoelectricity*, 1, 62 – 83.
14. Anatychuk L.I., Vikhor L.M., Kobylianskyi R.R., Kadeniuk T.Ya. (2017). Computer simulation and optimization of the dynamic operating modes of thermoelectric device for treatment of skin diseases. *J. Thermoelectricity*, 2, 46 – 57.
15. Anatychuk L.I., Vikhor L.M., Kobylianskyi R.R., Kadeniuk T.Ya., Zvarych O.V. (2017). Computer simulation and optimization of the dynamic operating modes of thermoelectric reflexotherapy device. *J. Thermoelectricity*, 3, 65 – 74.
16. Anatichuk L.I., Vykhor L.M., Kobylanskyi R.R., Kadenyuk T.Ya. (2017). Computer modeling and optimization of dynamic modes of operation of a thermoelectric device for cryodestruction. *Solid state physics and chemistry*, 18 (4), 455 – 459.
17. Anatychuk L., Vikhor L., Kotsur M., Kobylianskyi R., Kadeniuk T. (2018). Optimal control of time dependence of temperature in thermoelectric devices for medical purposes. *International Journal of Thermophysics* 39, 108. https://doi.org/10.1007/s10765-018-2430-z.
18. Anatychuk L.I., Kobylianskyi R.R., Fedoriv R.V. (2019). Methodology for taking into account the phase transition in biological tissue in computer simulation of the cryodestruction process. *J. Thermoelectricity,* 1, 46 – 58.
19. Anatychuk L.I., Kobylianskyi R.R., Fedoriv R.V. (2019). Computer simulation of human skin cryodestruction process in thermoeelctric cooling. *J.Thermoelectricity,* 2, 21 – 35.
20. Anatychuk L.I., Kobylianskyi R.R., Fedoriv R.V. (2020). Computer simulation of cyclic temperature effect on the human skin. *J. Thermoelectricity*, 2, 44 – 61.
21. Anatychuk L.I., Kobylianskyi R.R., Fedoriv R.V. (2020).Computer simulation of cyclic temperature effect on the oncological neoplasm of the human skin. *J. Thermoelectricity*, 3, 29 – 45.
22. Miller P., Metzner D. (1969). Cryosurgery for tumors of the head and neck. – *Trns. Am.Ophthalmol. Otolaringol. Soc.*, 73 (2), 300 – 309.
23. D'Hont G. La cryotherapie en ORL (1974). *Acta. Otorhinolaringol*., 28 (2), 274 – 278.
24. Mazur P. (1968). Physical-chemical factors underlying cell injury in cryosurgical freezing. In:*Cryosurgery* ed. by R. W. Rand, A. P. Rinfret, H. Leden – Springfield, Illinois, U.S.A.1968 p. 32 – 51.
25. Gill W., Fraser I. (1968). A look at cryosurgery. *Scot, Med*, I., 3, 268 – 273.
26. Van Venrjy G. (1975). Freeze-etching: freezing velocity and crystal size at different size locations in samples. *Cryobiology*, 12 (1), 46 – 61.
27. Bause H. (2004). Kryotherapie lokalisierter klassischer, neues Verfahren mit Peltier-Elementen (– 32°C) Erfahrungsbericht Hamangiome. *Monatsschr Kinderheilkd*. 152, 16 – 22.
28. COMSOL Multiphysics User's Guide (2010). COMSOLAB.

29. Jiang S.C., Ma N., Li H.J., Zhang X.X. (2002). Effects of thermal properties and geometrical dimensions on skin burn injuries. *Burns*, 28, 713 – 717.
30. Cetingul M.P., Herman C. (2008). Identification of skin lesions from the transient thermal response using infrared imaging technique. *IEEE*, 1219 – 1222.
31. Ciesielski M., Mochnacki B., Szopa R. (2011). Numerical modeling of biological tissue heating. Admissible thermal dose. *Scientific Research of the Institute of Mathematics and Computer Science,* 1 (10), 11 – 20.
32. Filipoiu Florin, Ioan Bogdan Andrei, Carstea Iulia Maria (2010). Computer-aided analysis of the heat transfer in skin tissue. *Proceedings of the 3rd WSEAS Int. Conference on Finite Differences – Finite Elements – Finite Volumes – Boundary Elements*, 53 – 59.
33. Carstea Daniela, Carstea Ion, Carstea Iulia Maria. (2011). Interdisciplinarity in computer-aided analysis of thermal therapies. *WSEAS Transactions on Systems and Control*, 6 (4), 115 – 124.
34. Deng Z.S. Liu J. (2005). Numerical simulation of selective freezing of target biological tissues following injection of solutions with specific thermal properties. *Cryobiology*, 50, 183 - 192.
35. Han Liang Lim, Venmathi Gunasekaran (2011). *Mathematical modeling of heat distribution during cryosurgery*. https://isn.ucsd.edu/last/courses/beng221/problems/2011/project10.pdf.
36. Shah Vishal N., Orlov Oleg I., Orlov Cinthia, Takebe Manabu, Thomas Matthew, and Plestis Konstadinos (2018). Combined cryo-maze procedure and mitral valve repair through a ministernotomy. *Multimed Man Cardiothorac Surg*. doi: 10.1510/mmcts.2018.022.
37. Rykaczewski Konrad (2019). Modeling thermal contact resistance at the finger-object interface. *Temperature*, 6 (1), 85 – 95.

Subminitted: 11.02.2022.

**Анатичук Л.І.,** *акад. НАН України* [1,2]
**Кобилянський Р.Р.,** *канд. фіз.-мат. наук* [1,2]
**Федорів Р.В.** [1,2]

[1] Інститут термоелектрики НАН та МОН України,
вул. Науки, 1, Чернівці, 58029, Україна;
[2] Чернівецький національний університет імені Юрія Федьковича,
вул. Коцюбинського 2, Чернівці, 58012, Україна
*e-mail: anatych@gmail.com*

## КОМП'ЮТЕРНЕ МОДЕЛЮВАННЯ РОБОЧОГО ІНСТРУМЕНТУ ТЕРМОЕЛЕКТРИЧНОГО ПРИЛАДУ ДЛЯ КРІОДЕСТРУКЦІЇ БЕЗ ВРАХУВАННЯ ФАЗОВОГО ПЕРЕХОДУ

*У роботі наведено результати комп'ютерного моделювання робочого інструменту термоелектричного приладу для кріодеструкції без врахування фазового переходу, а також циклічного температурного впливу на шкіру людини у динамічному режимі. Побудовано фізичну модель робочого інструменту, тривимірну комп'ютерну модель біологічної тканини з врахуванням теплофізичних процесів, кровообігу, теплообміну, процесів метаболізму та фазового переходу. Як приклад, розглянуто випадок, коли на поверхні шкіри знаходиться*

*робочий інструмент, температура якого змінюється циклічно за наперед заданим законом у діапазоні температур [– 50 ÷ + 50] °C. Визначено розподіли температури у різних шарах шкіри людини в режимах охолодження та нагріву. Отримані результати дають можливість прогнозувати глибину промерзання і прогрівання біологічної тканини при заданому температурному впливі.*

**Ключові слова:** кріодеструкція, робочий інструмент, температурний вплив, шкіра людини, динамічний режим, комп'ютерне моделювання.

## Література

1. Анатичук Л.І. Термоелектрика. Т.2. Термоелектричні перетворювачі енергії. Київ, Чернівці: Інститут термоелектрики, 2003. – 376 с.
2. Москалик І.А., Маник О.М. Про використання термоелектричного охолодження у практиці кріодеструкції // Термоелектрика. − № 6. – 2013. – С. 84 – 92.
3. Москалик І.А. Про використання термоелектричних приладів у кріохірургії // Фізика і хімія твердого тіла. – №4. – 2015. – С. 742 – 746.
4. Анатичук Л.І., Денисенко О.І., Кобилянський Р.Р., Каденюк Т.Я. Про використання термоелектричного охолодження в дерматології та косметології // Термоелектрика. − № 3. – 2015. – С. 57 – 71.
5. Кобилянський Р.Р., Москалик І.А. Комп'ютерне моделювання локального теплового впливу на біологічну тканину // Термоелектрика. − № 6. – 2015. – С.59 – 68.
6. Кобилянський Р.Р., Каденюк Т.Я. Про перспективи використання термоелектрики для лікування захворювань шкіри холодом // Науковий вісник Чернівецького університету: збірник наук. праць. Фізика. Електроніка. – Т. 5, Вип. 1. – Чернівці: Чернівецький національний університет, 2016. – С. 67 – 72.
7. Анатичук Л.І., Денисенко О.І., Кобилянський Р.Р., Каденюк Т.Я., Перепічка М.П. Сучасні методи кріотерапії в дерматологічній практиці // Клінічна та експериментальна патологія. – Том XVI. – №1 (59). – 2017. – С. 150 – 156.
8. Анатичук Л.І., Денисенко О.І., Шуленіна О.В., Микитюк О.П., Кобилянський Р.Р. Результати клінічного застосування термоелектричного приладу для лікування захворювань шкіри // Термоелектрика. − № 3. – 2018. – С. 52 – 66.
9. Кобилянський Р.Р., Маник О.М., Вигонний В.Ю. Про використання термоелектричного охолодження для кріодеструкції у дерматології // Термоелектрика. − № 6. – 2018. – С. 36 – 46.
10. Анатичук Л.І., Денисенко О.І., Кобилянський Р.Р., Степаненко В.І., Свирид С.Г., Степаненко Р.Л., Перепічка М.П. Термоелектричний прилад для лікування захворювань шкіри // Термоелектрика. − № 4. – 2019. – С. 62 – 73.
11. Анатичук Л.І., Тодуров Б.М., Кобилянський Р.Р., Джал С.А. Про використання термоелектричних мікрогенераторів для живлення електрокардіостимуляторів // Термоелектрика. − № 5. – 2019. – С. 60 – 88.
12. Анатичук Л.І., Вихор Л.М., Коцур М.П., Кобилянський Р.Р., Каденюк Т.Я. Оптимальне керування часовою залежністю температури охолодження в термоелектричних пристроях // Термоелектрика. − № 5. – 2016. – С. 5 – 11.

13. Анатичук Л.І., Кобилянський Р.Р., Каденюк Т.Я. Комп'ютерне моделювання локального теплового впливу на шкіру людини // Термоелектрика. − № 1. – 2017. – С. 69 – 79.
14. Анатичук Л.І., Вихор Л.М., Кобилянський Р.Р., Каденюк Т.Я. Комп'ютерне моделювання та оптимізація динамічних режимів роботи термоелектричного приладу для лікування захворювань шкіри // Термоелектрика. − № 2. – 2017. – С. 44 – 57.
15. Анатичук Л.І., Вихор Л.М., Кобилянський Р.Р., Каденюк Т.Я., Зварич О.В. Комп'ютерне моделювання та оптимізація динамічних режимів роботи термоелектричного приладу для рефлексотерапії // Термоелектрика. − № 3. – 2017. – С. 68 – 78.
16. Анатичук Л.І., Вихор Л.М., Кобилянський Р.Р., Каденюк Т.Я. Комп'ютерне моделювання та оптимізація динамічних режимів роботи термоелектричного приладу для кріодеструкції // Фізика і хімія твердого тіла. – Т.18. − № 4. – 2017. – С. 455 – 459.
17. L. Anatychuk, L. Vikhor, M. Kotsur, R. Kobylianskyi, T. Kadeniuk. Optimal Control of Time Dependence of Temperature in Thermoelectric Devices for Medical Purposes // International Journal of Thermophysics". – International Journal of Thermophysics (2018) 39, 108. https://doi.org/10.1007/s10765-018-2430-z.
18. Анатичук Л.І., Кобилянський Р.Р., Федорів Р.В. Методика врахування фазового переходу в біологічній тканині при комп'ютерному моделюванні процесу кріодеструкції // Термоелектрика. − № 1. – 2019. – С. 46 – 58.
19. Анатичук Л.І., Кобилянський Р.Р., Федорів Р.В. Комп'ютерне моделювання процесу кріодеструкції шкіри людини при термоелектричному охолодженні // Термоелектрика. − № 2. – 2019. – С. 21 – 35.
20. Анатичук Л.І., Кобилянський Р.Р., Федорів Р.В. Комп'ютерне моделювання циклічного температурного впливу на шкіру людини // Термоелектрика. − № 2. – 2020. – С. 48 – 64.
21. Анатичук Л.І., Кобилянський Р.Р., Федорів Р.В. Комп'ютерне моделювання циклічного температурного впливу на онкологічне новоутворення шкіри людини // Термоелектрика. − № 3. – 2020. – С. 29 – 46.
22. Miller P., Metzner D. (1969). Cryosurgery for tumors of the head and neck. – *Trns. Am.Ophthalmol. Otolaringol. Soc.*, 73 (2), 300 – 309.
23. D'Hont G. La cryotherapie en ORL (1974). *Acta. Otorhinolaringol*., 28 (2), 274 – 278.
24. Mazur P. (1968). Physical-chemical factors underlying cell injury in cryosurgical freezing. In:*Cryosurgery* ed. by R. W. Rand, A. P. Rinfret, H. Leden – Springfield, Illinois, U.S.A.1968 p. 32 – 51.
25. Gill W., Fraser I. (1968). A look at cryosurgery. *Scot, Med*, I., 3, 268 – 273.
26. Van Venrjy G. (1975). Freeze-etching: freezing velocity and crystal size at different size locations in samples. *Cryobiology*, 12 (1), 46 – 61.
27. Bause H. (2004). Kryotherapie lokalisierter klassischer, neues Verfahren mit Peltier-Elementen (– 32°C) Erfahrungsbericht Hamangiome. *Monatsschr Kinderheilkd*. 152, 16 – 22.
28. COMSOL Multiphysics User's Guide (2010). COMSOLAB.
29. Jiang S.C., Ma N., Li H.J., Zhang X.X. (2002). Effects of thermal properties and geometrical dimensions on skin burn injuries. *Burns*, 28, 713 – 717.
30. Cetingul M.P., Herman C. (2008). Identification of skin lesions from the transient thermal response using infrared imaging technique. *IEEE*, 1219 – 1222.

31. Ciesielski M., Mochnacki B., Szopa R. (2011). Numerical modeling of biological tissue heating. Admissible thermal dose. *Scientific Research of the Institute of Mathematics and Computer Science,* 1 (10), 11 – 20.
32. Filipoiu Florin, Ioan Bogdan Andrei, Carstea Iulia Maria (2010). Computer-aided analysis of the heat transfer in skin tissue. *Proceedings of the 3rd WSEAS Int. Conference on Finite Differences – Finite Elements – Finite Volumes – Boundary Elements*, 53 – 59.
33. Carstea Daniela, Carstea Ion, Carstea Iulia Maria. (2011). Interdisciplinarity in computer-aided analysis of thermal therapies. *WSEAS Transactions on Systems and Control*, 6 (4), 115 – 124.
34. Deng Z.S. Liu J. (2005). Numerical simulation of selective freezing of target biological tissues following injection of solutions with specific thermal properties. *Cryobiology*, 50, 183 - 192.
35. Han Liang Lim, Venmathi Gunasekaran (2011). *Mathematical modeling of heat distribution during cryosurgery*. https://isn.ucsd.edu/last/courses/beng221/problems/2011/project10.pdf.
36. Shah Vishal N., Orlov Oleg I., Orlov Cinthia, Takebe Manabu, Thomas Matthew, and Plestis Konstadinos (2018). Combined cryo-maze procedure and mitral valve repair through a ministernotomy. *Multimed Man Cardiothorac Surg*. doi: 10.1510/mmcts.2018.022.
37. Rykaczewski Konrad (2019). Modeling thermal contact resistance at the finger-object interface. *Temperature*, 6 (1), 85 – 95.

Надійшла до редакції: 11.02.2022.

**L.I. Anatychuk,** *Acad. NAS Ukraine* [1,2]
**R.R. Kobylianskyi,** *Cand. Sc (Phys &Math)* [1,2]
**A.V. Prybyla,** *Cand. Sc (Phys &Math)* [1,2]
**I.A. Konstantynovych,** *Cand. Sc (Phys &Math)* [1,2]
**V.V. Boychuk** [2]

[1]Institute of Thermoelectricity of the NAS and MES of Ukraine,
1, Nauky str., Chernivtsi, 58029, Ukraine;
[2]Yuriy Fedkovych Chernivtsi National University,
2, Kotsiubynsky str., Chernivtsi, 58012, Ukraine
*e-mail: anatych@gmail.com*

# COMPUTER SIMULATION OF THE THERMOELECTRIC HEAT FLOW SENSOR ON THE SURFACE OF THE HUMAN BODY

*This paper presents the results of computer simulation of cyclic temperature effect on the human skin in dynamic mode. A three-dimensional computer model of the biological tissue has been built with regard to thermophysical processes, blood circulation, heat exchange, metabolic processes and the phase transition. As an example, the case is considered when on the skin surface there is a working tool the temperature of which changes cyclically according to a predetermined law in the temperature range [– 50 ÷ + 50] °C. Temperature distributions in different human skin layers in heating and cooling modes have been determined. The results obtained make it possible to predict the depth of the biological tissue freezing and heating under a given temperature effect.*
**Key words:** temperature effect, human skin, dynamic mode, computer simulation.

## Introduction

It is known that various diseases of the human body are treated with the help of temperature effect [1 – 2]. However, the devices used for this purpose are in most cases bulky, without adequate temperature regulation and thermal regime reproduction capabilities. To obtain lower temperatures, liquid nitrogen systems are generally used [3], which significantly limits the possibilities of their use in medical institutions, where the supply of liquid nitrogen is rather problematic. Moreover, the use of liquid nitrogen or the Joule-Thomson effect during gas expansion does not allow for the implementation of precisely required temperature regimes, which also reduces the overall efficiency of using cold in treatment.

This problem can be solved with the use of thermoelectric cooling (heating) [4 – 13]. The studies of thermal effect on the biological tissue, creation of thermoelectric devices based on them and their use in medicine confirm their efficiency. However, thermoelectric medical devices have certain disadvantages. The main one is the lack of ability to manage cooling and heating processes in time. This significantly narrows the possibilities of heat and cold treatment.

Studies show that cooling rates play an important role in treatment [4 – 13]. Very fast cooling does not lead to the destruction of the biological tissues at all. On the contrary, moderate but cyclic cooling promotes effective destruction of tumours. Therefore, the time functions of cooling and heating are vital in the treatment of various diseases.

Thus, the problem lies in the necessity to create scientific fundamentals for the development and creation of thermoelectric medical devices of a new generation, allowing to reproduce the specified heating and cooling functions in the biological tissue. It should be noted that in most cases it is quite difficult to control the cyclic processes of heating and cooling of the biological tissue, therefore it is necessary to be able to predict the depth of heating and freezing of skin layers under a given temperature effect at different moments in time.

Therefore, *the purpose of the work* is to determine, using computer simulation, the temperature distribution in the layers of the human skin in dynamic mode under a given cyclic effect.

## 1. Physical model

According to the physical 2D model with axial symmetry (Fig. 1), a section of the biological tissue of the human body is a structure of three layers of skin (epidermis 1, dermis 2, subcutaneous layer 3) and internal biological tissue 4 and is characterized by the following thermophysical properties [14 – 20]: thermal conductivity $\kappa_i$, specific heat $C_i$,, density $\rho_i$, blood perfusion rate $\omega_{bi}$, blood density $\rho_b$, blood temperature $T_b$, blood heat capacity $C_b$ and specific heat release $Q_{meti}$ due to metabolic processes and latent heat of phase transition $L$. The thermophysical properties of the skin and the biological tissue of the human body in normal [21 – 25] and frozen states [26, 27] are shown in Tables 1, 2. The corresponding layers of the biological tissue 1 – 4 are considered as volume sources of heat $q_i$, where:

$$q_i = Q_{meti} + \rho_b \cdot C_b \cdot \omega_{bi} \cdot (T_b - T), \quad i = 1..4 . \tag{1}$$

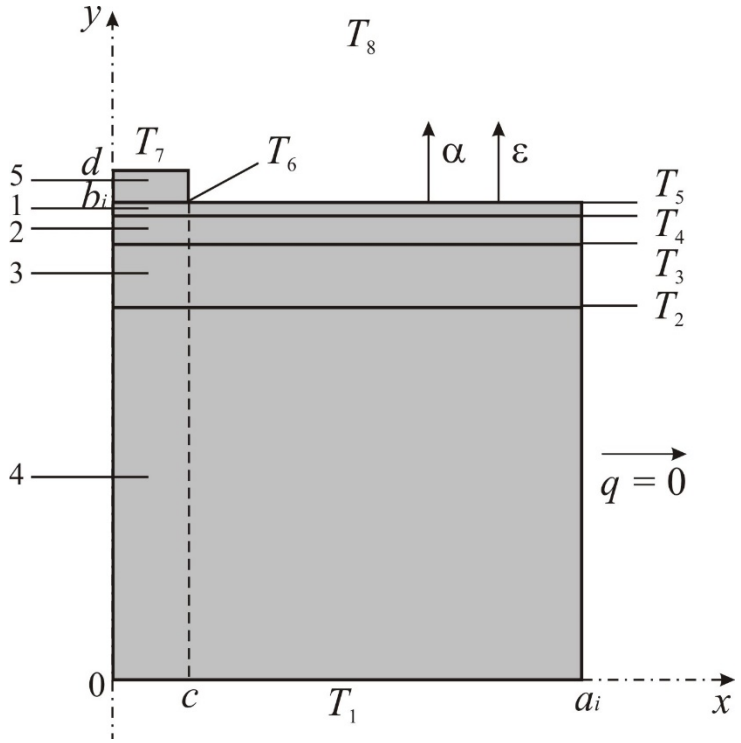


*Fig. 1. Physical 2D model of the human skin with axial symmetry: 1 – epidermis, 2 – dermis, 3 – subcutaneous layer, 4 – internal biological tissue, 5 – working tool.*

The geometric dimensions of each such layer 1 – 4 are $a$, $b$. On the surface of the skin there is a round working tool 5, the geometric dimensions of which are as follows: thickness $d$ = 1 mm and

diameter $c$ = 10 mm. According to medical recommendations and analysis of known cryoprobes used for cryodestruction, it was determined that the diameter of such probes is from 5 mm to 15 mm [28]. Therefore, in this paper, as an example, the average value of the diameter of the probe, which is $c$ = 10 mm, is taken. The temperatures at the boundaries of the corresponding layers 1 – 4 and the working tool 5 are $T_1$, $T_2$, $T_3$, $T_4$, $T_5$, $T_6$. The temperature inside the biological tissue is $T_1$ = + 37 °C. The temperature of the working tool varies in the range – $T_7$ = [- 50 ÷ + 50] °C. The ambient temperature is $T_8$ = + 22 °C. The surface of the human skin with temperature $T_6$ is in a state of heat exchange with the environment (heat exchange coefficient α and radiation coefficient ε) at temperature $T_8$. The side surface of the skin is adiabatically insulated.

*Table 1*

*Thermophysical properties of the biological tissue of the human body [21 – 25]*

| Biological tissue layers | Epidermis | Dermis | Subcutaneous layers | Internal tissue |
|---|---|---|---|---|
| Thickness, $l$ (mm) | 0.08 | 2 | 10 | 30 |
| Specific heat, $C$ ($J \cdot kg^{-1} \cdot K^{-1}$) | 3590 | 3300 | 2500 | 4000 |
| Thermal conductivity, κ ($W \cdot m^{-1} \cdot K^{-1}$) | 0.24 | 0.45 | 0.19 | 0.5 |
| Density, ρ ($kg \cdot m^{-3}$) | 1200 | 1200 | 1000 | 1000 |
| Metabolism, $Q_{met}$ ($W/m^3$) | 368 | 368 | 368 | 368 |
| Blood perfusion rate, $\omega_b$ (ml/s·ml) | 0 | 0.0005 | 0.0005 | 0.0005 |
| Blood density, $\rho_b$ ($kg \cdot m^{-3}$) | 1060 | 1060 | 1060 | 1060 |
| Blood heat capacity, $C_b$ ($J \cdot kg^{-1} \cdot K^{-1}$) | 3770 | 3770 | 3770 | 3770 |

*Table 2*

*Thermophysical properties of the biological tissue of the human body in the normal and frozen states [26, 27]*

| Thermophysical properties of the biological tissue | Value | Units of measurement |
|---|---|---|
| Heat capacity of normal biological tissue ($C_1$) | 3600 | $J/m^3$ °C |
| Heat capacity of frozen biological tissue ($C_2$) | 1800 | $J/m^3$ °C |
| Thermal conductivity of normal biological tissue ($\kappa_1$) | 0.5 | W/m °C |
| Thermal conductivity of frozen biological tissue ($\kappa_2$) | 2 | W/m °C |
| Latent heat of phase transition ($L$) | $250 \cdot 10^3$ | $J/m^3$ |
| Upper temperature of phase transition ($T_1$) | – 1 | °C |
| Lower temperature of phase transition ($T_2$) | – 8 | °C |

In this model, the thermal contact resistance between the working tool and the human skin is not taken into account, since it is estimated to be insignificant and equals $R_c = 2 \cdot 10^{-3}$ m$^2$·K/W [29].

## 2. Mathematical model

In its general form, the equation of heat exchange in the biological tissue is given by [30]:

$$C_i \cdot \frac{\partial T}{\partial t} = \nabla \cdot (\kappa_i \cdot \nabla T) + \rho_b \cdot C_b \cdot \omega_{bi} \cdot (T_b - T) + Q_{meti}, \quad i = 1..4, \tag{2}$$

where $C_i$, $\kappa_i$ are specific heat and thermal conductivity of corresponding skin layers, $\rho_b$ is blood density, $C_b$ is specific heat of blood, $\omega_{bi}$ is blood perfusion of corresponding layers, $T_b$ is blood temperature, $T$ is temperature of the biological tissue; $Q_{meti}$ is heat released due to metabolic processes in each layer.

The term on the left side of equation (2) represents the rate of change of thermal energy contained in a unit volume of the biological tissue. The three terms on the right side of this equation represent, respectively, the rate of change of thermal energy due to thermal conductivity, blood perfusion, and metabolic heat.

The equation of heat exchange in the biological tissue (2) is solved with the appropriate boundary conditions. The temperature on the surface of the working tool changes according to a given law in the temperature range $T_7$ = [– 50 ÷ + 50] °C. Inside the biological tissue, the temperature $T_1$ = + 37 °C. The side surfaces of the biological tissue are adiabatically isolated ($q$ = 0), and the upper surface of the skin is in a state of heat exchange (heat exchange coefficient α and radiation coefficient ε) with the environment at temperature $T_8$.

$$q_i(x,y,t)\Big|_{\substack{c \le x \le a \\ y = b_i}} = \alpha \cdot (T_8 - T_5) + \varepsilon \cdot \sigma \cdot (T_8^4 - T_5^4), \tag{3}$$

where $q_i(x,y,t)$ is the heat flux density of the i-th layer of the human skin, α is the convective heat exchange coefficient of the skin surface with the environment, $\varepsilon$ is the radiation coefficient,
σ is the Boltzmann constant, $T_5$ is the surface temperature of the human skin, $T_8$ is the ambient temperature ($T_8$ = + 22 °C).

At the initial time moment $t$ = 0 s it is assumed that the temperature in the entire skin volume is $T$ = + 37 °C, i.e. the initial conditions for solving equation (2) are as follows:

$$T_i(x, y, 0) = T_b, \qquad i = 1,...,4. \tag{4}$$

As a result of solving the initial-boundary problem (2)–(4), the distributions of temperature $T_i(x,y,t)$ and heat fluxes $q_i(x,y,t)$ in the corresponding layers of the skin at an arbitrary moment in time are determined. As an example, this paper considers the case in which the temperature of the working tool changes according to a given law in the temperature range $T_7$ = [– 50 ÷ + 50] °C. However, it should be noted that the proposed technique allows considering cases when the temperature of the working tool $T_f(t)$ changes in any temperature range or according to a predetermined function.

In the process of freezing, the cells will undergo a phase change at the freezing point, while the heat loss of the phase transition ($L$) will occur and the temperature in these cells will not change. The

phase transition in the biological cells occurs in the temperature range (– 1 ÷ – 8) °C. The properties of the skin and the biological tissue in normal and frozen states are shown in Tables 1, 2 [21 – 27]. In the temperature range (– 1 ÷ – 8) °C, when the cells are frozen, the heat of the phase transition is absorbed, which can be simulated by adding the appropriate value to the heat capacity [26, 27].

When human skin freezes, the capillary vessels constrict until all the blood in the capillaries freezes, and the value tends to zero. In addition, cells will not be able to generate metabolic heat when frozen, and $Q_{met\,i}$ will be zero at sub-zero temperatures.

In the frozen state the properties of the skin and the biological tissue will have the following values (5) – (8):

$$C_i = \begin{cases} C_1 & T \geq -1°C \\ \dfrac{L}{-1-(-8)} + \dfrac{C_1 + C_2}{2} & -8°C \leq T \leq -1°C \\ C_2 & T \leq -8°C \end{cases} \tag{5}$$

$$\kappa_i = \begin{cases} \kappa_1 & T \geq -1°C \\ \dfrac{\kappa_1 + \kappa_2}{2} & -8°C \leq T \leq -1°C \\ \kappa_2 & T \leq -8°C \end{cases} \tag{6}$$

$$Q_{met_i} = \begin{cases} 368 & T \geq -1°C \\ 0 & -8°C \leq T \leq -1°C \\ 0 & T \leq -8°C \end{cases} \tag{7}$$

$$\omega_{b_i} = \begin{cases} 0.0005 & T \geq -1°C \\ 0 & -8°C \leq T \leq -1°C \\ 0 & T \leq -8°C \end{cases} \tag{8}$$

## 3. Computer model

A three-dimensional computer model of the biological tissue was created in a cylindrical coordinate system, on the surface of which a medical working tool is located. The Comsol Multiphysics package of application programs [31], was used to build a computer model, which makes it possible to simulate thermophysical processes in the biological tissue, taking into account blood circulation, heat exchange, metabolic processes, and the phase transition.

The calculation of temperature distributions and heat flux density in the biological tissue was carried out using the finite element method, the essence of which is that the object under study is divided into a large number of finite elements and in each of them the value of the function is sought that satisfies the specified second-order differential equations with the corresponding boundary conditions. The accuracy of the solution to the problem depends on the level of division and is ensured by using a large number of finite elements [31].

As an example, Figs. 3 – 10 show the distribution of temperature and isothermal surfaces in the volume of the human skin, on the surface of which the working tool is placed, the temperature of which

changes cyclically according to a predetermined law in the temperature range [-50 ÷ +50] °C at different moments of time.

## 4. Results of computer simulation of cyclic temperature effects on the human skin in dynamic mode

According to known methods of cryodestruction and coagulation of the biological tissue [10, 11] the cooling rate should be at least (40 – 50) °C/min, and the heating rate should be (20 – 25) °C/min. Therefore, in this paper, as an example, we consider a case in which the temperature of the working tool $T_f(t)$ changes in the range of operating temperatures [– 50 ÷ + 50]°C as follows: first, cryodestruction of the skin is carried out with a cooled working tool at a temperature of $T$ = – 50 °C for $t$ = 120 s, then the temperature of the working tool changes from *-50°C* to *+50°C* for the next 240 s, after that, skin coagulation is performed with a heated working tool at temperature $T$ = + 50 °C for $t$ = 120 s, the next temperature decrease to $T$ = – 50 °C occurs for 120 s, then this temperature effect is repeated cyclically to achieve better destruction of the human skin. The specified cyclic temperature effect on the human skin is presented in Fig. 2.

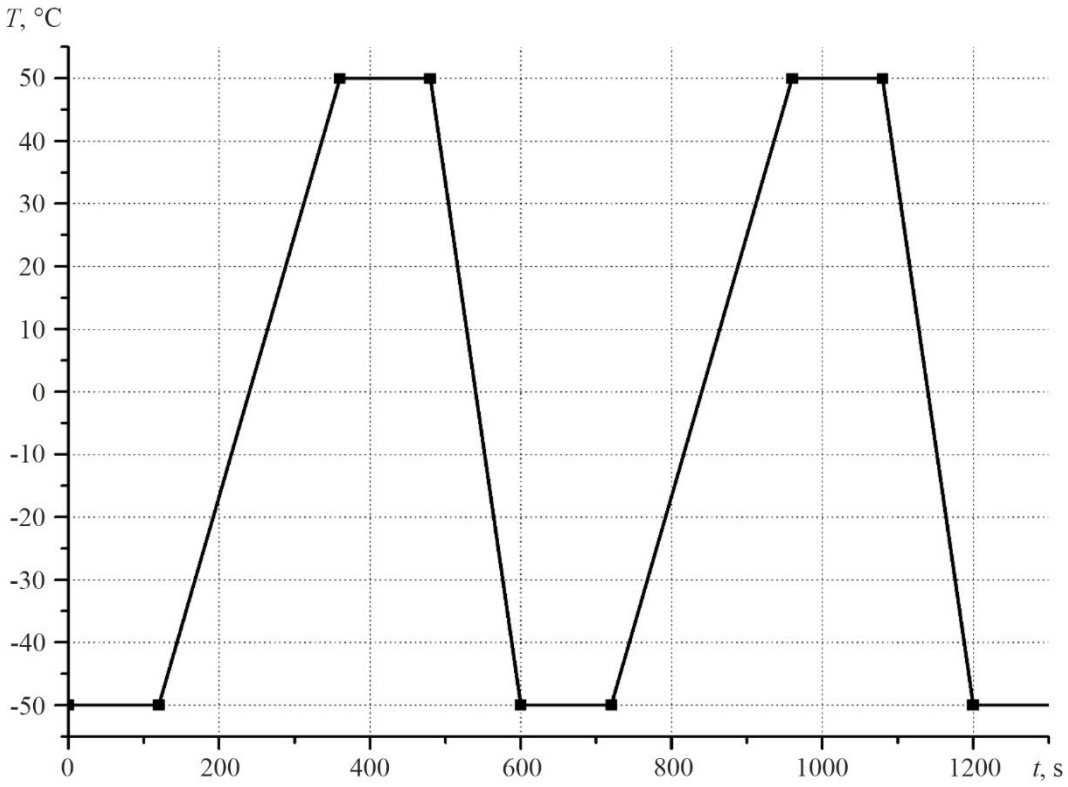


*Fig. 2. Dependence of the working tool temperature on time.*

Figs.3-10 show the distribution of temperature and isothermal surfaces in a cross-section of the biological tissue, on the surface of which the working tool is placed, the temperature of which changes according to the above law in the range of working temperatures [– 50 ÷ + 50]°C at the initial and final moments of the cooling-heating cycle.

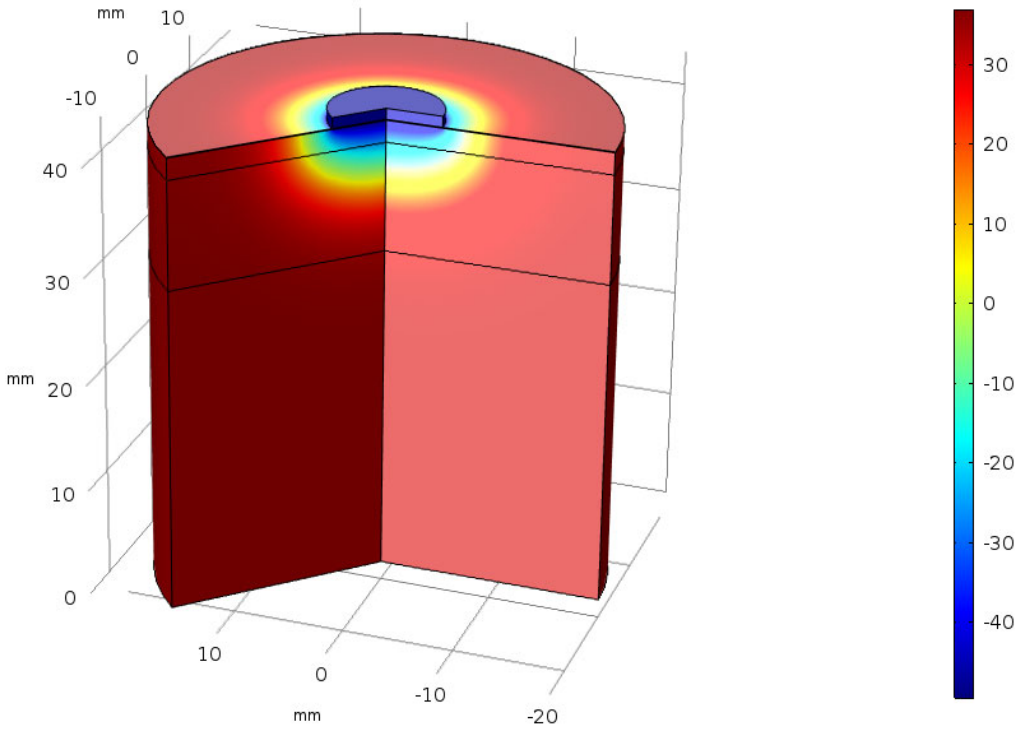


*Fig. 3. Temperature distribution in the volume of the skin on the surface of which the working tool is placed at a temperature of T=-50°C at the moment of time t=120 s*

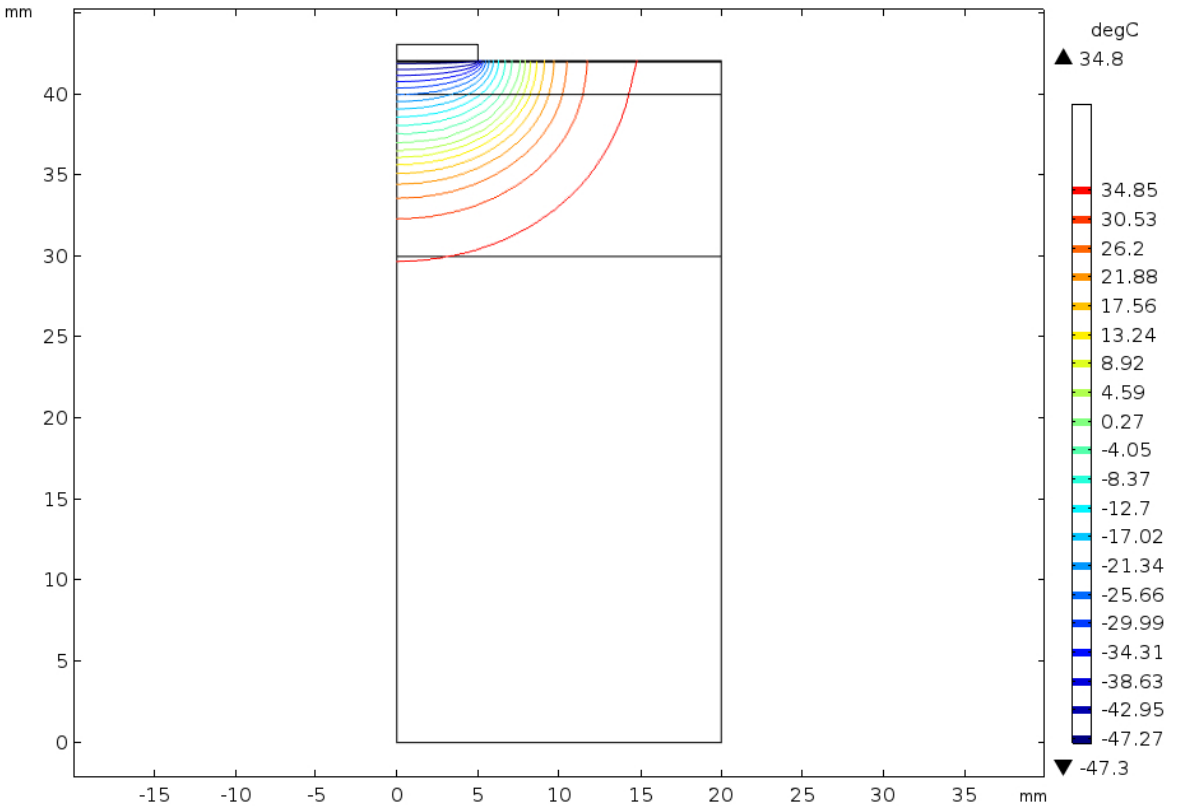


*Fig.4. Distribution of isothermal surfaces in the volume of the skin on the surface of which the working tool is placed at a temperature of T = – 50 °C at the moment of time t = 120 s.*

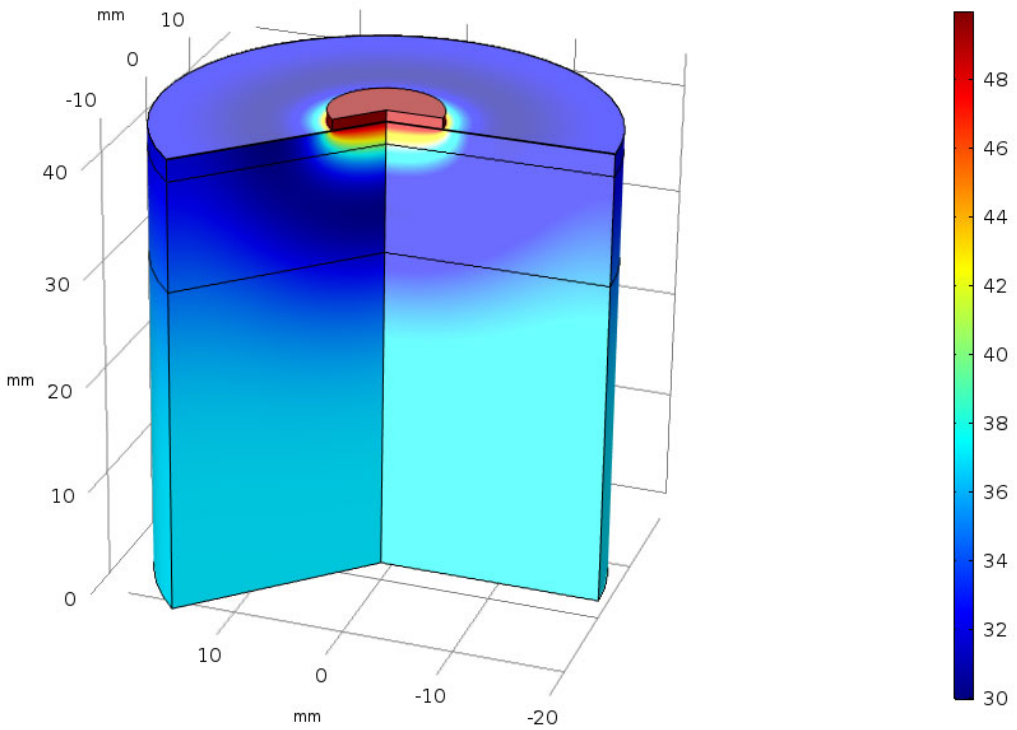


*Fig. 5. Temperature distribution in the volume of the skin on the surface of which the working tool is placed at a temperature of T = + 50 °C at the moment of time t = 480 s.*

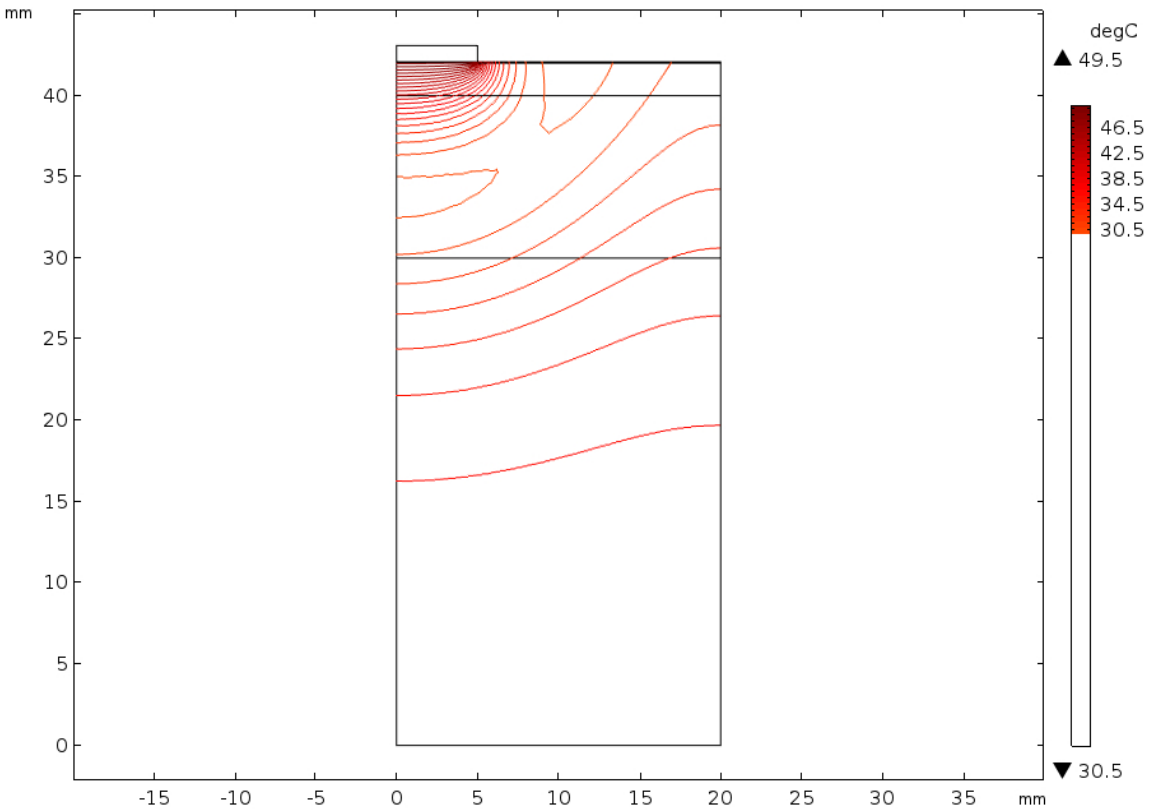


*Fig. 6. Distribution of isothermal surfaces in the volume of the skin on the surface of which the working tool is placed at a temperature of T = + 50 °C at the moment of time t = 480 s.*

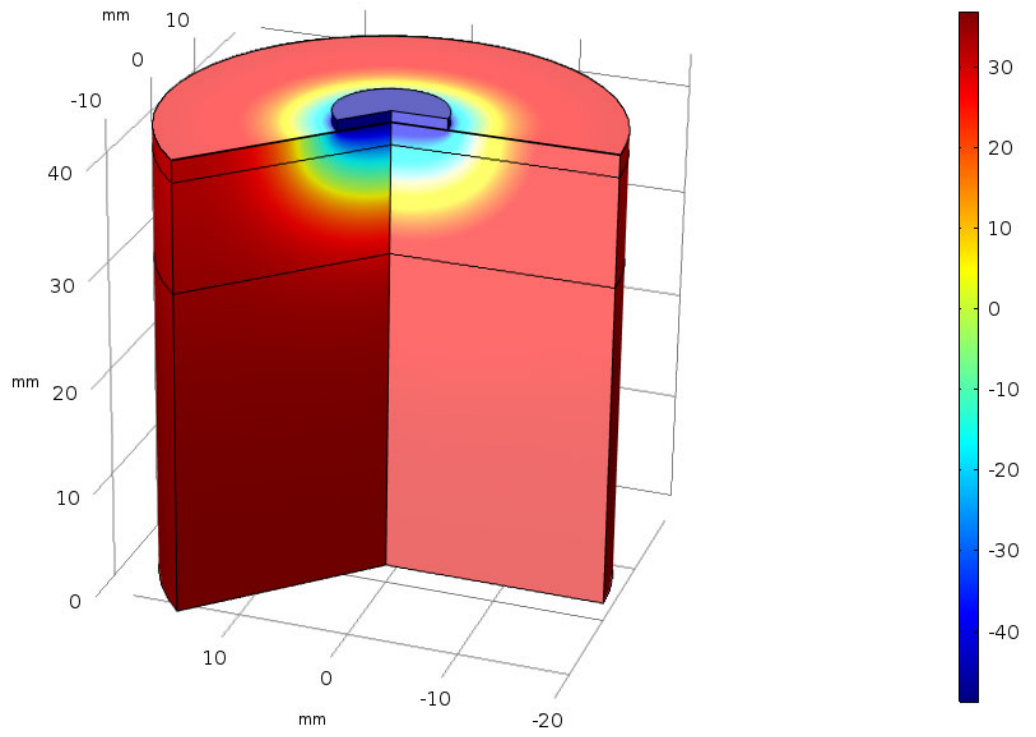


*Fig. 7. Temperature distribution in the volume of the skin on the surface of which the working tool is paced at a temperature of T = – 50 °C at the moment of time t = 720 s.*

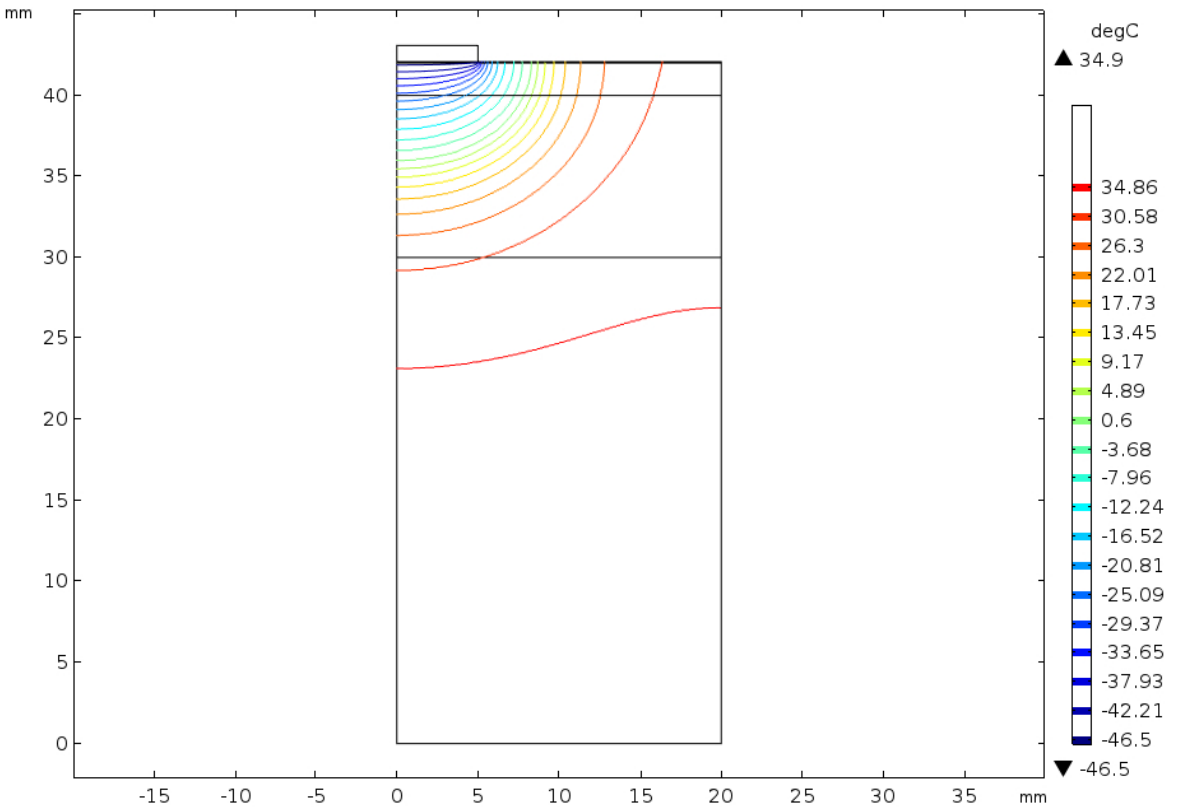


*Fig. 8. Distribution of isothermal surfaces in the volume of skin on the surface of which a working tool is placed at a temperature of T = – 50°C at the moment of time t = 720 s.*

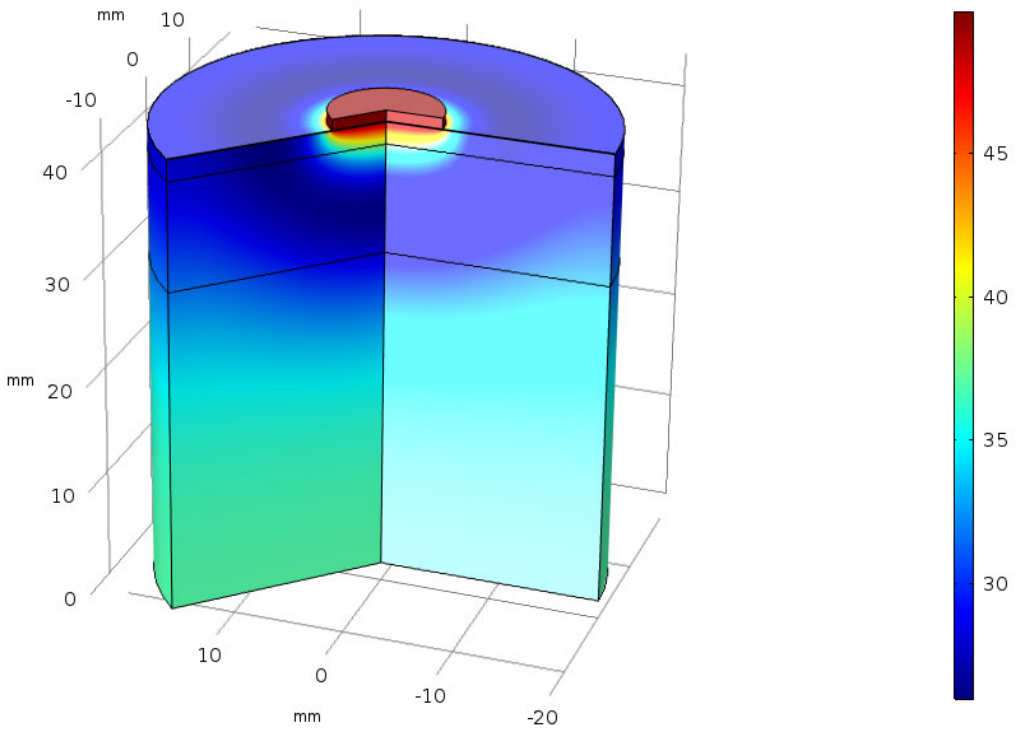


*Fig. 9. Temperature distribution in the volume of the skin on the surface of which the working tool is placed at a temperature of T = + 50°C at the moment of time t = 1080 s.*

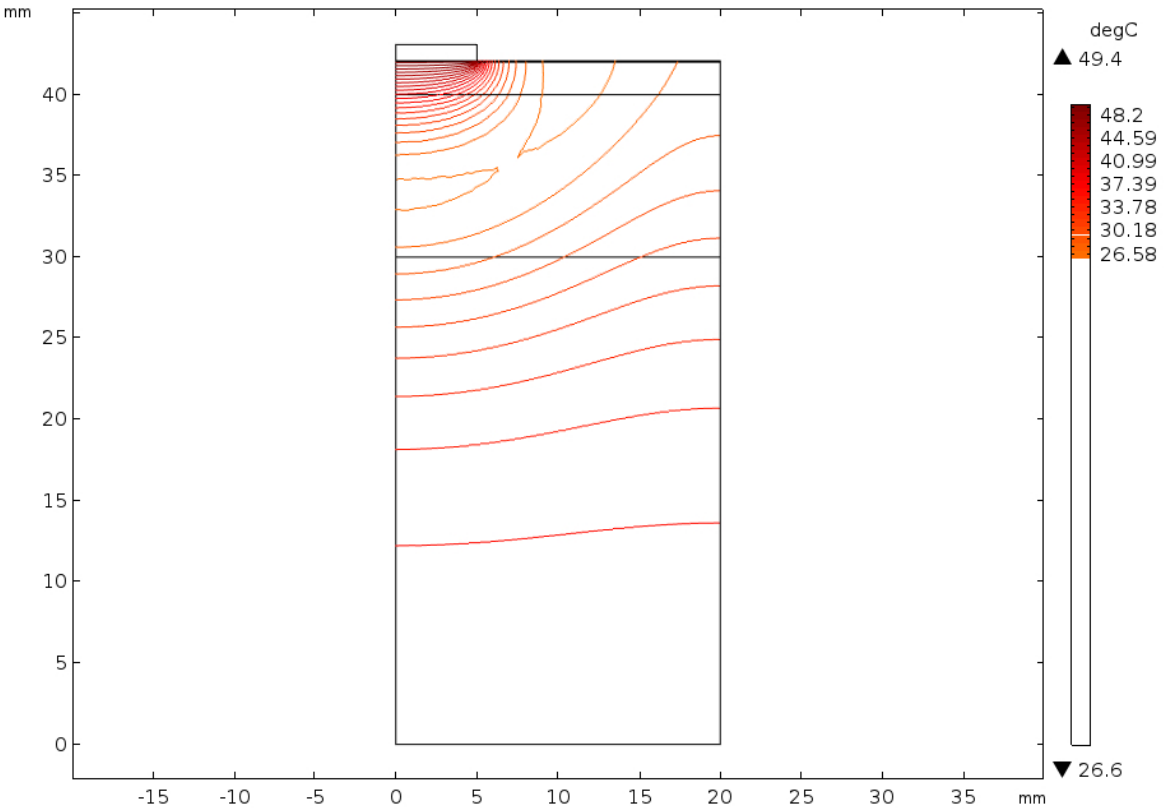


*Fig. 10. Distribution of isothermal surfaces in the volume of the skin on the surface of which the working tool is paced at a temperature of T = + 50 °C at the moment of time t = 1080 s.*

From Figs. 3 – 6 it can be seen that at $t = 120$ s the epidermis cools to a temperature of – 48.9 °C, at the epidermis-dermis boundary the temperature is – 48.3 °C, at the dermis-subcutaneous-fat tissue boundary the temperature is – 25.5 °C. And at $t = 480$ s, the temperature in the epidermis rises to + 49.8 °C, at the epidermis-dermis boundary the temperature is + 49.5 °C, at the dermis-subcutaneous-fat tissue boundary the temperature is + 40.3 °C. Since the upper layer of the skin (epidermis) has the smallest thickness and blood perfusion in it $\omega_b = 0$, the temperature inside this layer is close to the temperature of the working tool. Subsequently, with repeated cyclic temperature exposure (Figs. 7 – 10), it is observed that at $t = 720$ s after cooling, the temperature inside the skin, for example, at the dermis-subcutaneous-fat tissue boundary reaches – 28 °C, and at $t = 1080$ s after reheating, the temperature at the dermis-subcutaneous-fat tissue boundary is + 38 °C.

Computer simulation has shown that with an increase in the exposure (number of cycles) of temperature effect, deeper cooling of the skin layers and approximately equal heating of the skin are achieved. That is, with prolonged temperature effect in the range of [– 50 ÷ + 50] °C, it is possible to achieve destruction and coagulation of superficial skin neoplasms.

Thus, the obtained results allow predicting the depth of freezing and warming of the layers of the human skin with a given cyclic temperature exposure in order to achieve the maximum effect when performing cryodestruction or coagulation. The developed technique of computer simulation in dynamic mode makes it possible to determine temperature distributions in different layers of the human skin with a predetermined arbitrary function of temperature change of the working tool with time $T_f(t)$.

## Conclusions

1. A method for computer simulation of temperature distribution in the human skin in dynamic mode has been developed, allowing to predict the results of local temperature effect on the skin and determine at any moment in time the temperature distribution in the skin layers for a given time function of change in the temperature of the working tool $T_f(t)$.
2. Using computer simulation, temperature distributions in the skin layers were determined in heating and cooling modes with changes in the working tool temperature in the temperature range [– 50 ÷ + 50]°C according to a predetermined law. The results obtained make it possible to predict the depth of heating and freezing of biological tissue under a given cyclic temperature effect.

## References

1. Anatychuk L.I. (2003). *Thermoelectricity. Vol. 2. Thermoelectric power converters*. Kyiv, Chernivtsi: Institute of Thermoelectricity.
2. Anatychuk L.I., Denisenko O.I., Kobylianskyi R.R., Kadeniuk T.Ya., Perepichka M.P. (2017). Modern cryotherapy methods in dermatological practice. *Clinical and Experimental Pathology*, XVI, (59), 150 – 156.
3. Maruyama S., Nakagawa K., Takeda H. (2008). The flexible cryoprobe using Peltier effect for heat transfer control. *Journal of Biomechanical Science and Engineering*, 138 – 150.
4. Moskalyk I.A., Manyk O.M. (2013). On the use of thermoelectric cooling in the practice of cryodestruction. *J. Thermoelectricity*, 6, 84 – 92.
5. Anatychuk L.I., Denisenko O.I., Kobylianskyi R.R., Kadeniuk T.Ya. (2015). On the use of thermoelectric cooling in dermatology and cosmetology. *J. Thermoelectricity*, 3, 57 – 71.
6. Moskalyk I.A. (2015). On the use of thermoelectric devices in cryosurgery. *Physics and Chemistry*

*of the Solid State,* 4, 742 – 746.
7. Kobylianskyi R.R., Kadeniuk T.Ya. (2016). On the prospects of using thermoelectricity for treatment of skin diseases with cold. *Scientific Bulletin of Chernivtsi University: collected papers. Physics. Electronics*. 5 (1). – Chernivtsi: Chernivtsi National University, 67 – 72.
8. Miller P., Metzner D. (1969. Cryosurgery for tumors of the head and neck – *Trns. Am.Ophthalmol. Otolaringol. Soc.,* 73 (2), 300 – 309.
9. D'Hont G. (1974). La cryotherapie en ORL – *Acta. Otorhinolaringol. Belg*., 28 (2), 274 – 278.
10. Mazur P. (1968). Physical-chemical factors underlying cell injury in cryosurgical freezing. In: *Cryosurgery* ed. by R. W. Rand, A. P. Rinfret, H. Leden – Springfield, Illinois, U.S.A. 32 – 51.
11. Gill W., Fraser I. (1968). A look at cryosurgery. – *Scot, Med,* I., 13, 268– 273.
12. Van Venrjy G. (1975). Freeze-etching: freezing velocity and crystal size at different size locations in samples. *Cryobiology*, 2 (1), 46 – 61.
13. Bause H. (2004). Kryotherapie lokalisierter klassischer, Neues Verfahren mit Peltier-Elementen (– 32 °C) Erfahrungsbericht Hamangiome. *Monatsschr Kinderheilkd*, 152, 16 – 22.
14. Anatychuk L.I., Vikhor L.M., Kotsur M.P., Kobylianskyi R.R., Kadeniuk T.Ya. (2016). Optimal control of the time dependence of cooling temperature in thermoelectric devices. *J. Thermoelectricity,* 5, 5 – 11.
15. Anatychuk L.I., Kobylianskyi R.R., Kadeniuk T.Ya. (2017). Computer simulation of local thermal effect on the human skin. *J. Thermoelectricity*, 1, 69 – 79.
16. Anatychuk L.I., Vikhor L.M., Kobylianskyi R.R., Kadeniuk T.Ya. (2017). Computer simulation and optimization of the dynamic operating modes of a thermoelectric device for treatment of skin diseases. *J. Thermoelectricity*, 2, 44 – 57.
17. Anatychuk L.I., Vikhor L.M., Kobylianskyi R.R., Kadeniuk T.Ya., Zvarich O.V.(2017). Computet simulation and optimization of the dynamic operating modes of a thermoelectric device for reflexotherapy. *J. Thermoelectricity*, 3, 68 – 78.
18. Anatychuk L., Vikhor L., Kotsur M., Kobylianskyi R., Kadeniuk T. (2018). Optimal control of time dependence of temperature in thermoelectric devices for medical purposes. *International Journal of Thermophysics*, 39, 108. https://doi.org/10.1007/s10765-018-2430-z.
19. Anatychuk L.I., Kobylianskyi R.R., Fedoriv R.V. (2019). Methodology for taking into account the phase transition in the biological tissue during computer simulation of cryodestruction process. *J. Thermoelectricity*, 1, 46 – 58.
20. Anatychuk L.I., Kobylianskyi R.R., Fedoriv R.V. (2019). Computer simulation of cryodestruction process of the human skin with thermoelectric cooling. *J. Thermoelectricity*, 2, 21 – 35.
21. Jiang S.C., Ma N., Li H.J., Zhang X.X. (2002). Effects of thermal properties and geometrical dimensions on skin burn injuries. *Burns*, 28, 713 – 717.
22. Cetingul M.P., Herman C. (2008). Identification of skin lesions from the transient thermal response using infrared imaging technique. *IEEE*, 1219 – 1222.
23. Ciesielski M., Mochnacki B., Szopa R. (2011). Numerical modeling of biological tissue heating. Admissible thermal dose. *Scientific Research of the Institute of Mathematics and Computer Science*, 1 (10), 11 – 20.
24. Filipoiu Florin, Bogdan Andrei Ioan, Carstea Iulia Maria (2010). Computer-aided analysis of the heat transfer in skin tissue. *Proceedings of the 3rd WSEAS Int. Conference on Finite Differences* – Finite Elements – Finite Volumes – Boundary Elements, 53 – 59.
25. Carstea Daniela, Carstea Ion, Carstea Iulia Maria (2011). Interdisciplinarity in computer-aided analysis of thermal therapies. *WSEAS Transactions on Systems and Control*, 6 (4), 115 – 124.

26. Deng Z.S., Liu J. (2005). Numerical simulation of selective freezing of target biological tissues following injection of solutions with specific thermal properties. *Cryobiology*, 50, 183 - 192.
27. Han Liang Lim, Venmathi Gunasekaran (2011). *Mathematical modeling of heat distribution during cryosurgery.* https://isn.ucsd.edu/last/courses/beng221/problems/2011/project10.pdf.
28. Shah Vishal N., Orlov Oleg I, Orlov Cinthia, Takebe Manabu, Thomas Matthew, and Plestis Konstadinos (2018). Combined cryo-maze procedure and mitral valve repair through a ministernotomy. *Multimed Man Cardiothorac Surg*. doi: 10.1510/mmcts.2018.022.
29. Rykaczewski Konrad (2019). Modeling thermal contact resistance at the finger-object interface. *Temperature*, 6 (1), 85 – 95.
30. Pennes H.H. (1948). Analysis of tissue and arterial blood temperatures in the resting forearm *J. Appl. Physiol*. 1 (2), 93 – 122.
31. COMSOL Multiphysics User's Guide (2010). COMSOLAB.

Subminitted: 11.02.2022.

**Анатичук Л.І.,** *акад. НАН України* [1,2]
**Кобилянський Р.Р.,** *канд. фіз.-мат. наук* [1,2]
**Прибила А.В.,** *канд. фіз.-мат. наук* [1,2]
**Константинович І.А.,** *канд. фіз.-мат. наук* [1,2]
**Бойчук В.В.** [2]

[1] Інститут термоелектрики НАН та МОН України,
вул. Науки, 1, Чернівці, 58029, Україна;
[2] Чернівецький національний університет імені Юрія Федьковича,
вул. Коцюбинського 2, Чернівці, 58012, Україна
*e-mail: anatych@gmail.com*

## КОМП'ЮТЕРНЕ МОДЕЛЮВАННЯ ТЕРМОЕЛЕКТРИЧНОГО СЕНСОРА ТЕПЛОВОГО ПОТОКУ НА ПОВЕРХНІ ТІЛА ЛЮДИНИ

*У роботі представлено результати комп'ютерного моделювання циклічного температурного впливу на шкіру людини у динамічному режимі. Побудовано тривимірну комп'ютерну модель біологічної тканини з врахуванням теплофізичних процесів, кровообігу, теплообміну, процесів метаболізму та фазового переходу. Як приклад, розглянуто випадок, коли на поверхні шкіри знаходиться робочий інструмент, температура якого змінюється циклічно за наперед заданим законом у діапазоні температур [-50 ÷ +50] °C. Визначено розподіли температури у різних шарах шкіри людини в режимах охолодження та нагріву. Отримані результати дають можливість прогнозувати глибину промерзання і прогрівання біологічної тканини при заданому температурному впливі.*

**Ключові слова:** температурний вплив, шкіра людини, динамічний режим, комп'ютерне моделювання.

### Література

1. Анатичук Л.І. Термоелектрика. Т.2. Термоелектричні перетворювачі енергії. Київ, Чернівці: Інститут термоелектрики, 2003. – 376 с.

2. Анатичук Л.І., Денисенко О.І., Кобилянський Р.Р., Каденюк Т.Я., Перепічка М.П. Сучасні методи кріотерапії в дерматологічній практиці // Клінічна та експериментальна патологія. – Том XVI. – №1 (59). – 2017. – С. 150 – 156.
3. Maruyama S., Nakagawa K., Takeda H. (2008). The flexible cryoprobe using Peltier effect for heat transfer control. *Journal of Biomechanical Science and Engineering*, 138 – 150.
4. Москалик І.А., Маник О.М. Про використання термоелектричного охолодження у практиці кріодеструкції // Термоелектрика. − № 6. – 2013. – С. 84 – 92.
5. Анатичук Л.І., Денисенко О.І., Кобилянський Р.Р., Каденюк Т.Я. Про використання термоелектричного охолодження в дерматології та косметології // Термоелектрика. − №3. – 2015. – С. 57 – 71.
6. Москалик І.А. Про використання термоелектричних приладів у кріохірургії // Фізика і хімія твердого тіла. – №4. – 2015. – С. 742 – 746.
7. Кобилянський Р.Р., Каденюк Т.Я. Про перспективи використання термоелектрики для лікування захворювань шкіри холодом // Науковий вісник Чернівецького університету: збірник наук. праць. Фізика. Електроніка. – Т. 5, Вип. 1. – Чернівці: Чернівецький національний університет, 2016. – С. 67 – 72.
8. Miller P., Metzner D. (1969. Cryosurgery for tumors of the head and neck – *Trns. Am.Ophthalmol. Otolaringol. Soc.,* 73 (2), 300 – 309.
9. D'Hont G. (1974). La cryotherapie en ORL – *Acta. Otorhinolaringol. Belg*., 28 (2), 274 – 278.
10. Mazur P. (1968). Physical-chemical factors underlying cell injury in cryosurgical freezing. In: *Cryosurgery* ed. by R. W. Rand, A. P. Rinfret, H. Leden – Springfield, Illinois, U.S.A. 32 – 51.
11. Gill W., Fraser I. (1968). A look at cryosurgery. – *Scot, Med,* I., 13, 268– 273.
12. Van Venrjy G. (1975). Freeze-etching: freezing velocity and crystal size at different size locations in samples. *Cryobiology*, 2 (1), 46 – 61.
13. Bause H. (2004). Kryotherapie lokalisierter klassischer, Neues Verfahren mit Peltier-Elementen (– 32 °C) Erfahrungsbericht Hamangiome. *Monatsschr Kinderheilkd*, 152, 16 – 22.
14. Анатичук Л.І., Вихор Л.М., Коцур М.П., Кобилянський Р.Р., Каденюк Т.Я. Оптимальне керування часовою залежністю температури охолодження в термоелектричних пристроях // Термоелектрика. − № 5. – 2016. – С. 5 – 11.
15. Анатичук Л.І., Кобилянський Р.Р., Каденюк Т.Я. Комп'ютерне моделювання локального теплового впливу на шкіру людини // Термоелектрика. − № 1. – 2017. – С.69 – 79.
16. Анатичук Л.І., Вихор Л.М., Кобилянський Р.Р., Каденюк Т.Я. Комп'ютерне моделювання та оптимізація динамічних режимів роботи термоелектричного приладу для лікування захворювань шкіри // Термоелектрика. − № 2. – 2017. – С.44 – 57.
17. Анатичук Л.І., Вихор Л.М., Кобилянський Р.Р., Каденюк Т.Я., Зварич О.В. Комп'ютерне моделювання та оптимізація динамічних режимів роботи термоелектричного приладу для рефлексотерапії // Термоелектрика. − № 3. – 2017. – С. 68 – 78.
18. Anatychuk L., Vikhor L., Kotsur M., Kobylianskyi R., Kadeniuk T. (2018). Optimal control of time dependence of temperature in thermoelectric devices for medical purposes. *International Journal of Thermophysics*, 39, 108. https://doi.org/10.1007/s10765-018-2430-z.
19. Анатичук Л.І., Кобилянський Р.Р., Федорів Р.В. Методика врахування фазового переходу в біологічній тканині при комп'ютерному моделюванні процесу кріодеструкції // Термоелектрика. − № 1. – 2019. – С. 46-58.
20. Анатичук Л.І., Кобилянський Р.Р., Федорів Р.В. Комп'ютерне моделювання процесу кріодеструкції шкіри людини при термоелектричному охолодженні // Термоелектрика. −

№ 2. – 2019. – С. 21-35.

21. Jiang S.C., Ma N., Li H.J., Zhang X.X. (2002). Effects of thermal properties and geometrical dimensions on skin burn injuries. *Burns*, 28, 713 – 717.
22. Cetingul M.P., Herman C. (2008). Identification of skin lesions from the transient thermal response using infrared imaging technique. *IEEE*, 1219 – 1222.
23. Ciesielski M., Mochnacki B., Szopa R. (2011). Numerical modeling of biological tissue heating. Admissible thermal dose. *Scientific Research of the Institute of Mathematics and Computer Science*, 1 (10), 11 – 20.
24. Filipoiu Florin, Bogdan Andrei Ioan, Carstea Iulia Maria (2010). Computer-aided analysis of the heat transfer in skin tissue. *Proceedings of the 3rd WSEAS Int. Conference on Finite Differences* – Finite Elements – Finite Volumes – Boundary Elements, 53 – 59.
25. Carstea Daniela, Carstea Ion, Carstea Iulia Maria (2011). Interdisciplinarity in computer-aided analysis of thermal therapies. *WSEAS Transactions on Systems and Control*, 6 (4), 115 – 124.
26. Deng Z.S., Liu J. (2005). Numerical simulation of selective freezing of target biological tissues following injection of solutions with specific thermal properties. *Cryobiology*, 50, 183 - 192.
27. Han Liang Lim, Venmathi Gunasekaran (2011). *Mathematical modeling of heat distribution during cryosurgery.* https://isn.ucsd.edu/last/courses/beng221/problems/2011/project10.pdf.
28. Shah Vishal N., Orlov Oleg I, Orlov Cinthia, Takebe Manabu, Thomas Matthew, and Plestis Konstadinos (2018). Combined cryo-maze procedure and mitral valve repair through a ministernotomy. *Multimed Man Cardiothorac Surg*. doi: 10.1510/mmcts.2018.022.
29. Rykaczewski Konrad (2019). Modeling thermal contact resistance at the finger-object interface. *Temperature*, 6 (1), 85 – 95.
30. Pennes H.H. (1948). Analysis of tissue and arterial blood temperatures in the resting forearm *J. Appl. Physiol*. 1 (2), 93 – 122.
31. COMSOL Multiphysics User's Guide (2010). COMSOLAB.

Надійшла до редакції: 11.02.2022.

*L.I. Anatychuk*

**L.I. Anatychuk,** *Acad. NAS Ukraine* [1,2]
**A.V. Prybyla,** *Cand. Sc (Phys &Math)* [1,2]

[1]Institute of Thermoelectricity of the NAS and MES of Ukraine,
1, Nauky str., Chernivtsi, 58029, Ukraine;
[2]Yuriy Fedkovych Chernivtsi National University,
2, Kotsiubynsky str., Chernivtsi, 58012, Ukraine
*e-mail: anatych@gmail.com*

*A.V. Prybyla*

# THERMOELECTRIC GENERATOR USING TEMPERATURE DIFFERENCES IN LUNAR SOIL

*The paper investigates the possibilities of creating a thermoelectric generator on the Moon. The temperature and thermal conditions in the lunar soil are analyzed. The specific power, weight and cost of such a generator are calculated. A thermoelectric generator and solar batteries are compared under the conditions of their use on the Moon.*

**Key words:** thermoelectric ground generator, Moon, design.

## Introduction

*General characterization of the problem*. The progress of mankind is related to constant search and improvement of technologies that provide it with new opportunities both on Earth and in the exploration of the surrounding outer space. Scientists' views have long been aimed at colonizing the nearest planets of the solar system. The first step for this is an attempt to create a space base on the surface of the nearest satellite of the Earth – the Moon.

Ensuring the operation of the lunar base is connected with the needs of its power supply with electrical energy. The main sources of energy currently known to mankind are divided into renewable - energy of the Sun, wind, hydropower of rivers, internal heat of the Earth, and non-renewable - fossil mineral fuel and nuclear energy. For obvious reasons, not all of these sources can be used on the surface of the Moon.

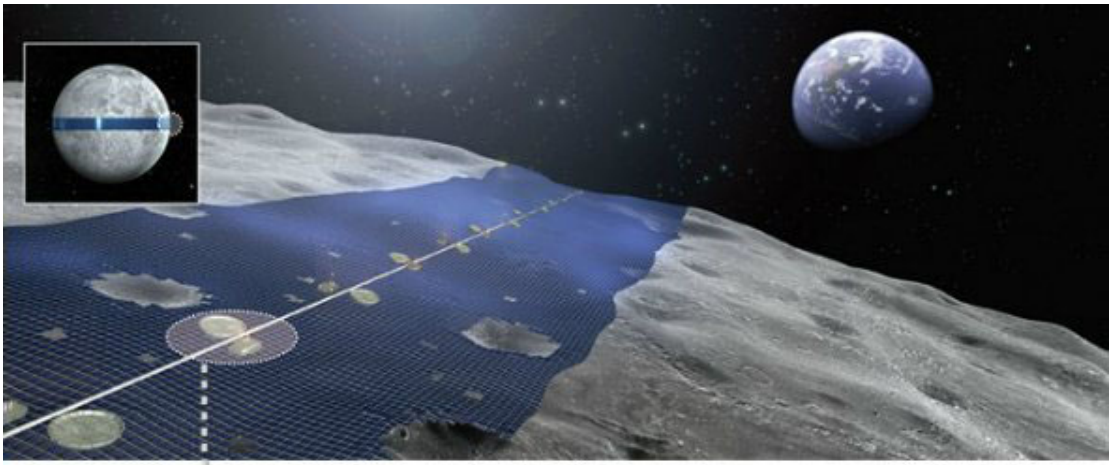

*Fig. 1. A variant of a solar power plant on the surface of the Moon, proposed by the Shimizu Corporation of Japan [1].*

One of the most interesting sources in this context is the energy of the Sun. For its conversion, solar batteries are used, which with a conversion factor of 10 – 30 % provide good opportunities for generating electrical energy (Fig. 1). However, they also have a number of disadvantages. This is, in particular, a relatively short service life, especially in conditions of harsh cosmic radiation, dependence on the presence of solar radiation (lunar "day" and "night"), as well as relatively large mass and size indicators, which significantly increases the cost of implementing such a project.

An alternative method of energy conversion is the use of temperature differences in the lunar soil, which arise as a result of the thermal action of solar radiation, through thermoelectric energy conversion [2]. Such generators have already been developed and operate in the Earth conditions [3 – 5]. They have a long service life (about 30 years), low weight and dimensions, and are also resistant to mechanical loads and cosmic radiation, which is especially important in the conditions of this task. The characteristics of such thermoelectric converters largely depend on the magnitude of the temperature difference in the soil. Under the conditions of the Moon, the temperature difference in the meter-long near-surface layer of the soil is about 164 K (surface temperature + 127 °C, temperature at a depth of 1 m – 37 °C) for the lunar "day" and 136 K (surface temperature – 173 °C, temperature at a depth of 1 m – 37 °C) for the lunar "night". These are much more favourable indicators for thermoelectricity than for similar generators on Earth (near-surface temperature differences in the Earth's soil range from several to ten degrees).

Therefore, the purpose of this work is to study the possibilities of creating a thermoelectric generator that uses differences in the lunar soil.

## Generators using temperature differences in the Earth

The Institute of Thermoelectricity of the National Academy of Sciences and the Ministry of Education and Science of Ukraine has developed a series of ground-based thermoelectric generators (GTEG), which have been successfully operating for decades and provide power to various low-power devices, including special-purpose equipment, protective and security systems, electronic devices of autonomous weather stations, etc. (Fig. 2). The specific power of such thermogenerators is about 5 W/m$^2$ at a temperature difference of < 10 K.

*Fig. 2. Appearance of GTEG Altec-8027.*

The physical model and diagram of the operating principle of a thermoelectric generator using soil thermal energy are shown in Fig. 3.

The thermoelectric generator located in the soil consists of a heat-receiving collector 1, a heat pipe 2, a highly efficient multi-element battery 3, a heat sink 4, a radiator 5, a body 6 and thermal insulation 7. The operating principle of the thermogenerator is as follows: the heat flow $q$, present in the soil, falls on the heat-receiving pad 1, is led to the hot junctions of the thermopile 3 by the heat pipe 2, is led to the radiator 5 by the heat pipe 4 and dissipates into the lower layers of the soil. To reduce heat loss, the body 6 of the thermogenerator is filled with heat-insulating material. As heat passes through the thermopile, a temperature gradient is created thereupon, which leads to the generation of electric power $W$. It should be noted that during the day, the direction of heat flow may change to the opposite. This allows you to use such a converter not only during the day, but also at night, when there is no direct flow of solar radiation to the Earth's surface.

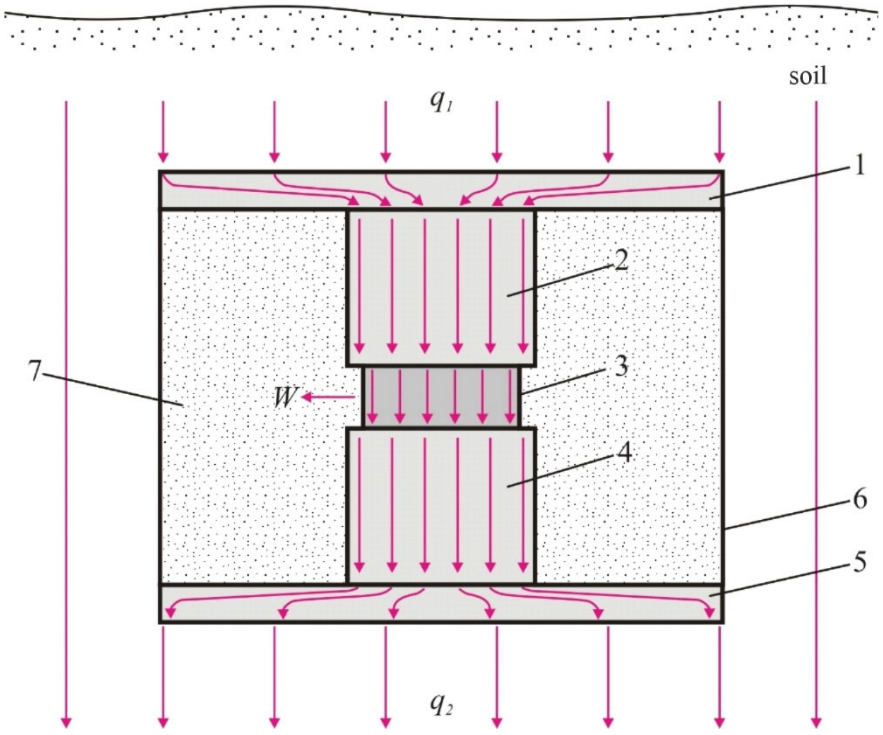


*Fig. 3. Physical model of a thermal generator located in soil.*

The specified physical model, with regard to some differences, can be used to describe a thermoelectric generator on the Moon.

## Using the idea of a ground generator on the Moon

As mentioned above, the temperature conditions in the meter-long near-surface layer of the lunar soil are as follows:

- for a lunar "day"

surface temperature + 127 °C;

temperature at a depth of 1 m – 37 °C;

- for a lunar "night"

surface temperature – 173 °C;

temperature at a depth of 1 m – 37 °C.

Such a temperature difference is favorable for thermoelectric conversion of energy, therefore, during the design of the generator, the conditions of equality of thermal resistances of GTEG and the specified layer of the lunar soil were ensured.

Fig. 4 shows a physical model of a thermoelectric generator on the surface of the Moon.

The source of heat for the generator is the flow of solar radiation $q_1$, which hits the surface of aluminum foil 1 with a special selective coating that provides the best absorption of thermal energy. The aluminum foil serves as a heat energy concentrator to the legs of thermoelectric material based on bismuth telluride (*BiTe*) *n*-2 and *p*-3 type of conductivity. The aluminum concentrator 4 serves to divert the thermal energy $q_2$ from the thermoelectric material to the lunar soil. The gap between the aluminum plates is filled with a vacuum, and heat flux $q_{loss}$ takes place in it by radiation. To reduce it, a thin mirror

plate 5 was introduced into the generator design. The figure shows an elementary section of such a generator for one pair of thermoelectric material legs.

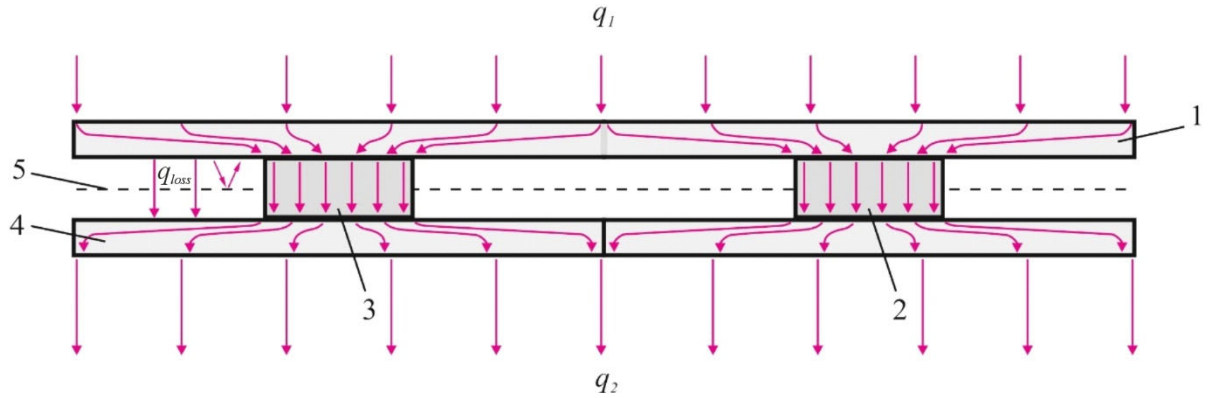


*Fig. 4. Physical model of a thermal generator located in lunar soil.*

According to the proposed physical model, the design of the generator was calculated, as well as its specific indicators. Calculations were performed using computer simulation methods using the Comsol Multiphysics application program package.

The dimensions of the heat concentrator were determined from the conditions of ensuring the uniformity of the heat flow at the minimum possible thickness. Therefore, the calculated thickness of the heat concentrator is 50 μm.

In addition, an evaluation of heat losses in the gaps between heat concentrators by radiation was carried out. They make up ~ 16 % of the amount of useful heat flow and lead to a decrease in the efficiency of energy conversion. To reduce them, a thin mirror plate (5 in Fig. 4) was introduced into the generator design, which allows to reduce losses to 7 %, and the introduction of two similar plates reduces heat losses to 5 %.

Thus, the final design of the GTEG based on 1 $m^2$ of the Moon's area is as follows:

- number of thermoelectric material legs – 3124;
- height of legs – 2 mm;
- cross section of legs – 1 x 1 mm;
- thickness of heat concentrators – 50 μm.

In this case, under the conditions of a lunar "day", the electric power generated by GTEG is $W_e$ = 96 W/$m^2$ (for comparison, the solar generator version produces electric power $W_e$ = 100 W/$m^2$).

The specific power of the generator in relation to its mass is $W_p$ = 230 W/kg (for comparison, the solar photovoltaic generator has a specific power of $W_p$ = 21 W/kg).

Consequently, in terms of energy indicator, GTEG is on the same level as photovoltaic solar, but has a 6-fold lower specific gravity, which is important given the significant costs of delivering cargo to the Moon. In addition, the operating life of the GTEG is up to 30 years, which significantly exceeds the capabilities of a solar generator, whose resource is 5 – 10 years.

In addition, unlike a photovoltaic solar generator, GTEG can be used in the conditions of the lunar "night", while the electric power generated by it will be $W_e \approx$ 10 W/$m^2$).

## Peculiarities of using the ground generator at the poles of the Moon

An important factor in the use of a thermoelectric generator on the Moon is the geographical location of the lunar base.

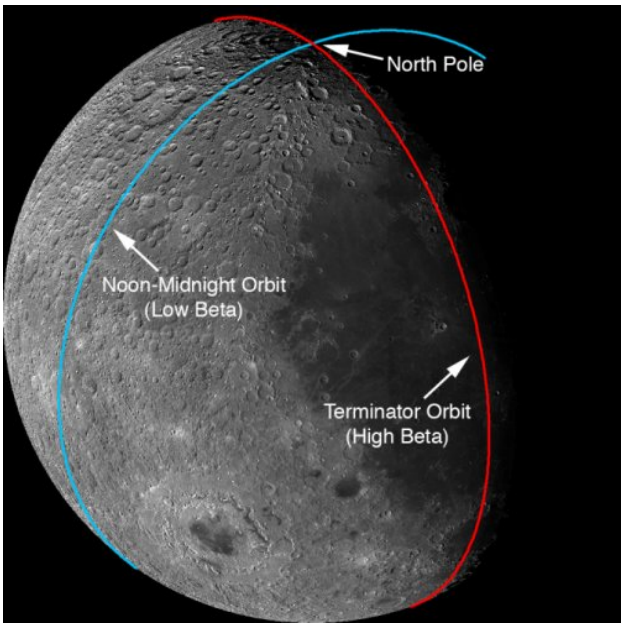


*Fig. 5. Photo of the Moon [6].*

In the case of the location of the lunar base at the poles, there are some peculiarities related to the angle of incidence of solar radiation on the surface of the Moon. The solar rays at the poles fall tangentially to the surface, which significantly changes the temperature and thermal conditions in the thickness of the lunar soil. On the other hand, lighting conditions at the poles of the Moon are more stable than in the equatorial zone.

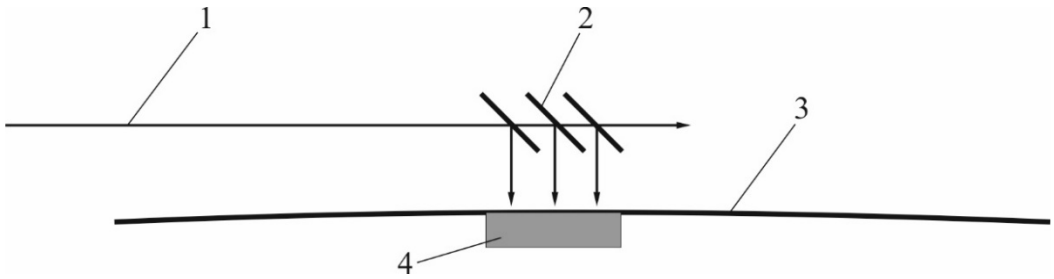


*Fig. 6. Location of a thermoelectric generator at the pole of the Moon: 1 – solar rays, 2 – guiding elements, 3 – the surface of the Moon, 4 – thermoelectric generator.*

Under such conditions, the use of the thermoelectric generator design proposed above is impossible. The way out of this situation is to use guiding elements in the GTEG design that provide the necessary conditions for the functioning of the generator. Fig. 6 shows a schematic representation of the guiding plates located on the surface of the Moon in the pole area.

## Conclusions

1. The possibility of creating a thermoelectric generator using the temperature difference in the lunar soil has been confirmed.
2. It has been calculated that under the conditions of a lunar "day" the electric power generated by the GTEG is $W_e = 96$ W/m$^2$.
3. It has been determined that the specific power of the generator in relation to its mass is $W_p = 230$ W/kg.
4. It has been established that a thermoelectric generator under lunar night conditions can develop a power of up to $W_e \approx 10$ W/m$^2$.

## References

1. https://www.shimz.co.jp.
2. Anatychuk L.I. (2005). *Thermoelectricity Vol.2 – Thermoelectric Power Converters*. Kyiv: Institute of Thermoelectricity.
3. Anatychuk L.I., Mykytiuk P.D. (2003). Thermal generators using heat flows in soils. *J. Thermoelectricity*, 3, 86 – 95.
4. Mykytiuk P.D. (2009). Thermal generators with renewable sources of thermal energy. *Autonomous Energy*, 26, 61 – 68.
5. Dudal V.O., Kuz R.V. (2016). Temperature distributions in soil and possibilities of underground thermoelectric generators. *J. Thermoelectricity*, 2, 89 – 95.
6. https://www.nasa.gov.

Subminitted: 20.01.2022.

**Анатичук Л.І.,** *акад. НАН України* [1,2]
**Прибила А.В.,** *канд. фіз.-мат. наук* [1,2]

[1] Інститут термоелектрики НАН та МОН України,
вул. Науки, 1, Чернівці, 58029, Україна;
[2] Чернівецький національний університет імені Юрія Федьковича,
вул. Коцюбинського 2, Чернівці, 58012, Україна
*e-mail: anatych@gmail.com*

# ТЕРМОЕЛЕКТРИЧНИЙ ГЕНЕРАТОР, ЩО ВИКОРИСТОВУЄ ПЕРЕПАДИ ТЕМПЕРАТУР У МІСЯЧНОМУ ГРУНТІ

*У роботі виконано дослідження можливостей створення термоелектричного генератора на Місяці. Проаналізовано температурні і теплові умови у місячному ґрунті. Розраховані питомі потужність, вагу і вартість такого генератора. Здійснено порівняння термоелектричного генератора і сонячних батарей в умовах їх використання на Місяці.*

**Ключові слова:** термоелектричний ґрунтовий генератор, Місяць, проектування.

## Література

1. https://www.shimz.co.jp.
2. L.I. Anatychuk, “Thermoelectricity Vol.2 – Thermoelectric Power Converters”, Institute of Thermoelectricity, Kyiv, 2005.
3. Анатичук Л.І. Термогенератори, що використовують теплові потоки в грунтах / Анатичук Л.І., Микитюк П.Д. // Термоелектрика. – 2003. – №3. – С. 86 – 95.
4. Микитюк П.Д. Термогенератори з відновлюваними джерелами теплової енергії / Микитюк П.Д. // Автономна енергетика. – 2009. – № 26. – С. 61 – 68.
5. Дудаль В.О. Розподіли температур у ґрунті і можливості підземних термоелектричних генераторів / Дудаль В.О., Кузь Р.В. // Термоелектрика. – 2016. – № 2. – С. 89 – 95.
6. https://www.nasa.gov.

Надійшла до редакції: 20.01.2022.

**L.I. Anatychuk,** *Acad. NAS Ukraine* [1,2]
**M.V. Havryliuk,** [1]
**V.V. Lysko,** *Cand.Sc (Phys-Math)* [1,2]

[1]Institute of Thermoelectricity of the NAS and MES of Ukraine,
1, Nauky str., Chernivtsi, 58029, Ukraine;
[2]Yuriy Fedkovych Chernivtsi National University,
2, Kotsiubynsky str., Chernivtsi, 58012, Ukraine
*e-mail: anatych@gmail.com*

# EQUIPMENT FOR DETERMINING THERMOELECTRIC PROPERTIES OF MATERIAL BY MODIFIED HARMAN'S METHOD

*The results of the development of equipment for determining the thermoelectric properties of materials – electrical conductivity, thermal conductivity, the Seebeck coefficient and thermoelectric figure of merit in the temperature range of 30 – 500 °C using modified Harman's method are presented. Measurement errors are estimated and reduction methods are described. The results of measurements of material samples based on $Bi_2Te_3$ obtained using the described equipment are shown.*

**Key words:** Harman's method, thermoelectric figure, absolute method.

## Introduction

*General characterization of the problem.* Thermoelectric energy converters find more and more applications in various fields of science and technology, in particular in medicine, metrology, space and military technology, electronics, household and computer technology, etc.

Recent years have seen increasing interest in the creation of thermoelectric generators, which are used for the conversion of heat from industry and internal combustion engines, which opens up new opportunities for "green" technologies. Special attention is drawn to the creation of TEGs on vehicles, primarily cars. The use of such thermoelectric generators allows you to get a fuel economy of 5 – 10 %. Such works are being intensively developed in the USA, Japan, and Western Europe. In doing so, the typical operating temperature range for thermoelectric energy converters is 50 – 300 °C. For this interval, materials based on *Bi-Te* are most suitable, and an additional improvement in efficiency can be achieved by using materials with programmable heterogeneity, namely functionally graded materials.

One of the main factors affecting the quality of thermoelectric energy converters is the figure of merit of thermoelectric materials they are made of. Advances in the technology of obtaining materials are directly related to the accuracy of determining their parameters, since further improvement of the quality of materials is possible only if a clear connection is established between the technological actions during the obtaining of the material and its properties.

*Analysis of the literature.* The most attractive for the creation of high-precision measuring equipment for determining the thermoelectric properties of materials are the use of the absolute method and Harman's method. The main disadvantages of the absolute method [1, 2] are the complexity of the design of the sample holder, and, therefore, the process of setting up the sample for measurement, and

the need for a long time to reach stationary mode by the system, which makes the measurement process quite long. In addition, in order to increase the accuracy of the measurements, the samples used in the measurements are quite large – with a diameter of about 6 – 8 mm and a length of 8 – 15 mm, which, when examining a large number of samples, leads to significant losses of material, in addition, reduces the speed of reaching stationary mode by the system. Harman's method is devoid of such shortcomings of the absolute method [3, 4]. Much smaller samples are used to determine thermoelectric properties by this method, and the structure of the sample holder itself is simple and convenient to use.

The essence of Harman's method is as follows. A sample of thermoelectric material is fixed in the thermostat on two current leads (Fig. 1).

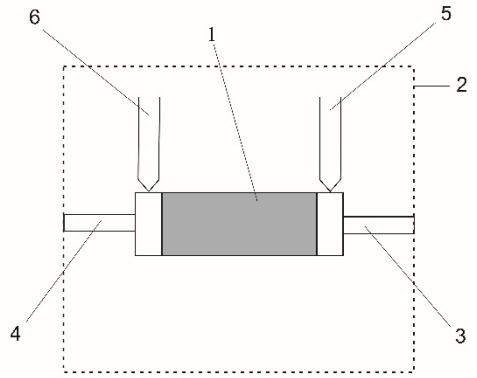


*Fig. 1. Schematic of Harman's method. 1 – sample, 2 – thermostat, 3, 4 – current leads, 5, 6 – thermocouples.*

The values of the thermoelectric figure of merit, as well as the thermal conductivity, electrical conductivity, and the Seebeck coefficient, are determined by the resistances of the sample and the voltage drops on the sample, measured when passing direct and alternating current therethrough:

$$Z = \frac{1}{T_{av}}\left(\frac{R_{\approx}}{R_{=}} - 1\right)\left(1 + \sum_i \gamma_i\right),$$

$$\alpha = \frac{U_{=} - U_{\approx}}{\Delta T},\ \sigma = \frac{1}{R_{\approx}}\frac{l}{S},\ \kappa = \frac{\alpha^2\sigma}{Z},$$

where $R_{\approx}$, $U_{\approx}$ are the resistance of the sample and the voltage drop on it when alternating current is passed, $R_{=}$, $U_{=}$ are the resistance of the sample and the voltage drop on it when direct current is passed, $T_{av}$ is the average temperature of the sample, $l$, $S$ are the length and area of the sample cross-section, $\gamma_i$ are correction factors that take into account the heat exchange of the sample and current leads with the thermostat. These factors depend on a large number of parameters, namely the radiation coefficients of the sample, contact plates and current leads, their temperature dependences, as well as the exact values of electrical conductivity and thermal conductivity of wire materials, the radiation coefficient of chamber walls and its temperature dependence, exact geometric dimensions of current leads, etc.

Work [5] presents an analysis of the errors in measuring the figure of merit using Harman's method and shows that the main source of errors when using Harman's method is the heat exchange of the sample with the environment through current leads and radiation. To minimize these errors, the technique of modified Harman's method is proposed, which makes it possible to measure the properties of the thermoelectric material with a high speed of response, and at the same time take into consideration the heat exchange of the sample with the thermostat, measuring all the necessary values for this during one experiment.

*The purpose of the work* is to develop high-speed, high-precision equipment for determining the thermoelectric properties of a material using modified Harman's method in the temperature range of 30 – 500 °C, which takes into consideration possible measurement errors, and the equipment itself is made on a modern element basis, using computer processing of measurement results.

## 1. Description of experimental installation

Installation for measuring the properties of parameters of TEM samples using modified Harman's method is schematically shown in Fig. 2.

The installation consists of a measuring unit, a control unit and a pumping vacuum post. The control unit includes sources of direct and alternating current with appropriate ammeters, voltage and temperature meters, and a thermoregulation system.

The main unit of the installation is a measuring unit with a TEM sample holder. The design of the measuring unit is shown in Fig. 3.

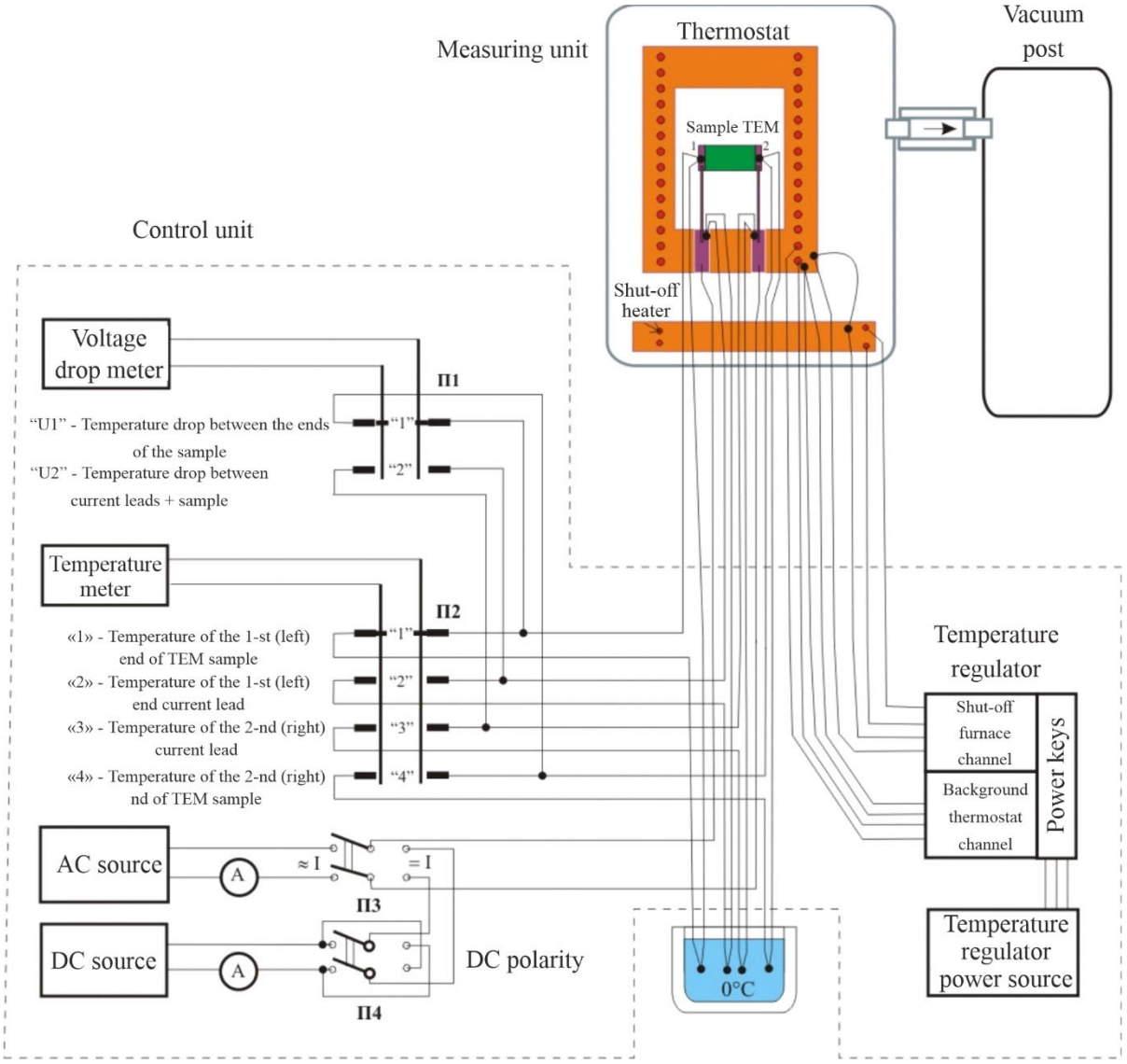


*Fig. 2. Schematic of the installation for measuring parameters of TEM samples.*

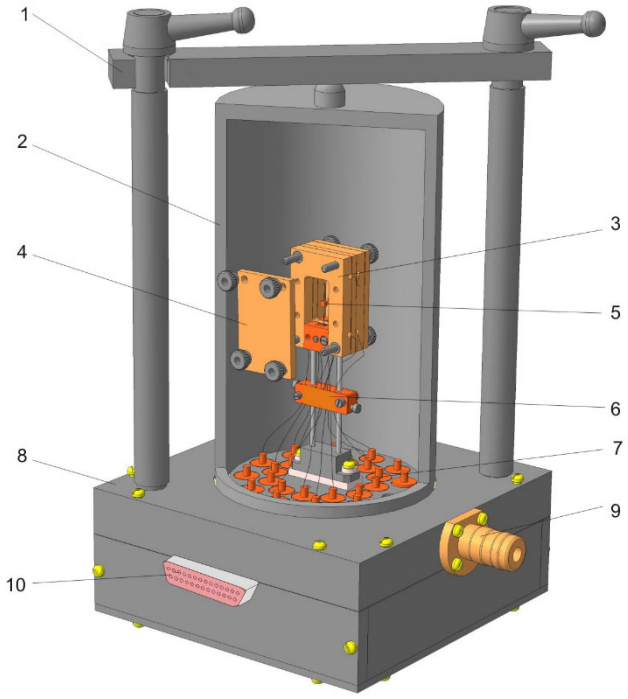


*Fig. 3. Design of the measuring unit.*

*1 – vacuum cap clamp,*
*2 – vacuum cap,*
*3 – thermostat,*
*4 – removable cover of the thermostat,*
*5 – sample holder probes,*
*6 – shut-off heater,*
*7 – pressure leads,*
*8 – the base of the measuring unit,*
*9 – vacuum fitting,*
*10 – connector.*

A TEM sample holder is fixed on the base of the measuring unit body, on thin stainless legs (Fig. 4). The holder itself is a metal collapsible thermostat, in the middle of which there is a niche with two pads on thin, elastic stainless racks. These pads are used as TEM sample holders, as well as current leads and contact elements of potential and temperature sensors. The racks themselves are mounted in heat spreader plates, which have good thermal contact with the base of the thermostat, but are electrically isolated from it. The pads, which in their area are comparable to the area of the ends of the TEM sample, are parallel to each other and are located at a distance from each other that is comparable to the length of the TEM sample. The pads are capable of holding the sample in suspension due to friction and elasticity of the racks. Pads and heat spreader plates, each having one measuring thermocouple and together with the current leads being one whole, form the probes. The probes in the installation are replaceable. This makes it possible to easily change them during routine or repair work, or to install others – for different sizes of samples. For measurement, the TEM sample is inserted between the probe pads through the removable side covers of the thermostat and soldered to them for better thermal and electrical contact.

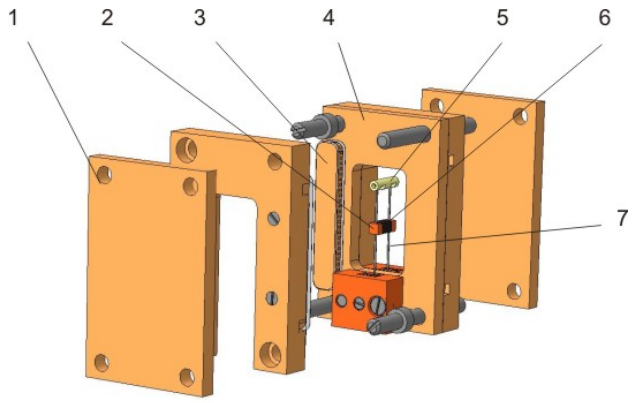


*Fig. 4. Sample arrangement in the holder. 1 – Thermostat cover, 2 – probe pads, 3 – heating element, 4 – thermostat base, 5 – ceramic screed, 6 – TEM sample, 7 – probe rack.*

The thermostat is active. Resistive heating elements and thermocouples are mounted in its walls and the required temperature is maintained with the help of a thermoregulator. To prevent thermal distortions in the thermostat, a shut-off heater is attached to its legs, the temperature of which is maintained by the thermoregulator at a given level. Moreover, all conductors leaving the thermostat are in contact with the shut-off heater and, thus, acquire the same temperature as it. This significantly reduces heat loss from the thermostat through the conductors. The conductors themselves are connected through sealed leads to the connector and further, through the measuring cable, to the control unit. The thermostat is covered with a cap, from under which air can be pumped out with the help of a vacuum post, or the air can be replaced with an inert gas. Measuring TEM samples in a vacuum or in an inert atmosphere reduces measurement errors, and also protects the TEM sample and the surface of the thermostat from oxidation during high-temperature measurements. The vacuum cap has clamping structural elements for better tightness.

## 2. Description of the measurement technique

Determination of the thermoelectric properties of the material by modified Harman's method is carried out as follows. A sample of thermoelectric material is fixed between two contact plates with high thermal and electrical conductivity on the current conductors in the thermostat. The side surface of the sample and contact plates is covered with a thin, uniform layer of material with a low emissivity. To further increase the accuracy, the measurement process is carried out consecutively twice at two different temperatures, and the magnitude of errors caused by radiation from the surface of the sample and contact plates is experimentally determined. In doing so, the temperature of the thermostat at which the first measurement is made is lower than the temperature at which the second measurement is made and is such that the errors caused by radiation from the surface of the sample and contact plates are insignificant and can be neglected. Since at the first temperature the contribution of radiation is insignificant, it is believed that all the heat is transferred through the current leads to the thermostat by thermal conductivity, therefore it is possible to determine the heat transfer coefficient $K_2$ along the current leads by thermal conductivity by passing an alternating current through the sample and measuring the magnitude of the voltage drops on the sample $U_1$ and on the current leads $U_2$:

$$K_2 = \frac{1}{2}\frac{Q_1 + Q_2}{\left(T_{av} - T_0\right)}. \tag{1}$$

where: $Q_1 = IU_1$ is the Joule heat released in the sample, $Q_2 = IU_2$ is the Joule heat released in each of the current leads, $T_{av} = (T_1+T_2)/2$ is the average value of temperatures measured on the sample ends, $T_0$ is thermostat temperature.

At the second temperature value, voltage drops on the sample and current leads are measured, as well as temperatures at the ends of the sample and the thermostat when alternating current is passed through the sample, voltage drop on the sample, voltage drops on the current leads to the sample, temperatures at the ends of the sample and the thermostat when direct current is passed therethrough. The ohmic voltage drop on the sample $U\sigma$ is determined when alternating current is passed or at the moment direct current is turned on, and thermoEMF $U\alpha$ is determined when direct current is passed. The value of thermoelectric figure of merit, the Seebeck coefficient and electrical conductivity, as well as thermal conductivity are found, with account of heat transfer through current leads and radiation.

To do this, based on the Wiedemann-Franz law, by the results of measurements of temperatures and voltage drops on the sample and current leads at two temperatures $T'$ and $T'$ of the thermostat, the heat transfer coefficient along the current leads at temperature $T''$ is determined

$$K_2(T^{"}) = K_2(T^{'})\frac{U_2(T^{'})}{U_2(T^{"})}\frac{T^{"}}{T^{'}}. \tag{2}$$

Thus, the total heat flow at a higher temperature is divided into heat flow by thermal conduction through current leads and heat flow by radiation. Since the surfaces of the sample and the contact plates are covered with the same coating, the effective radiation heat transfer coefficient $K_{eff}$ can be used at temperature $T''$

$$K_{eff} = \frac{Q_1 - \left(2K_2 \cdot (T_{av} - T_0) - Q_2\right)}{\left(T_{av} - T_0\right)}. \tag{3}$$

Analysis of the accuracy of the proposed method of determining the thermoelectric properties of materials is given in [5]. The distributions of electric potential and temperature in the sample, contact plates, and current leads were obtained by computer simulation, which made it possible to optimize the measurement scheme and obtain the values of possible errors in the determination of the thermoelectric figure of merit associated with heat transfer by radiation. Errors in determining the thermoelectric figure of merit by the proposed method, associated with heat transfer through current leads and radiation, in the temperature range of 30 – 500 ºC should not exceed 2 %.

Typical results of measuring the temperature dependences of parameters of the sample of *n*-type $Bi_2Te_3$ thermoelectric material are presented in Fig. 5.

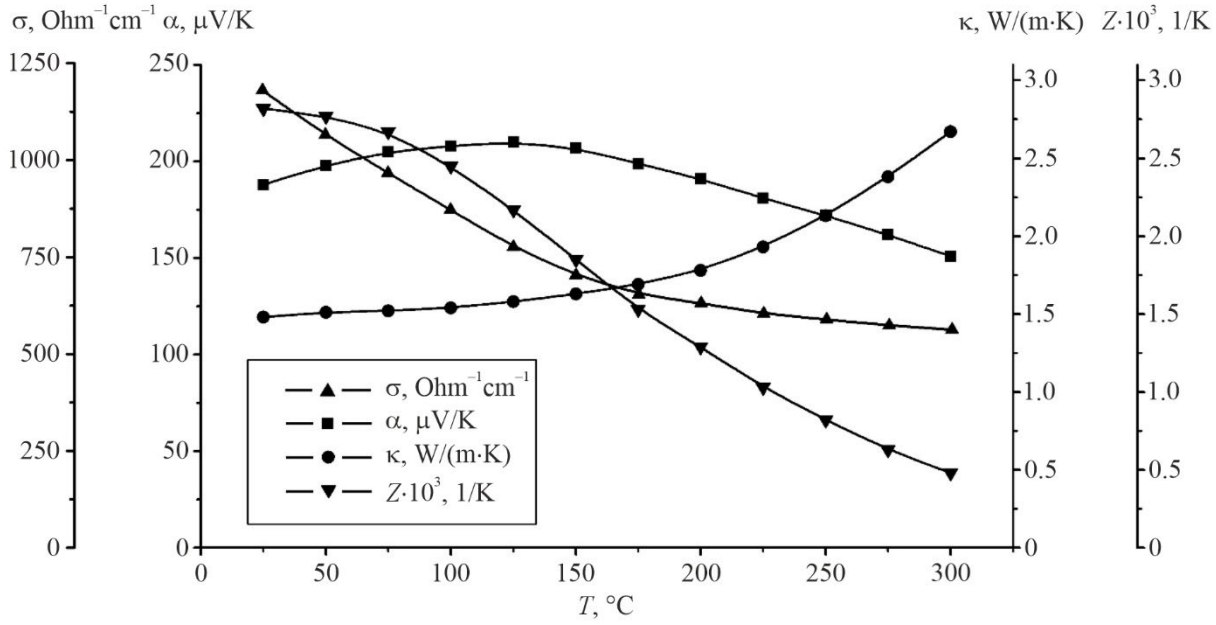


*Fig. 5. Temperature dependences of the properties of n-type thermoelectric material sample based on $Bi_2Te_3$.*

An experimental comparison of the results obtained by modified Harman's method on the equipment described above with the results obtained on the installation for measuring the properties of thermoelectric materials, built on the absolute method, was carried out [6 – 7]. It was established that deviations in the results increase with a rise in temperature and are within 6 – 7 % in the temperature range of 200 ÷ 300 ºC.

## Conclusions

1. High-speed, high-precision equipment has been developed for determining the thermoelectric properties of a material by modified Harman's method in the temperature range of 30 – 500 °C using computer processing of measurement results, which takes into account and eliminates possible measurement errors.
2. It has been established that the errors in determining the thermoelectric figure of merit by the proposed method, related to heat transfer by radiation, in the temperature range of 30 – 500 °C will not exceed 2 %.
3. A comparison of the results obtained by modified Harman's method with the results obtained at the installation for measuring the properties of thermoelectric materials by the absolute method was carried out.
4. It was established that deviations in the results increase with a rise in temperature and are within 6 – 7 % in the range of 200 ÷ 300 °C.

## References

1. Anatychuk L.I., Lysko V.V. (2014). On improvement of the accuracy and speed in the process of measuring characteristics of thermoelectric materials. *Journal of Electronic Materials,* 43 (10), 3863 – 3869. https://doi.org/10.1007/s11664-014-3300-5.
2. Anatychuk L.I., Havryliuk M.V., Lysko V.V. (2015). Absolute method for measuring of thermoelectric properties of materials. *Materials Today: Proceedings,* 2 (2), 737 – 743. https://doi.org/10.1016/j.matpr.2015.05.110.
3. Harman T.C., Cahn J.H., and Logan M.J. (1959). Measurement of thermal conductivity by utilization of the Peltier effect. *Journal of Applied Physics*, 30(9), 1351 – 1359.
4. Buist R.J. (1992). A new methodology for testing thermoelectric materials and devices. *Proc. of the 11th Intern. Conf. on Thermoelectrics*, Arlington, Texas, 1992, p. 196-209.
5. Anatychuk L.I., Lysko V.V. (2012). Modified Harman's method. *AIP Conf. Proc.* №1449, 373 – 376.
6. Anatychuk L.I., Lysko V.V. (2020).*Thermoelectricity: Vol. 5. Metrology of Thermoelectric Materials.* – Chernivtsi: Bukrek. ISBN 978-617-7770-40-3.
7. Anatychuk L.I., Havryliuk M.V., Lysko V.V. (2018). Ways for quality improvement in the measurement of thermoelectric material properties by the absolute method. *J. Thermoelectricity,* 2, 90 – 100.
8. Anatychuk L.I., Havryliuk M.V., Lysko V.V., Tiumentsev V.A. (2018). Automation and computerization of measurements of thermoelectric parameters of materials. *J. Thermoelectricity,* 3, 80 – 100.

Submitted 18.01.2022.

**Анатичук Л.І.,** *акад. НАН України* [1,2]
**Гаврилюк М.В.** [1]
**Лисько В.В.,** *канд. фіз.-мат. наук* [1,2]

[1] Інститут термоелектрики НАН та МОН України,
вул. Науки, 1, Чернівці, 58029, Україна;
[2] Чернівецький національний університет імені Юрія Федьковича,
вул. Коцюбинського 2, Чернівці, 58012, Україна
*e-mail: anatych@gmail.com*

# ОБЛАДНАННЯ ДЛЯ ВИЗНАЧЕННЯ ТЕРМОЕЛЕКТРИЧНИХ ВЛАСТИВОСТЕЙ МАТЕРІАЛУ МОДИФІКОВАНИМ МЕТОДОМ ХАРМАНА

*Наведено результати розробки обладнання для визначення термоелектричних властивостей матеріалів – електропровідності, теплопровідності, коефіцієнту термоЕРС та термоелектричної добротності в інтервалі температур 30 – 500 °С з використанням модифікованого методу Хармана. Оцінено похибки вимірювань та описано методи їх зниження. Показано результати вимірювань зразків матеріалів на основі $Bi_2Te_3$, отримані за допомогою описанного обладнання.*

**Ключові слова:** метод Хармана, термоелектрична добротність, абсолютний метод.

## Література

1. Anatychuk L.I., Lysko V.V. (2014). On improvement of the accuracy and speed in the process of measuring characteristics of thermoelectric materials. *Journal of Electronic Materials,* 43 (10), 3863 – 3869. https://doi.org/10.1007/s11664-014-3300-5.
2. Anatychuk L.I., Havryliuk M.V., Lysko V.V. (2015). Absolute method for measuring of thermoelectric properties of materials. *Materials Today: Proceedings,* 2 (2), 737 – 743. https://doi.org/10.1016/j.matpr.2015.05.110.
3. Harman T.C., Cahn J.H., and Logan M.J. (1959). Measurement of thermal conductivity by utilization of the Peltier effect. *Journal of Applied Physics*, 30(9), 1351 – 1359.
4. Buist R.J. (1992). A new methodology for testing thermoelectric materials and devices. *Proc. of the 11th Intern. Conf. on Thermoelectrics*, Arlington, Texas, 1992, p. 196-209.
5. Anatychuk L.I., Lysko V.V. (2012). Modified Harman's method. *AIP Conf. Proc.* №1449, 373 – 376.
6. Anatychuk L.I., Lysko V.V. (2020).*Thermoelectricity: Vol. 5. Metrology of Thermoelectric Materials.* – Chernivtsi: Bukrek. ISBN 978-617-7770-40-3.
7. Anatychuk L.I., Havryliuk M.V., Lysko V.V. (2018). Ways for quality improvement in the measurement of thermoelectric material properties by the absolute method. *J. Thermoelectricity,* 2, 90 – 100.
8. Anatychuk L.I., Havryliuk M.V., Lysko V.V., Tiumentsev V.A. (2018). Automation and computerization of measurements of thermoelectric parameters of materials. *J. Thermoelectricity,* 3, 80 – 100.

Надійшла до редакції: 18.01.2022.

# TO THE 85th ANNIVERSARY
# OF LUKYAN IVANOVYCH ANATYCHUK

July 15, 2022 marked the 85th birthday of the world-renowned thermoelectric scientist, director of the Institute of Thermoelectricity of the NAS of Ukraine and the Ministry of Education and Science of Ukraine, Doctor of Physical and Mathematical Sciences, Professor, Academician of the NAS of Ukraine, Head of the Department of Thermoelectricity and Medical Physics of the Educational and Scientific Institute of Physical, Technical and Computer Sciences of Yuriy Fedkovych Chernivtsi National University, President of the International Thermoelectric Academy, Head of the Scientific Coordination Council of the Western Scientific Center of the NAS and MES of Ukraine in Chernivtsi region, Honorary Academician of the International Academy of Refrigeration, Honorary Professor of Yuriy Fedkovych Chernivtsi National University and Wuhan University, Honorary Citizen of the village of Kolinkivtsi and the city of Chernivtsi.

L.I. Anatychuk is a well-known scientist in thermoelectricity, an important scientific and technical direction that involves the direct, machine-free thermal into electrical energy conversion, with great potential for practical applications. The founder of modern thermoelectricity was the director of the Leningrad Institute of Semiconductors, Academician A.F. Ioffe. There were close scientific ties between this Institute and Chernivtsi State University in Ukraine, thanks to which L.I. Anatychuk, while still a University student, became a disciple of academician Ioffe.

In 1960, after graduating from the University, L.I. Anatychuk received an invitation to become an employee of the A.F. Ioffe Institute, but Lukyan Ivanovich chose a different path – he devoted himself to the development of thermoelectricity in his homeland, dreaming of creating the same institute as Academician Ioffe's.

In 1964, after completing his postgraduate studies, he defended his candidate's thesis, and in 1974 – his doctoral thesis. In 1973, on the initiative of L.I. Anatychuk, the Department of Thermoelectricity was opened at Chernivtsi State University, which he headed and which he still manages today. This created unique conditions for special training of personnel in thermoelectricity and intensive development and implementation of the latest thermoelectric equipment.

Taking into account its high demand, in 1980 a design bureau of thermoelectric instrument-making "Phonon" was opened in Chernivtsi, with L.I. Anatychuk as its director.

Using its own funds, "Phonon" design bureau built a special laboratory building and a pilot production building, equipped with the latest equipment.

During 10 years of its activity, about 300 devices were developed and manufactured, mainly for space and defense purposes, the chief designer of most of them was L.I. Anatychuk. On his initiative,

two state programs on thermoelectricity were developed. "Phonon" design bureau became the leading organization on thermoelectricity in the country. In 1985, he was elected a corresponding member of the National Academy of Sciences of Ukraine.

The collapse of the USSR and the independence of Ukraine opened new horizons for the development of "Phonon" design bureau. In 1990 it was reorganized into Institute of Thermoelectricity of the National Academy of Sciences and the Ministry of Education and Science of Ukraine. Thus, L.I. Anatychuk's dream of creating a research Institute of Thermoelectricity came true. The pilot production of "Phonon" design bureau was reorganized into "Altec-M" LLC.

*Laboratory building of Institute of Thermoelectricity*

The international activities of the institute expanded. Scientific and business ties were established with many thermoelectric organizations around the world. The international prestige of the Institute grew. It was recognized as one of the leading scientific centers in thermoelectricity. In 1992, L.I. Anatychuk was elected an Academician of the NAS of Ukraine. In 1994, on the initiative of L.I. Anatychuk, the International Thermoelectric Academy (ITA) was founded. It united about 100 leading scientists in thermoelectricity from 24 countries of the world. L.I. Anatychuk is invariably elected its president. MTA carries out international scientific coordination and organizes forums on thermoelectricity.

In 2007, the RAPID educational, scientific and production complex was created on the basis of the Institute of Thermoelectricity, the Department of Thermoelectricity of the Chernivtsi National University and “Altec-M” LLC. The complex provides a full cycle of innovation activities – from training personnel, scientific research and to their implementation.

Under the scientific leadership of L.I. Anatychuk, the Institute is further developing the theory of thermoelectricity, thermoelectric materials science and technology of thermoelectric devices. A generalized theory of thermoelectric energy conversion, information-energy theory of thermoelectric devices, theory of reliability of thermoelectric systems have been created, the theory and technology of functionally graded materials have been developed, new methods of manufacturing thermoelectric materials and progressive technologies for creating thermoelectric energy converters have been devised. This has made it possible to manufacture internationally competitive thermoelectric devices.

The Institute pursues joint research with thermoelectric companies and research centers from 22 countries. It supplies thermoelectric products to the USA, Japan, France, Poland, Germany, China, Turkey, Israel and other countries. The most important is the development and supply of thermoelectric equipment for space programs. About 500 thermoelectric devices are successfully operating on Earth satellites, interplanetary stations and the International Space Station.

The use of thermoelectricity in medicine is also developing intensively. More than 35 thermoelectric devices have been developed for the diagnosis and treatment of various diseases.

L.I. Anatychuk has trained 9 doctors and 18 candidates of science, written 13 monographs and a handbook on thermoelectricity, delivered 215 reports at scientific conferences, published 365 scientific articles, and is the author of 283 patents. He is the founder and editor-in-chief of the international “Journal of Thermoelectricity".

L.I. Anatychuk has been awarded 7 state orders and other state and departmental awards; Gold Medal of the National Academy of Sciences of Ukraine; Honorary Gold Prize of the International Thermoelectric Academy; Award of the International Thermoelectric Society (IST), which noted: "Professor L.I. Anatychuk is known for more than sixty years of promotion of development and leadership in the field of thermoelectric research and development, as well as the implementation of thermoelectric technologies worldwide."

On the occasion of his 85th birthday, L.I. Anatychuk was awarded the Honorary Award of the Chernivtsi Regional State Administration "To the Glory of Bukovina".


*Honorary Award of the Chernivtsi Regional State Administration "To the Glory of Bukovina"*


*At the unveiling of the monument to A.F. Ioffe. S. Fedenyak, a student, is speaking*

L.I. Anatychuk deeply respects the memory of Academician A.F. Ioffe. On the initiative of L.I. Anatychuk, a monument to A.F. Ioffe was erected in his homeland in Ukraine, in the city of Romny, near the school where he studied.

L.I. Anatychuk's scientific successes only increase over time. He believes that his highest achievements are still ahead, therefore, he is full of enthusiasm and energy for their implementation.

# LUKYAN IVANOVYCH ANATYCHUK ABOUT HIS ACTIVITIES

Dear colleagues!

Let me first use the opportunity given to me to express my heartfelt gratitude for the sincere congratulations on my 85th birthday that have come from foreign countries, from my native Ukraine, including from my colleagues – employees of the Institute and the Department of Thermoelectricity.

Frankly speaking, while preparing for this speech, I was somewhat embarrassed, because I understood that from me – a person who has already lived for so many years - you expect something special, interesting and instructive. However, over the long period of our joint activities, I have given you so many instructions that repeating them today would be a very dubious matter.

The great Voltaire, an outstanding French philosopher of the 17th century, helped me out.

While rereading Voltaire's works, which, believe me, is a great pleasure, I came across a very interesting saying:

**“For the foolish, old age is a burden,**
**For the ignorant it is winter, but for the man of science**
**it is the time of golden harvest”.**

Trying to apply these words to myself, I, frankly, did not believe them at first, because I was convinced that my most productive creative time was between the ages of 40 and 50. I believed that at this stage of life a person is still full of youthful energy and is already quite experienced in his field.

*F. Voltaire – an outstanding French philosopher of the 17th century*

To determine where the truth lies, I plotted the number of my scientific achievements, expressed in published articles, monographs, and patents, over time.

They are shown in the figure, where the *x*-axis shows the years of life, and the *y*-axis shows the magnitude of these scientific achievements. The figure shows

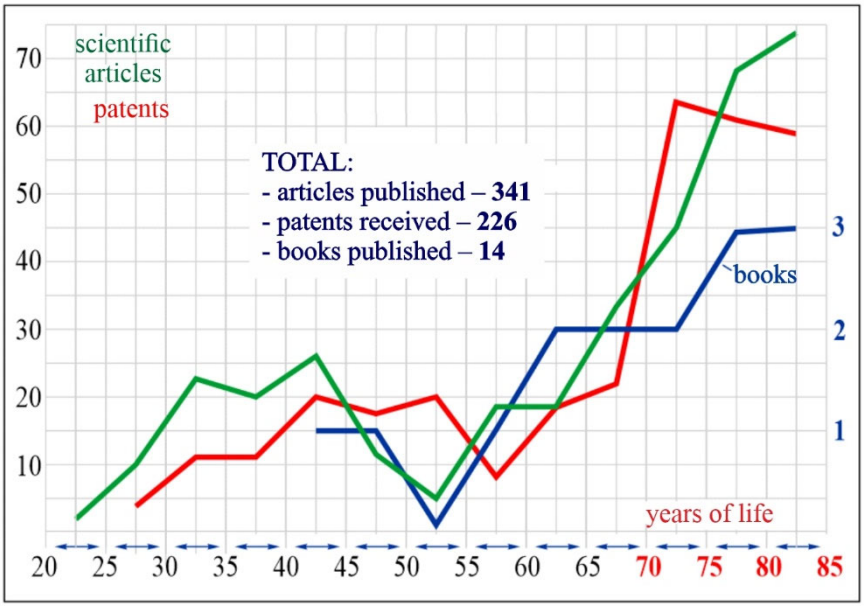


First, that over nearly 60 years of creative work, I have published 341 articles, received 220 patents, and published 12 monographs. It is especially gratifying to report on mys participation in the writing of the prestigious book "Kelvin, Thermodynamics, and the Natural World," published in the UK by WIT Press.

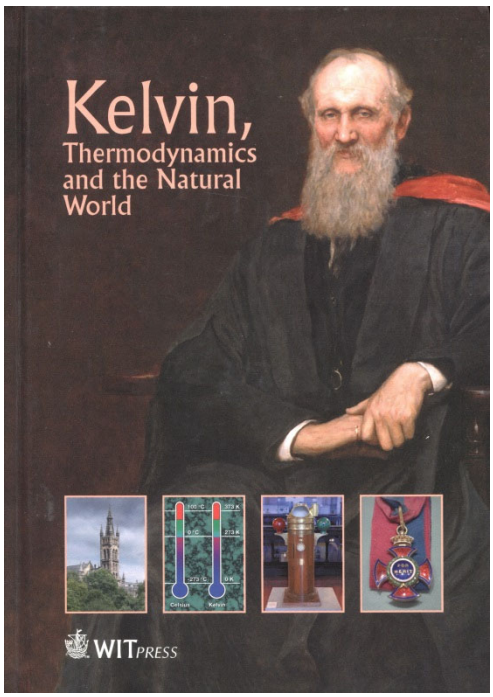


*In this book I had the honor of writing the chapter "Kelvin and Thermoelectricity."*

The book was written for the International Forum on Thermoelectricity, dedicated to W. Thomson and organized by the International Thermoelectric Academy in Belfast, Thomson's homeland.


*Queen's University Belfast*

In my opening speech at the Forum, I noted that Belfast is the place where the Titanic was built. It is interesting that during its construction, the developers of the Titanic were approached by German thermoelectric specialists with a proposal to install an infrared thermoelectric device on it that would detect the presence of obstacles (rocks, icebergs) in the fog at a distance of up to 1 km. However, the developers were so confident in the reliability of their future ship that they refused such a proposal. The result of this erroneous decision is known to everyone. It is instructive for those who ignore thermoelectricity.

Secondly, it follows from the drawing that Voltaire was indeed right – my scientific achievements at the advanced age of 70 – 85 years are almost three times greater than those I expected at 40 – 45 years. So, indeed, at the advanced age the time of the "golden harvest" has come. Moreover, from the trends of growth of achievements it follows that the time of the "golden harvest" should continue in future years.

This inspires optimism and a desire for further creative scientific work. Therefore, I have already created a plan for my scientific activities for the coming years and am making efforts to implement it every day. At the same time, I very much hope for your active assistance in this matter.

## ARTICLE SUBMISSION GUIDELINES

For publication in a specialized journal, scientific works are accepted that have never been printed before. The article should be written on an actual topic, contain the results of an in-depth scientific study, the novelty and justification of scientific conclusions for the purpose of the article (the task in view).

The materials published in the journal are subject to internal and external review which is carried out by members of the editorial board and international editorial board of the journal or experts of the relevant field. Reviewing is done on the basis of confidentiality. In the event of a negative review or substantial remarks, the article may be rejected or returned to the author(s) for revision. In the case when the author(s) disagrees with the opinion of the reviewer, an additional independent review may be done by the editorial board. After the author makes changes in accordance with the comments of the reviewer, the article is signed to print.

The editorial board has the right to refuse to publish manuscripts containing previously published data, as well as materials that do not fit the profile of the journal or materials of research pursued in violation of ethical norms (for instance, conflicts between authors or between authors and organization, plagiarism, etc.). The editorial board of the journal reserves the right to edit and reduce the manuscripts without violating the author's content. Rejected manuscripts are not returned to the authors.

**Submission of manuscript to the journal**

The manuscript is submitted to the editorial office of the journal in paper form in duplicate and in electronic form on an electronic medium (disc, memory stick). The electronic version of the article shall fully correspond to the paper version. The manuscript must be signed by all co-authors or a responsible representative.

In some cases it is allowed to send an article by e-mail instead of an electronic medium (disc, memory stick).

English-speaking authors submit their manuscripts in English. Russian-speaking and Ukrainian-speaking authors submit their manuscripts in English and in Russian or Ukrainian, respectively. Page format is A4. The number of pages shall not exceed 15 (together with References and extended abstracts). By agreement with the editorial board, the number of pages can be increased.

To the manuscript is added:

1. Official recommendation letter, signed by the head of the institution where the work was carried out.

2. License agreement on the transfer of copyright (the form of the agreement can be obtained from the editorial office of the journal or downloaded from the journal website – Dohovir.pdf). The license agreement comes into force after the acceptance of the article for publication. Signing of the license agreement by the author(s) means that they are acquainted and agree with the terms of the agreement.

3. Information about each of the authors – full name, position, place of work, academic title, academic degree, contact information (phone number, e-mail address), ORCID code (if available). Information about the authors is submitted as follows:

authors from Ukraine - in three languages, namely Ukrainian, Russian and English;

authors from the CIS countries - in two languages, namely Russian and English;

authors from foreign countries – in English.

4. Medium with the text of the article, figures, tables, information about the authors in electronic form.

5. Colored photo of the author(s). Black-and-white photos are not accepted by the editorial staff. With the number of authors more than two, their photos are not shown.

**Requirements for article design**

The article should be structured according to the following sections:

- *Introduction*. Contains the problem statement, relevance of the chosen topic, analysis of recent research and publications, purpose and objectives.
- *Presentation of the main research material* and the results obtained.
- *Conclusions* summing up the work and the prospects for further research in this direction.
- *References*.

The first page of the article contains information:

1) in the upper left corner – UDC identifier (for authors from Ukraine and the CIS countries);

2) surname(s) and initials, academic degree and scientific title of the author(s);

3) the name of the institution where the author(s) work, the postal address, telephone number, e-mail address of the author(s);

4) article title;

5) abstract to the article – not more than 1 800 characters. The abstract should reflect the consistent logic of describing the results and describe the main objectives of the study, summarize the most significant results;

6) key words – not more than 8 words.

***The text*** of the article is printed in Times New Roman, font size 11 pt, line spacing 1.2 on A4 size paper, justified alignment. There should be no hyphenation in the article.

**Page setup**: "mirror margins" – top margin – 2.5 cm, bottom margin – 2.0 cm, inside – 2.0 cm, outside – 3.0 cm, from the edge to page header and page footer – 1.27 cm.

**Graphic materials**, pictures shall be submitted in color or, as an exception, black and white, in .opj or .cdr formats, .jpg or .tif formats being also permissible. According to author's choice, the tables and partially the text can be also in color.

*Figures* are printed on separate pages. The text in the figures must be in the font size 10 pt. On the charts, the units of measure are separated by commas. Figures are numbered in the order of their arrangement in the text, parts of the figures are numbered with letters – a, b, .. On the back of the figure, the title of the article, the author (authors) and the figure number are written in pencil. Scanned images and graphs are not allowed to be inserted.

*Tables* are provided on separate pages and must be executed using the MSWord table editor. Using pseudo-graph characters to design tables is inadmissible.

*Formulae* shall be typed in Equation or MatType formula editors. Articles with formulae written by hand are not accepted for printing. It is necessary to give definitions of quantities that are first used in the text, and then use the appropriate term.

*Captions to figures and tables* are printed in the manuscript after the references.

*Reference list* shall appear at the end of the article. References are numbered consecutively in the order in which they are quoted in the text of the article. References to unpublished and unfinished works are inadmissible.

**Attention!** In connection with the inclusion of the journal in the international bibliographic abstract database, the reference list should consist of two blocks: CITED LITERATURE and REFERENCES (this requirement also applies to English articles):

CITED LITERATURE – sources in the original language, executed in accordance with the

Ukrainian standard of bibliographic description DSTU 8302:2015. With the aid of VAK.in.ua (http://vak.in.ua) you can automatically, quickly and easily execute your "Cited literature" list in conformity with the requirements of State Certification Commission of Ukraine and prepare references to scientific sources in Ukraine in understandable and unified manner. This portal facilitates the processing of scientific sources when writing your publications, dissertations and other scientific papers.

REFERENCES – the same cited literature list transliterated in Roman alphabet (recommendations according to international bibliographic standard APA-2010, guidelines for drawing up a transliterated reference list "References" are on the site http//www.dse.org.ua, section for authors).

**To speed up the publication of the article, please adhere to the following rules:**

- in the upper left corner of the first page of the article – the UDC identifier;
- family name and initials of the author(s);
- academic degree, scientific title;

begin a new line, Times New Roman font, size 12 pt, line spacing 1.2, center alignment;

- name of organization, address (street, city, zip code, country), e-mail of the author(s);

begin a new line 1 cm below the name and initials of the author(s), Times New Roman font, size 11 pt, line spacing 1.2, center alignment;

- the title of the article is arranged 1 cm below the name of organization, in capital letters, semi-bold, font Times New Roman, size 12 pt, line spacing 1.2, center alignment. The title of the article shall be concrete and possibly concise;
- the abstract is arranged 1 cm below the title of the article, font Times New Roman, size 10 pt, in italics, line spacing 1.2, justified alignment in Ukrainian or Russian (for Ukrainian-speaking and Russian-speaking authors, respectively);
- key words are arranged below the abstract, font Times New Roman, size 10 pt, line spacing 1.2, justified alignment. The language of the key words corresponds to that of the abstract. Heading "Key words" - font Times New Roman, size 10 pt, semi-bold;
- the main text of the article is arranged 1 cm below the abstract, indent 1 cm, font Times New Roman, size 11 pt, line space spacing 1.2, justified alignment;
- formulae are typed in formula editor, fonts Symbol, Times New Roman. Font size is "normal" – 12 pt, "large index" – 7 pt, "small index" – 5 pt, "large symbol" – 18 pt, "small symbol" – 12 pt. The formula is arranged in the text, center aligned and shall not occupy more than 5/6 of the line width, formulae are numbered in parentheses on the right;
- dimensions of all quantities used in the article are represented in the International System of Units (SI) with the explication of the symbols employed;
- figures are arranged in the text. The figures and pictures shall be clear and contrast; the plot axes – parallel to sheet edges, thus eliminating possible displacement of angles in scaling; figures are submitted in color, black-and-white figures are not accepted by the editorial staff of the journal;
- tables are arranged in the text. The width of the table shall be 1 cm less than the line width. Above the table its ordinary number is indicated, right alignment. Continuous table numbering throughout the text. The title of the table is arranged below its number, center alignment;

• references should appear at the end of the article. References within the text should be enclosed in square brackets behind the text. References should be numbered in order of first appearance in the text. Examples of various reference types are given below.

**Examples of LITERATURE CITED**

*Journal articles*

Anatychuk L.I., Mykhailovsky V.Ya., Maksymuk M.V., Andrusiak I.S. Experimental research on thermoelectric automobile starting pre-heater operated with diesel fuel. *J.Thermoelectricity*. 2016. №4. P.84–94.

*Books*

Anatychuk L.I. *Thermoelements and thermoelectric devices. Handbook.* Kyiv, Naukova dumka, 1979. 768 p.

*Patents*

*Patent of Ukraine №* 85293. Anatychuk L.I., Luste O.J., Nitsovych O.V. Thermoelement.

*Conference proceedings*

Lysko V.V. *State of the art and expected progress in metrology of thermoelectric materials.* Proceedings of the XVII International Forum on Thermoelectricity (May 14-18, 2017, Belfast). Chernivtsi, 2017. 64 p.

*Authors' abstracts*

Kobylianskyi R.R. *Thermoelectric devices for treatment of skin diseases*: extended abstract of candidate's thesis. Chernivtsi, 2011. 20 p.

**Examples of REFERENCES**

*Journal articles*

Gorskiy P.V. (2015). Ob usloviakh vysokoi dobrotnosti i metodikakh poiska perspektivnykh sverhreshetochnykh termoelektricheskikh materialov [On the conditions of high figure of merit and methods of search for promising superlattice thermoelectric materials]. *Termoelektrichestvo - J.Thermoelectricity,* 3, 5 – 14 [in Russian].

*Books*

Anatychuk L.I. (2003). *Thermoelectricity. Vol.2. Thermoelectric power converters*. Kyiv, Chernivtsi: Institute of Thermoelectricity.

*Patents*

*Patent of Ukraine №* 85293. Anatychuk L. I., Luste O.Ya., Nitsovych O.V. Thermoelements [In Ukrainian].

*Conference proceedings*

Rifert V.G. Intensification of heat exchange at condensation and evaporation of liquid in 5 flowing-down films. In: *Proc. of the 9th International Conference Heat Transfer.* May 20-25, 1990, Israel.

*Authors'abstracts*

Mashukov A.O. *Efficiency hospital state of rehabilitation of patients with color carcer.* PhD (Med.) Odesa, 2011 [In Ukrainian].